On the Annual Cycle over the Atlantic Sector. The Relative Role of Land and Ocean.

Michela Biasutti

A dissertation submitted in partial fulfillment
of the requirements for the degree of

Doctor of Philosophy

University of Washington

2003

Program Authorized to Offer Degree: Atmospheric Sciences

ProQuest Information and Learning Company
300 North Zeeb Road
P.O. Box 1346
Ann Arbor, MI 48106-1346

In presenting this dissertation in partial fulfillment of the requirements for the Doctoral degree at the University of Washington, I agree that the Library shall make its copies freely available for inspection. I further agree that extensive copying of this dissertation is allowable only for scholarly purposes, consistent with "fair use" as prescribed in the U.S. Copyright Law. Requests for copying or reproduction of this dissertation may be referred to Bell and Howell Information and Learning, 300 North Zeeb Road, Ann Arbor, MI 48106-1346, to whom the author has granted "the right to reproduce and sell (a) copies of the manuscript in microform and/or (b) printed copies of the manuscript made from microform."

Signature Michelle Zbanth

Date August 13th, 2003

University of Washington

Graduate School

This is to certify that I have examined this copy of a doctoral dissertation by

Michela Biasutti

and have found that it is complete and satisfactory in all respects,
and that any and all revisions required by the final
examining committee have been made.

Co-Chairs of Supervisory Committee:

David S. Battisti

Edward S. Sarachik

Reading Committee:

David S. Battisti

Edward S. Sarachik

Dennis L. Hartmann

Date: August 13th, 2003

University of Washington

Abstract

On the Annual Cycle over the Atlantic Sector.
The Relative Role of Land and Ocean.

by Michela Biasutti

Co-Chairs of Supervisory Committee:

Professor David S. Battisti
Atmospheric Sciences

Professor Edward S. Sarachik
Atmospheric Sciences

This study investigates how local and remote forcings shape the annual cycle of surface temperature and precipitation in the tropical Atlantic ocean, Africa, and South America.

We use an atmospheric general circulation model with prescribed SST or coupled to a slab ocean model, and prescribe insolation over land and SST—or, in the coupled case, insolation and ocean heat transport convergence (OHTC)—independently of each other. The annual cycle in a simulation in which only one forcing varies annually indicates the importance of that particular forcing for the observed annual cycle. Additional experiments in which we specify the elevated condensational heating in selected regions are used to distinguish between circulations driven by elevated heating and circulations driven by boundary layer processes.

SST determines the location of the maritime ITCZ and influences precipitation in equatorial coastal regions and the Sahel. The circulation generated by the ITCZ elevated heating generates the low-level convergence and precipitation response in the coastal regions. Changes in subtropical SST are advected inland and force changes in sea level pressure, low-level convergence, and precipitation in the Sahel.

The Atlantic ITCZ intensity is modulated by the precipitation intensity in Africa and South America. Reduced land precipitation cools the upper troposphere and enhances the convective available potential energy in the ITCZ region, thereby making precipitation more intense.

In coupled experiments, annual variations in the continental climate impact the position of the Atlantic ITCZ. The annual changes in Saharan surface temperature affect the strength of the northern subtropical Trades, while changes in continental precipitation affect the surface wind in proximity of the ITCZ. Both processes trigger a coupled response in the equatorial Atlantic surface wind, the ITCZ, and the cross-equatorial SST gradient, whose net effect is the meridional displacement of the ITCZ.

It is shown that the annual cycles of precipitation and temperature over the continents are as important as the annual cycle of insolation over the ocean and of OHTC in forcing the annual march of the Atlantic ITCZ seen in the control simulation.

TABLE OF CONTENTS

List of Figures iii

List of Tables vi

Chapter 1: Introduction 1

Chapter 2: The Model 5

Chapter 3: Experimental Design 11

Chapter 4: Uncoupled Experiments: the local and remote response to SST and insolation 16

4.1 Outlook 16

4.2 On the simulated climatologies 17

4.3 The effect of SST 23

4.4 The effect of Insolation 27

4.5 Statistical Significance and Non-Additive Effects 31

4.6 Summary 32

Chapter 5: Uncoupled Experiments: Mechanisms of local and remote response to SST and insolation 37

5.1 Outlook 37

5.2 Local control of continental precipitation 39

5.3 Local control of oceanic precipitation 43

5.4 Oceanic Control of Continental Precipitation 47

5.5 Continental Control of Oceanic Precipitation 53

5.6 Summary and Discussion 58

Chapter 6: Coupled Experiments: Terrestrial influence on the Atlantic ITCZ **63**

6.1 Outlook 63

6.2 The ITCZ response to a steady continental forcing 63

6.3 The ITCZ response to an annually varying continental forcing 69

6.4 The ITCZ response to annually varying local forcings 81

6.5 Summary and Discussion 83

Chapter 7: Conclusions **87**

7.1 Results 87

7.2 Implications 89

Bibliography **92**

LIST OF FIGURES

2.1 Climatological annual cycle of surface air temperature in observation and the control simulation 7

2.2 Climatological annual cycle of precipitation and surface wind in observations and the control simulation 9

2.3 Atlantic sector: Orography. 10

4.1 Surface air temperature biases in simulation with perpetual forcings 18

4.2 Precipitaion biases in simulations with perpetual forcings. 19

4.3 The annual cycle of the CTL run, presented as anomalies from the month of March. 21

4.4 The portion of the annual cycle of surface air temperature that can be attributed solely to seasonal changes in SST 24

4.5 The portion of the annual cycle of precipitation that can be attributed solely to seasonal changes in SST. 26

4.6 The portion of the annual cycle of surface air temperature that can be attributed solely to seasonal changes in insolation. 28

4.7 The portion of the annual cycle of precipitation that can be attributed to seasonal changes in insolation. 30

4.8 Statistical significance of the surface temperature response to SST, insolation, and their interaction. 33

4.9 Statistical significance of the precipitation response to SST, insolation, and their interaction. 34

4.10 Percentage of the annual variations in surface air temperature and precipitation that can be ascribed to SST, insolation, and their interaction. 35

5.1 The annual cycle of precipitation in the CTL, PMS, and PVE simulations . . 38

5.2 The insolation-induced seasonal changes in net energy flux in the atmospheric column and precipitation. 41

5.3 Vertical structure of the atmosphere in Africa 42

5.4 Seasonal movement of the ITCZ 44

5.5 Seasonal changes in P-E in the ITCZ region. 45

5.6 September-March sea level pressure and surface wind anomalies in the PVE simulation 48

5.7 The development of SAT, wind, and precipitation anomalies over Africa in response to the September-March SST change. 50

5.8 Seasonal changes in $\theta_e$and SLP in the PVE simulation. 52

5.9 Remotely forced seasonal changes in precipitation and low-level wind in the Atlantic ITCZ. 54

5.10 Seasonal changes in the vertical structure of the atmosphere in the ITCZ . . 55

6.1 The June-March difference in condensational heating over South America and Africa. 64

6.2 The surface wind and ITCZ response forced over the ocean by the constant condensational heating anomalies over land. 65

6.3 The annual cycle of the response of the Central Atlantic to land condensational heating. 68

6.4 The annual cycle of insolation over land. 70

6.5 The precipitation response to the annual cycle of insolation over land. 72

6.6 The annual cycle of precipitation, SST, and surface wind in the Central Atlantic in simulations with different annual forcings. 73

6.7 The annual cycle of the response of precipitation, SST, and surface wind in the Central Atlantic to annually varying continental forcing. 74

6.8 The surface air temperature response to the annual cycle of insolation over land. 76

6.9 The winter-time latent heat flux response to the annual cycle of insolation over land. 76

6.10 The latent heat flux and surface wind response to the annual cycle of insolation over land. 78

6.11 The response to the annual cycle of insolation over land. 80

6.12 The annual cycle of precipitation, SST, and surface wind in the Central Atlantic in simulations with different annual forcings. 82

6.13 Harmonic dial of the annual cycle of precipitation and surface air temperature in experiments with different annual forcing. 84

LIST OF TABLES

3.1 List of experiments presented in Chapter 4: name, insolation forcing, SST boundary conditions, interpretation 12

3.2 List of experiments presented in Chapter 5: name, insolation forcing, SST boundary conditions, condensational heating over land, condensational heating over in the oceanic ITCZ region. 13

3.3 List of the uncoupled experiments presented in Chapter 6: name, insolation forcing over land, SST boundary conditions, elevated condensational heating over South America and Africa. 14

3.4 List of the coupled experiments presented in Chapter 6: name, insolation forcing over land, Q-flux, elevated condensational heating over South America and Africa. 14

ACKNOWLEDGMENTS

It is a pleasure to acknowledge the role that many teachers and friends have played in making my time in Seattle, in the Department of Atmospheric Sciences, and in JISAO a time of growth, accomplishment, and joy.

The whole department has provided a great learning environment: I have appreciated the breadth and depth of the program, the openness of the teachers to a sincere interactions with their students, and the atmosphere of collegiality that makes the department serene and fertile for collaboration inside and outside the department itself. I have always felt that the love of the game is what keeps people in this department going and this makes for a very welcoming and safe environment in which I could try things out and learn the game.

Case in point: my committee. I have known Mike Wallace, Dennis Hartmann, Chris Bretherton, and Eric Steig first and foremost as teachers, then as committee members. They have been a great resource: knowledgeable, approachable, interested in my thoughts and work.

My deepest gratitude goes to David Battisti and Ed Sarachik. David and Ed, you, together, have supported me over the years, each in your own way. You have answered the little questions, and taught me how to answer the big ones, you had faith in me, you helped me see the fun in my work when I wasn't able to see it alone, you have learned to work with me while I was learning to work with you, all of us contributing their strengths (and their quirks) as equals. Seven years make a strong connection. Let's keep it alive.

I would have quit before the end of the first year, had it not been for the class of '96. Thank you all guys. Dan, I am particularly happy that you've been around through all of this: it's been so helpful to always be able to ask any questions that came to mind, to feel the pride of answering a question when I could, to bitch and moan with an old friend when I needed to, to share a celebration when we had reason for it, to share a laughter at any

time.

Chris Thompson, Martin Widmann, John Chiang have been a blessing: just enough ahead of me to have a clearer sight of the path, close enough that they could be comrades on the workplace and friends outside. I hope you know how dear you are to me.

Todd Mitchell has been a welcoming and very helpful presence in JISAO. Thank you.

Camille Li, Justin Wettstein, and Kevin Rennert have been great office mates, and god knows how one needs those in a place like JISAO! I especially appreciate how y'all brought a waft of fresh air (figuratively, of course...) into JISAO, the friendliness, the weird music, the sense that we are working together, even as each sits in front of his or her computer. Kevin, a particular thanks to you on pokey's behalf.

Not by science alone lives woman, and my "civilian" life has been greatly enriched because of many friendships outside the workplace. Fiamma Straneo and Rosalba Ciampi have been my first friends on this side of the ocean and a godsend. Chris Flanagan and Eric Dee: you have been a true home. Chris, on top of everything else, I also have to thank you for my health. That my stomach is feeling great while I am writing this dissertation is a tribute to your art. My deepest thanks to all the Pokeys met in Food Not Bombs, besides Chris and Eric, especially Eric W., Brian, Jameson: I have seen the best of America in you, I have learned a ton, and I had the time of my life. MaryLou, Dean, Mike, Fabio, Chris, and many more friends, including those who've moved on to godknowswhere but are still in my heart: thanks, you've made my time in Seattle a lot of fun and have given me a tremendous amount of support and joy. Martin, thanks for your love, patience, and support (more on this later this summer!). David, Lynn, Eric, Adrian, and Nathaniel, thanks for opening your house and welcoming me into your family circle: my time playing and cooking and running around and reading stories with you has been a true source of happiness.

Finally, my folks and friends in Italy have endured my absence, have worked hard to stay deeply connected with me nonetheless, and have supported me in the path that I have chosen, even if it takes me away from them. I am deeply touched and grateful.

DEDICATION

To parents, teachers, friends, and numerous beings,
who have given guidance and support along the path.

May the the merits of this work benefit all beings.

Chapter 1

INTRODUCTION

A number of short-term climate forecast techniques have recently been developed for specific land regions of the tropics, in particular Northeast Brazil (e.g. Folland et al., 2001) and the Sahel (e.g. Ward, 1998). These techniques are based on proven interannual (or longer) correlations of global sea surface temperature (SST) with air temperature and precipitation in the given regions which are interpreted as prove that SST anomalies cause precipitation anomalies. Most past research on precipitation variability has focused on land regions where precipitation is scarce and the human and economic impact of climate variability is large. Yet, the reach of the SST influence might be broader. For example, variability in precipitation in central Africa is also correlated with global SST (not shown). Moreover, interpreting the simultaneous correlation of SST and precipitation in central African as prove of a one-way influence of SST on continental precipitation might not be warranted. Given that the amount of rainfall in central Africa is substantial, and that the reach of convection-driven circulation is broad, we might expect a mutual influence between the oceanic and continental climate.

The correlations between continental and oceanic climates are hard won (e.g Folland et al., 1986, for the Sahel and Uvo et al., 1998, for Northeast Brazil), since long time series are needed to gather the statistics of SST anomalies from the annual cycle and for local temperature and precipitation anomalies. Yet there is no process in the atmosphere on these longer time scales that doesn't also act on the shorter annual time scale. Thus one is tempted to turn to the annual cycle as a convenient analogue for the longer time-scale variability. The difficulty, of course, is that everything varies annually so that perfect correlations tell us nothing about the influence of SST on the annual cycle over land.

Thus, in this study, we will employ a general circulation model (GCM) to identify the processes that govern the annual cycle of tropical precipitation over both the continents and the Atlantic ocean, with a special focus on the mechanisms of oceanic influence over continental precipitation, and mechanisms of terrestrial influence over the oceanic ITCZ.

The annual cycle over land can be thought of as forced locally by the direct action of the sun and remotely by circulations forced primarily by SST and, secondarily, by other land masses. This distinction can be applied to monsoon regions as well, because the reversal of land-sea temperature gradients that drives the monsoon is determined primarily by land temperature changes, and therefore primarily by insolation. If local and remote sources of annual variability could be separated, then where and when the remote effects of SST are important could be quantified simply by decomposing and analyzing the annual cycle.

This separation clearly cannot be done observationally, but can be done in atmospheric models of the annual cycle. Thus Shukla and Fennessy (1994) investigated the Asian summer monsoon in a set of six-month-long atmospheric GCM (AGCM) simulations with seasonally varying SST and insolation, fixed SST and seasonally varying insolation, and seasonally varying SST and fixed insolation; they concluded that the annual cycle of SST is just as important as the annual cycle of solar forcing in the establishment of the summer Asian monsoon. Li and Philander (1997), using an atmospheric GCM forced by specified SST, suppressed the annual cycle of SST by replacing it with an unchanging annual mean while leaving the annual solar variation untouched. They found that even over the unchanging ocean in the Gulf of Guinea, an annual cycle of the model meridional winds could be induced by the annual variation of temperature over land forced locally by the annual cycle of solar heating. Similarly Fu et al. (2001) selectively suppressed the annual cycle of SST in different regions to examine effects of SST on precipitation in the Amazon basin.

In the first part of this study, we employ an AGCM in a manner similar to Li and Philander (1997) but, instead of specifying an unchanging mean SST, we specify constant values of SST at various phases of the annual cycle and allow the sun to vary through its annual cycle. To complete the separation, we specify constant values of the sun at two (extreme) phases of its annual cycle and allow the SST to vary annually. This separation of local and remote effects allows us to estimate not only where SST is important, but also

when.

The effect of SST on land is totally taken into account in such AGCM experiments, but the effect of land on the oceanic climate is artificially constrained by the specification of SST. In the second part of this study, we couple a slab ocean model (SOM) to the AGCM, so that SST can respond to the terrestrial forcing via thermodynamic processes (i.e. in response to changes in surface heat fluxes), albeit not via ocean dynamics. This is still a strong limitation, especially in the equatorial region, where Ekman transport and upwelling force the annual appearance of the equatorial cold tongue.

We concentrate on the Atlantic because there the annual cycle is relatively pure: internal variability is small compared to annual variability (Carton and Zhou, 1997) and occurs mostly on decadal time scales. In the Pacific, by contrast, a good deal of the annual cycle is due to averaging of mostly longer term ENSO variability that is tied to the annual cycle.

Moreover, understanding the relationship between the climate of the Atlantic and that of Africa and South America in AGCM and AGCM+SOM model configurations will have important ramifications. First, current coupled general circulation models do a terrible job at simulating the climate of the Atlantic without using flux adjustments (Davey et al., 2002) . In order to identify what processes might be responsible for this failure, it is wise to look at a simpler model that can reproduce the annual cycle of the Atlantic climate, and identify the mechanisms controlling the annual cycle in this simplified context. That knowledge can then be a starting point for diagnosing the source of error in the more complete coupled model. Second, we anticipate that mechanisms important for the annual cycle in the tropical Atlantic are also relevant to interannual variability (Hastenrath, 1984). AGCM+SOM configurations have been widely and successfully used to simulate the Atlantic interannual variability (e.g., Seager et al., 2001; Saravanan and Chang, 1999), indicating that any insight on the annual cycle gained from the same configuration might be applicable to the interannual variability problem. Third, understanding the first order response of the tropical Atlantic sector to large changes in external forcing—such as changes in local insolation— can offer guidance in organizing the climate information in the paleo records from the Atlantic ocean, Africa, and South America into a cohesive picture.

This thesis is based on Biasutti et al. (2003c, a, b) and is organized as follows. Chap-

ter 2 introduces our model in its uncoupled and coupled configurations, and evaluates its performance in simulating the climate of the Atlantic sector (here defined as the tropical Atlantic, South America, and Africa) against observations. Chapter 3 gives an overview of our modeling strategy and provides a reference for all the experiments presented in this work.

Chapter 4 describes the results of our main uncoupled experiments. We will show that annual changes in SST determine the annual meridional march of the oceanic ITCZ and precipitation over equatorial coastal regions and heavily affect precipitation in the Sahel. We will also show that annual changes of insolation over land determine the gross features of the annual cycle of continental precipitation, namely the north-south displacement following summer insolation, and also affect the intensity of precipitation in the oceeanic ITCZ. Chapter 4 also discusses the degree to which local and remote forcings either add up linearly or interact non-linearly in producing the annual cycle of surface temperature and precipitation at any given location. Chapter 5 brings the focus on the mechanisms responsible for the behavior detailed in Chapter 4, and isolates the effect of boundary layer processes from the effect of the elevated heating in regions of persistent precipitation. Specifically, we will show that the influence of SST on the equatorial coastal regions is mediated by the maritime ITCZ, but the influence on the Sahel is direct.

Chapter 6 describes the results of our coupled experiments. We will show that temperature and precipitation variations over the continents trigger a coupled response in the tropical Atlantic surface wind, the ITCZ, and the cross-equatorial SST, whose net effect is the meridional displacement of the ITCZ. Furthermore, we will isolate and compare the relative importance of local insolation, ocean heat transport, continental surface temperature, and continental precipitation for the development of the annual cycle of SST and precipitation over the Atlantic ocean. We will show how suppressing the annual cycle over land suppresses the annual march of the oceanic ITCZ.

Chapter 7 summarizes our work and draws conclusions and implications.

Chapter 2

THE MODEL

The atmospheric model used in this study is the Community Climate Model version 3 (CCM3) developed at NCAR, run at the standard resolution T42L19 (triangular spectral truncation at wavenumber 42, corresponding to a grid about 2.8° × 2.8°; and 19 mixed sigma and pressure vertical levels). The NCAR Land Surface Model (LSM, Bonan, 1996) is coupled to the atmospheric component to simulate the effect of vegetation and soil hydrology on land-atmosphere exchanges (Bonan, 1998). A detailed description of the model, its dynamical core, its physical parameterizations, and its overall performance, can be found in Kiehl et al. (1998); Hack et al. (1998); Bonan (1998) and other papers in the same special issue of Journal of Climate (volume 11, June 1998). Fu et al. (2001) have used the same atmospheric model, but coupled to a different land surface model (BATS, Dickinson et al., 1993), to determine how SST influences precipitation in the equatorial Amazon, and found that the model qualitatively agrees with observations, and is therefore suitable for this kind of experiment.

For the coupled experiments described in Chapter 6, we have coupled CCM3 in the tropical Atlantic to a fixed 50m depth ocean mixed layer. Outside the tropical Atlantic, the SST field is prescribed, and the transition is eased over 10 degrees of latitude. This configuration allows for thermodynamic atmosphere-ocean interactions (but no ocean dynamics) in the tropical Atlantic, while at the same time minimizes the influence of the midlatitudes and of other oceans on the tropical Atlantic climate.

The effect of ocean dynamics on the annual cycle of SST is parameterized in the slab ocean model (SOM) by specifying an annually varying heat flux correction (referred to as the Q-flux). The Q-flux is derived from an uncoupled simulation that used fixed monthly mean observed SST; it is calculated as the difference between the mixed layer heat content tendency and the heat flux provided by the atmosphere (the sum of turbulent surface fluxes

and radiative fluxes). The application of the Q-flux can be interpreted as the imposition of the ocean heat transport convergence into the oceanic mixed layer, although in reality it also corrects for biases in the atmospheric fluxes. Note that the Q-flux is calculated from monthly mean SST tendency and atmospheric fluxes, and this mean value is then linearly interpolated to obtain the instantaneous values used in the integration. This procedure introduces a small additional bias in the simulated climatology. Saravanan and Chang (2000) and Chiang et al. (2003), each using a configuration similar to the one used in this study, have shown that CCM3 coupled to a slab ocean model simulates the mean state and the variability of the tropical Atlantic climate fairly well.

The climate simulated in a control simulation by the uncoupled AGCM model and that simulated by the coupled AGCM+SOM model are very similar to each other, and differences between the two simulations are negligible when compared to the difference between the simulations and the observations. Thus, here we will verify against observations only the AGCM control simulation.

We compare precipitation, surface air temperature, and surface winds simulated by the uncoupled control run (CTL) with those observed (the GPCP precipitation product, Huffman et al., 1997) or produced by the NCEP reanalysis project (for surface air temperature and wind, Kalnay et al., 1996). Note that the observed and reanalyzed climatologies refer to different time periods, and that the CTL climatology is obtained from a run with climatological SST boundary conditions (Shea et al., 1992), themselves different from the ones used by the reanalysis (Reynolds and Smith, 1994; Parker et al., 1996). Therefore, in-detail agreement should not be expected.

Figure 2.1 compares the reanalyzed and simulated March, June, September, and December surface air temperature. The differences over the ocean are consistent with the discrepancies in the SST products noted above. Over the continents the temperature pattern is quite similar to that observed, and the progression of the annual cycle is well simulated. This consistency goes beyond the obvious cooling in the winter and warming in the summer, and can be found in some of the spatial details. For example, over northern Africa the isotherms are quite zonal in March, but a localized maximum confined to western Africa develops in June; in the Amazon basin a temperature maximum develops in September. Nevertheless,

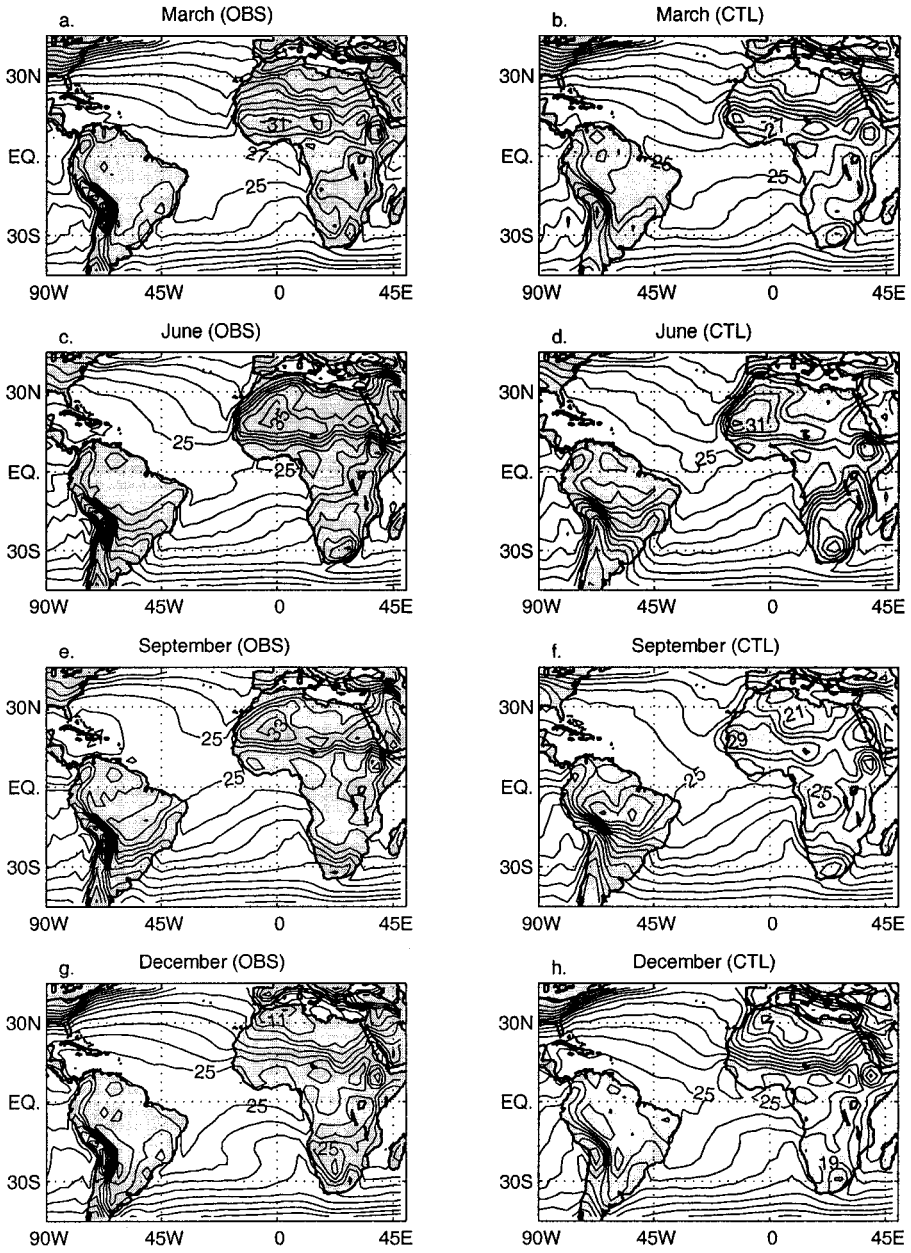

Figure 2.1: Climatological annual cycle of surface air temperature in the NCEP reanalysis (OBS, left column) and the control run (CTL, right column). All fields are regridded to the T42 grid. "Surface" is defined as the 0.995 sigma level in the NCEP model, and as the 0.992 sigma level in CCM. The contour interval is 2° C. The CTL run reproduces quite well the evolution of the annual cycle, although it consistently underestimates continental temperatures.

the model has a substantial cold bias throughout the year in the Sahara desert (because the soil albedo is too high, as reported by Bonan, 1998), Chile and Argentina, and—to a lesser degree—South Africa. A warm bias is present in the Amazon basin during austral winter and spring.

Figure 2.2 compares observed rainfall and reanalyzed surface winds with the CTL simulation. The CCM3 reproduces fairly well the seasonal movement of the ITCZ and the succession of dry and wet seasons over the continents. The agreement is less satisfactory when we compare the mean precipitation, instead of the seasonal changes. The CCM3 exhibits a substantial bias over central equatorial Africa, where it produces twice the observed precipitation all year round, and in the mountainous regions of southern Africa and South America (wet bias during March and December). In general the ITCZ is displaced somewhat too far to the south, and the Caribbean region is too wet during boreal summer and fall. While the wet bias in the equatorial and southwestern Africa is a shortcoming specific to the CCM3, the other biases (position of the ITCZ, orographic effect over the Andes during the summer months, and wet Caribbeans) are shared with the NCEP reanalysis (not shown). The fact that a model simulation (i.e. the reanalysis) constrained to be close to the observed circulation produces errors in the rainfall field similar to those seen in the CCM3 suggests that such common biases are due to the inadequate representation of convection in current GCMs, and that the CCM3 is otherwise capable of producing a realistic large scale circulation. Figure 2.2 shows that the low-level circulation is in fact satisfactory, aside for the exaggerated strength of the wind over the Sahara and in southern Africa: the local orography (Fig. 2.3) is not properly represented at the T42 resolution, and does not constitute an efficient barrier to the moist wind blowing into Africa from the Indian ocean. Most likely, the excessive moisture thus spuriously imported into Africa causes the excessive precipitation.

In summary, the CCM3 reproduces fairly well the main patterns of the seasonal evolution of temperature and precipitation in the tropical Atlantic, South America, and Africa, but presents substantial biases in the amount of continental precipitation. Thus, our model results can be applied to the annual cycle in the real world only as long as no pretense is made of explaining the subtleties of the observed climatology. In particular, we caution the

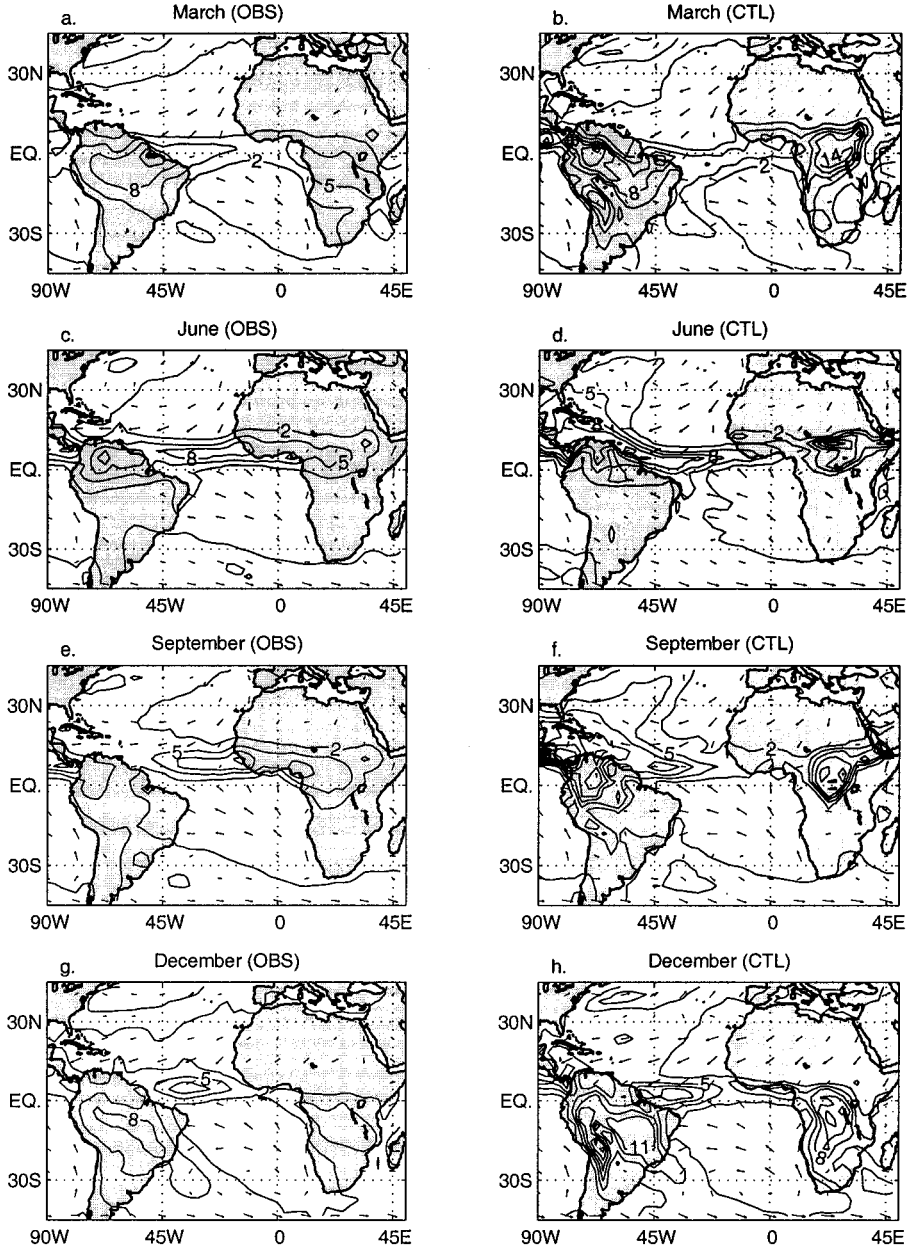

Figure 2.2: Climatological annual cycle of precipitation and surface wind in the GPCP dataset and NCEP reanalysis, respectively (OBS, left column) and in the control run (CTL, right column). All fields are regridded to the T42 grid. "Surface" is defined as the 0.995 sigma level in the NCEP model, and as the 0.992 sigma level in CCM. The contour interval for precipitation is 3mm/day, starting with the 2mm/day contour. The smallest arrow plotted corresponds to a 2m/s wind. The CTL run reproduces quite well the evolution of the annual cycle, although it consistently overestimates African rainfall, and displaces the ITCZ to the south.

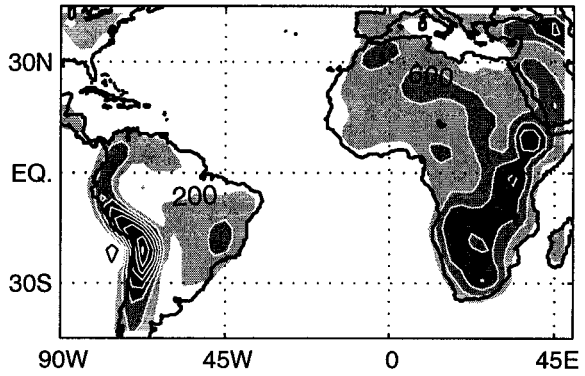

Figure 2.3: The region of interest, and its orography at T42 resolution. The contour interval is 400m, starting at the -200m value. (Negative altitudes below -200m—due to Gibbs fringes—are contoured in black, barely visible west of the Andes.) At T42 resolution the highest peak in the Andes is 3000m high.

reader about the risk that the effect of continental precipitation might be exaggerated in our study, due to the conspicuous wet bias of the model over equatorial South America and Africa.

Chapter 3

EXPERIMENTAL DESIGN

The main purpose of this study is to separate the response of the climate of the Atlantic Ocean and of Africa and South America to local and remote forcings on the annual time-scale. For the tropical land masses, the local annual forcing comes, to zeroth order, from the insolation overhead , and the remote annual forcing comes—via the atmospheric circulation—from the annual cycle of SST. An analogous decomposition applies to the case of the ocean: the local annual forcing comes from the insolation overhead and the ocean heat transport convergence (parameterized in our model by the Q-flux), and the remote annual forcing comes—via the atmospheric circulation—from the annual cycle of insolation over land.

A way to separate the local and remote response is, therefore, to run a set of experiments in which the direct (local) annual forcing is applied either to the ocean or to the land and to investigate the response to such forcing over both the ocean and the land regions. Over land the local forcing is insolation; over the ocean the local forcing is the prescribed SST, in the case of uncoupled experiments, or the combination of insolation and Q-flux in the case of the coupled experiments.

Table 3.1 gives a brief reference for the experiments presented in Chapter 4. We ran a control simulation (CTL), four main experiments (PMS, PSS, PVE, and PWSol) and two additional experiment (PMAS, PM). In the first two experiments, insolation cycles through the annual climatology, while the SST is kept fixed either to the March value (Perpetual March SST, PMS) or to the September value (Perpetual September SST, PSS). In the second two experiments, conditions are reversed: SST cycles through its annual climatology, while the insolation is kept fixed either to the boreal spring equinox value (Perpetual Vernal Equinox, PVE) or to the boreal winter solstice value (Perpetual Winter Solstice, PWSol)[1].

[1]In the PVE and PWSol runs the phenology of the vegetation, describing the leaf and

Table 3.1: List of experiments presented in Chapter 4: name, insolation forcing, SST boundary conditions, interpretation

Name	**Insolation**	**SST**	**Month to month changes are due to seasonal changes in:**
CTL	Climatological	Climatological SST	Insolation and SST (Fig. 4.3)
PMS	Climatological	**Perpetual March SST**	Insolation only (Figs. 4.6-4.7)
PSS	Climatological	**Perpetual September SST**	
PVE	**Perpetual Vernal Equinox**	Climatological SST	SST only (Figs. 4.4-4.5)
PWSol	**Perpetual Winter Solstice**	Climatological SST	
PMAS	Climatological	**Perpetual March Atlantic SST** (Climatological SST elsewhere)	Insolation and SST everywhere *except* in the Atlantic (not shown)
PM	Perpetual Vernal Equinox	Perpetual March SST	N/A (not shown)

In the fifth experiment (PMAS, Perpetual March Atlantic SST) both the insolation and the Pacific and Indian SSTs are allowed to vary according to their climatology, and only SST in the Atlantic is held fixed at the March value. We will not show the PMAS simulation, but we will use results from it as an aid for the interpretation of the main experiments. In all these cases we ran the CCM3 for at least 8 years and disregarded the first few years, in which the model had not yet fully reached equilibrium. The last experiment is a perpetual March experiment (PM, with perpetual vernal equinox insolation and perpetual March SST boundary conditions). PM will only be used in sec. 4.5 (in conjunction with PVE, PMS, and CTL) to measure the statistical significance of our results.

The annual cycle in the PMS and PSS experiments—in which insolation varies annually while SST is fixed at March or September value—is the effect of insolation changes *over land*; thus the experiments indicate where the annual cycle over land is driven locally, and where the annual cycle over the ocean is affected by continental changes (with the restriction of a non-interactive ocean—this restriction will be removed in Chapter 6). The PVE and PWSol experiments—in which SST varies annually while insolation is fixed at March 21st or December 22nd value—indicate where the annual cycle of precipitation over the ocean is

---

stem area, is also held fixed at the March and December values, respectively. Note that we have verified that an experiment with fixed vernal equinox insolation and annually varying phenology gave results virtually indistinguishable from those obtained from the PVE run.

Table 3.2: List of experiments presented in Chapter 5: name, insolation forcing, SST boundary conditions, condensational heating over land, condensational heating over in the oceanic ITCZ region.

Name	**Insolation**	**SST**	**Land Condensational Heating**	**ITCZ Condensational Heating**
CTL	Climatological	Climat.	Calculated (= Climat.)	Calculated (= Climat.)
PMS	Climatological	March	Calculated (~ Climat.)	Calculated (~ March.)
PVE	Vernal Equinox	Climat.	Calculated (~ March)	Calculated (~ Climat.)
PM	Vernal Equinox	March	Calculated (~ March)	Calculated (~ March)
PMw/SIQ	Vernal Equinox	March	Calculated (~ Climat.)	Imposed (= Sept.)
PMw/JAf+SAQ	Vernal Equinox	March	Imposed over South America & Africa (= June.)	Calculated (~ Climat.)
PMw/JAfQ	Vernal Equinox	March	Imposed over Africa (= June.)	Calculated (~ Climat.)
PMw/JSAQ	Vernal Equinox	March	Imposed over South America (= June.)	Calculated (~ Climat.)
PMw/JTQ	Vernal Equinox	March	Imposed over Tropics *except* Atlantic (= June.)	Calculated (~ Climat.)

driven by the local SST, and where the annual cycle over land is affected by SST changes.

Table 3.2 gives a brief reference for the experiments presented in Chapter 5. Our analysis of the mechanisms responsible for the uncoupled results is largely based on two of the experiments introduced above, namely the PMS simulation (in which only insolation is varying, and SST is prescribed to March value) and the PVE simulation (in which only SST is varying, and insolation is kept fixed at March 21st value). In addition, we refer to other experiments in which both insolation and SST are kept fixed at March values, but the elevated condensational heat released in convection in selected areas is prescribed to be constant with values taken either from the PVE experiment or the PMS experiment. We compare these additional experiments with the PM run in order to assess the atmospheric response to elevated condensational heating, when everything else is left unchanged. We caution the reader that, because the heating is specified, these experiments are not constrained to conserve heat.

Tables 3.3 and 3.4 give an overview of the uncoupled and coupled experiments presented in Chapter 6. Recall that the focus of Chapter 6 will be the influence of land on the annual cycle over the Atlantic when SST is allowed to interact thermodynamically with the

Table 3.3: List of the uncoupled experiments presented in Chapter 6: name, insolation forcing over land, SST boundary conditions, elevated condensational heating over South America and Africa.

Name	**Insolation over Land**	**SST**	**Land Condensational Heating**
CTL	Climatological	Climatological	Calculated (= Climat.)
PM	Vernal Equinox (3/21)	March	Calculated ($\sim$ March)
PMw/JQ	Vernal Equinox (3/21)	March	Prescribed (= June)
PSw/MQ	Autumnal Equinox (9/23)	September	Prescribed (= March)
PSw/JQ	Autumnal Equinox (9/23)	September	Prescribed (= June)
LPVE	Vernal Equinox (3/21)	Climatological	Calculated ($\sim$ March)

Table 3.4: List of the coupled experiments presented in Chapter 6: name, insolation forcing over land, Q-flux, elevated condensational heating over South America and Africa.

Name	**Land Insolation**	**Ocean Insolation**	**Q-flux**	**Land Condensational Heating**
CpldCTL	Climatological	Climatological	Climatological	Calculated (= Climat.)
CpldPJQ	Climatological	Climatological	Climatological	Prescribed (= June)
CpldPMQ	Climatological	Climatological	Climatological	Prescribed (= March)
CpldLPVE	Vernal Eq'x (3/21)	Climatological	Climatological	Calculated ($\sim$ March)
CpldLPVE$\overline{\text{Q}}$flux	Vernal Eq'x (3/21)	Climatological	Annual Mean	Calculated ($\sim$ Climat.)
CpldLOPVE	Vernal Eq'x (3/21)	Vernal Eq'x (3/21)	Climatological	Calculated ($\sim$ March)

atmosphere. To deconstruct the annual cycle of the Atlantic ITCZ into locally forced and remotely forced processes, we treat the ocean forcings and the land forcings as independent. Accordingly, our simulations are distinguished by independently considering the annual cycle of insolation over land, SST (for the uncoupled simulations) and insolation over the ocean and Q-flux (for the coupled simulations). Note that, in order to make a fairer comparison between the coupled and uncoupled simulations, we have performed an uncoupled run in which insolation is fixed at the March 21st value over land only, but varies annually over the ocean (Land only Perpetual Venal Equinox, LPVE). Because the SST is prescribed independently of insolation and the tropical atmosphere by itself responds weakly to changes in insolation, the LPVE simulation and the PVE simulations give very similar results in the tropical Atlantic.

In most of the simulations presented in Chapter 6, the elevated condensational heating is calculated by the convective parameterization in CCM3, but in selected simulations (see Tables 3.3 and 3.4) we have discarded, *over land only*, the condensational heating calculated by the model, and instead have prescribed a constant value (obtained from the PMS simulation, and corresponding to either June or March insolation values). By prescribing the continental condensational heating, we decouple continental convection from continental surface temperature, and we can observe the response of the ocean to each forcing separately.

Throughout this study, we focus on the monthly-mean, large-scale fields, with the understanding that the large scale features are the backdrop for rain-bearing synoptic and mesoscale processes. Thus, while recognizing the singularity of rain events at each location and in each season, we hope to build a conceptual model that can explain the coarse features of the simulated annual cycle in the Atlantic sector and, by extension, in the Tropics.

Chapter 4

UNCOUPLED EXPERIMENTS: THE LOCAL AND REMOTE RESPONSE TO SST AND INSOLATION

4.1 Outlook

The main purpose of the uncoupled experiments presented in this chapter is to separate the response of the climate of Africa and South America to local and remote forcings on the annual time-scale. For the tropical land masses, the local annual forcing comes, to zeroth order, from the insolation overhead , and the remote annual forcing comes—via the atmospheric circulation—from the annual cycle of SST. As a way to separate the local and remote response, therefore, we have run a set of experiments in which only one of the two annual forcings is present (either the annual cycle of SST or the annual cycle of insolation). In this chapter, we report on the response to each isolated forcing over both the oceanic and the continental regions.

Instead of presenting the annual cycle as an anomaly from the annual mean, we present it as changes from a single reference month, namely March (note that we we will refer to the "differences from the reference month March" as to "anomalies"). The only reason for this choice is that it makes the discussion in the next sections more effective, but any other method to describe the evolution of the annual cycle, such as differences from any other reference month or from the annual mean, would be equivalent. For example, the temperature difference June-March in the PMS simulation will give us an estimate of the amount of March to June seasonal change that can be ascribed solely to the corresponding changes in insolation. Similarly, the temperature difference June-March in the PVE simulation estimates the change ascribable solely to changes in SST.

In Section 4.3 and Section 4.4 we will refer to such seasonal changes as to the "portion" of the annual cycle due to each individual forcing. Yet, the reader should keep in mind

that these "portions" do not add up linearly to the full control annual cycle. Moreover, because the climate system is non-linear and has long-term memory, the response to the same prescribed forcing may be different when the forcing is applied to a different basic state. Therefore, estimates of the response to insolation changes or SST changes can be different for different experiments. For example, the difference June(PMS)-March(PMS) estimates the effect of insolation in a world with perpetual March SST, while June(PSS)-March(PSS) estimates the same quantity, but for a world with perpetual September SST. The two estimates turn out to be somewhat different (see Section 4.4). Similar considerations apply for the case of the PVE simulation (from which we can infer the effect of SST under perpetual boreal spring insolation) and the PWSol simulation (from which we can infer the effect of SST under perpetual boreal winter insolation). In the next sections we will present the different estimates and comment on their differences and the effect of non-linearities, but will focus mostly on those structures that are more robust.

4.2 On the simulated climatologies

4.2.1 Comments on the fixed-boundary-conditions simulation

Because the memory of the land-atmosphere system is longer than a month, the climate of any given month is dependent upon the history of the system in the previous months. Therefore, March(PMS) and March(PVE) can be expected to differ from March(CTL), and similarly, September(PSS) and December(PWSol) should differ from September(CTL) and December(CTL). Figures 4.1 and 4.2 show how important this effect is on surface air temperature and precipitation, respectively.

As expected, temperature effects are virtually limited to the land, where the soil maintains its memory from one month to the next via its moisture content. Over the ocean, air temperature is "slave" to SST and the memory of the system is artificially suppressed in an AGCM simulation. As a result, SAT anomalies over the ocean are quite closely confined to coastal regions (although, in the PWSol simulation, wintertime advection from the cold continent makes them reach as far as 45° W in the North Atlantic). The surface air temperature anomalies due to fixed insolation are a reflection of the change in annual

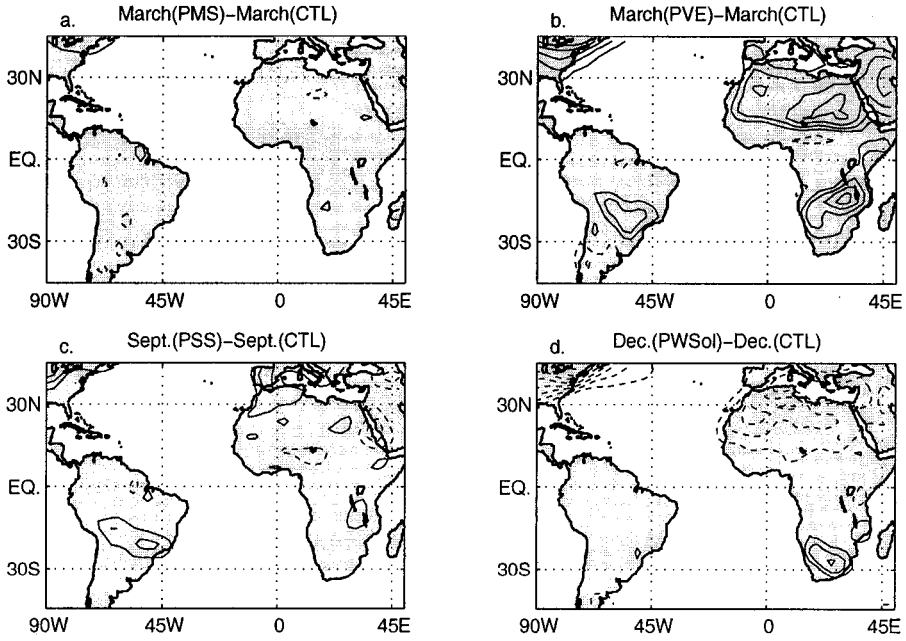

Figure 4.1: Surface air temperture anomalies (SAT) from the CTL run: (a) March(PMS)-March(CTL); (b) March(PVE)-March(CTL); (c) September(PSS)-September(CTL); (d) December(PWSol)-December(CTL). The contour interval is 1°C in all panels; the zero contour is omitted. The memory inherent in land surface properties records the history of the forcing, so that having the same forcing of the CTL run during a specific month does not ensure the same climate for that month. SAT anomalies in the fixed insolation runs reflect differences in annual mean insolation.

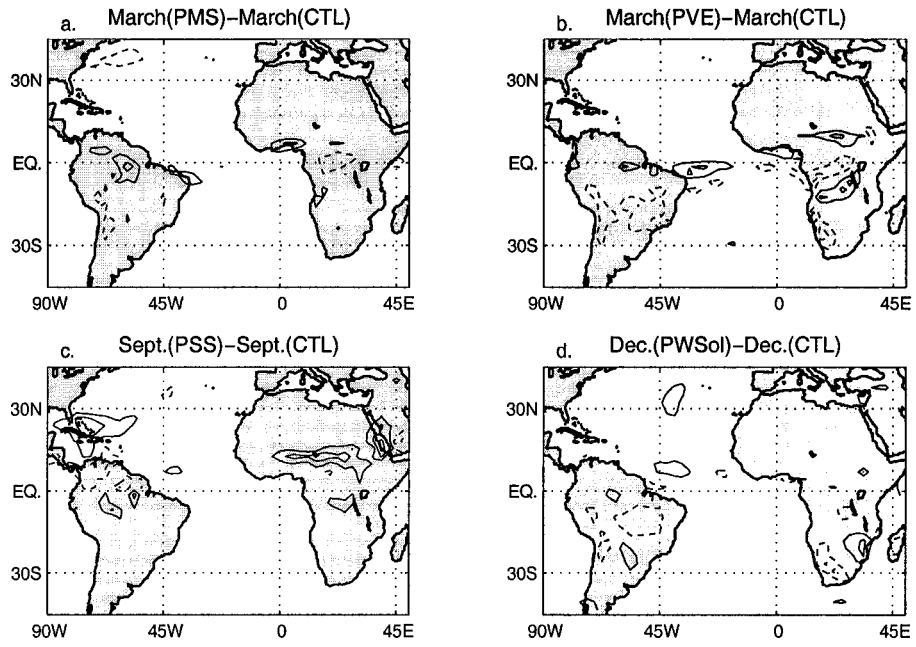

Figure 4.2: Rainfall anomalies from the CTL run: (a) March(PMS)-March(CTL); (b) March(PVE)-March(CTL); (c) September(PSS)-September(CTL); (d) December(PWSol)-December(CTL). The contour interval is 2mm/day in all panels; the zero contour is omitted. The memory inherent in land surface properties records the history of the forcing, so that having the same forcing of the CTL run during a specific month does not ensure the same climate for that month.

mean insolation: March insolation is up to 20Wm^{-2} larger than the annual average in the Tropics, and December insolation is 50 to 150Wm^{-2} less (more) than the annual average in the northern (southern) Tropics. The surface air temperature anomalies due to fixed SST conditions are much smaller than those due to fixed insolation, because in the former case the effect is only indirect, via the changes in circulation and precipitation associated with SST.

In contrast, changes in precipitation (Fig. 4.2) are not confined to the continents, but extend into the Caribbean Sea and the equatorial Atlantic Ocean, and their magnitude is comparable to that of continental anomalies. Over land, anomalies are a response to changes in low level stability and soil moisture; over the ocean they are a dynamical response.

Finally, we wish to point out that the equilibrium states in the four experiments do not inordinately diverge from a "reasonable" climate. If, for example, evaporation exceeded precipitation over a certain land region during March, a simulation with perpetual March forcing would reach equilibrium by drying the soil out in that region. It turns out that these conditions are not met in any of the experiments, and the simulated annual mean soil moisture falls in every case within the range seen in the the control climatology (not shown). Still, each simulation equilibrates to a different annual mean soil moisture content and surface temperature, and such difference can account for some of the non-linearities that will be discussed in the next sections.

4.2.2 The annual cycle of the control simulation

The CTL simulation shows the combined climate response to seasonal changes in both SST and insolation, thus providing a reference against which one can separately compare the anomalies due to SST and those due to insolation. Figure 4.3 shows the anomalies with respect to March values of surface air temperature and precipitation in the CTL simulation, an alternate view of the right-hand column of Figs. 2.1 and 2.2. In addition, the rightmost panel shows the anomalies from the March value of the zonally averaged boundary conditions: insolation at the top of the atmosphere and SST (which has been zonally averaged in the Atlantic basin only). The SST anomalies are strongest in September

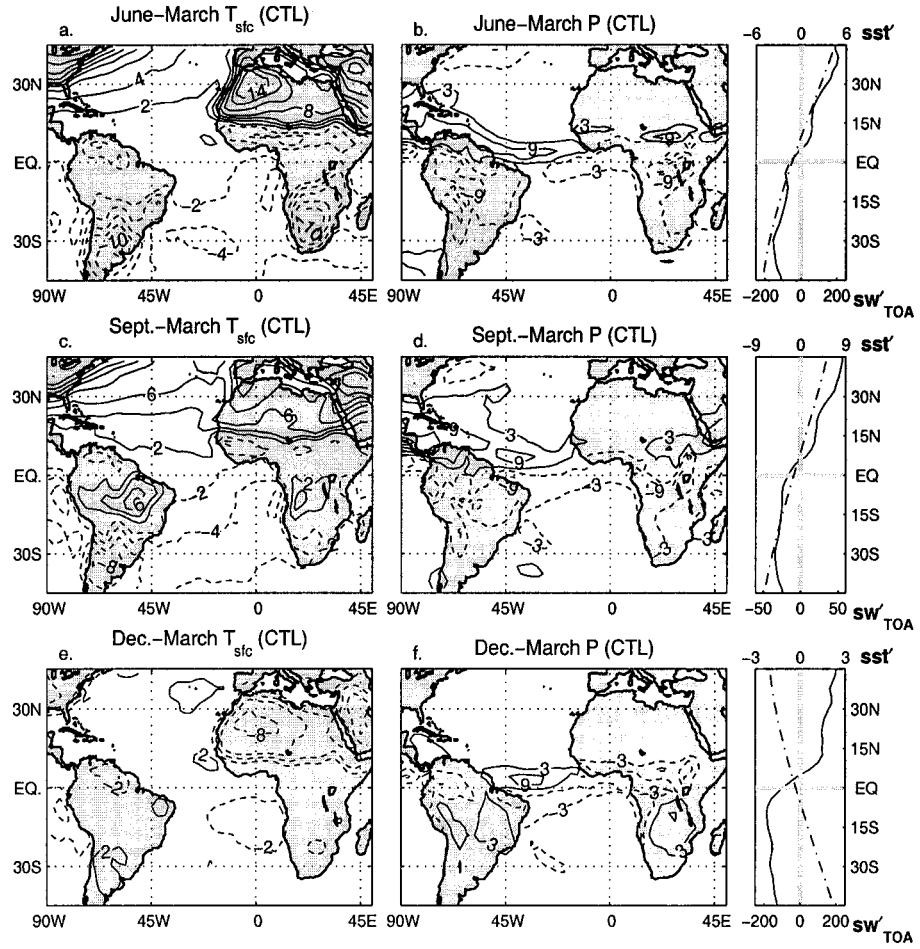

Figure 4.3: The annual cycle of the CTL run, presented as anomalies from the month of March. Left column: surface air temperature (contour interval of 2°C; the zero contour is omitted); central column: precipitation (contour interval of 6mm/day, starting at ±2mm/day; right column: zonally averaged insolation at the top of the atmosphere (dash-dotted line; bottom x-axis; units of Wm^{-2}) and zonally averaged Atlantic SST (solid line; top x-axis; units of °C).

(note the change of scale among panels in 4.3) and are always positive in most of the northern part of the domain (north of about 5°N), and negative in the southern part. The insolation anomalies are weak in September (with the Northern Hemisphere receiving a slightly higher insolation than in March), and four times as large—and, of course, of different signs—in the two solstice months, June and December.

Temperature anomalies over land have mostly the sign expected from the insolation anomalies, suggesting that insolation is the dominant forcing. On the other hand, two features suggest that SST must play a non-negligible role on land surface temperature: (i), the December temperature anomalies are much smaller than those of June (cf. Figs. 4.3a and 4.3e), even though the insolation forcing is of equal magnitude, and (ii), in September, between 15°N and 15°S, the temperature anomalies over land in Africa and South America have signs opposite to those of the solar forcing anomalies. (Note that while (i) holds true in observations (not shown), (ii) is true only in South America and not in Africa, where anomalies are slightly negative. Surface air temperature anomalies in the model are too strongly positive; they are associated with excessive negative precipitation anomalies and consequently excessive reduction in latent heat loss.)

The second column of Fig.4.3 shows the annual cycle of precipitation and indicates that, as expected, the ITCZ moves following the warmest waters, and is at its southernmost position during March. Over land, precipitation anomalies have a more complicated structure, but the general picture is of positive anomalies to the north and negative anomalies to the south during June and September, and the opposite during December. This pattern is consistent with continental precipitation following the maximum in insolation.

The modeling results presented in the next two sections support the conclusions suggested above, and evidence a more complex relation between continental and oceanic precipitation that is not readily visible from the analysis of the annual cycle in the control simulation.

4.3 The effect of SST

Figure 4.4 shows the portion of the annual cycle of surface air temperature that can be attributed solely to changes in SST. In the first two columns are mapped the two different estimates—obtained from the PVE and PWSol run—of the surface air temperature (SAT) response to the evolution of seasonal SST anomalies; the zonal average of the final SST anomaly is shown in the third column. For example, Fig. 4.4a shows the June-March SAT difference in the PVE run. In this case June and March are distinguished only by the value of the SST boundary condition, because the insolation is kept fixed at the vernal equinox value; therefore their difference indicates the response to June-March SST. Fig. 4.4b shows the same quantity, but for a run with a different basic state: a different model world, with perpetual winter insolation. The June-March SST (zonally averaged in the Atlantic domain) responsible for both these anomalies is plotted in the last column.

Over most of the ocean, the June-March SAT anomalies due to SST are indistinguishable from the total anomalies (shown in Fig. 4.3), with the noticeable exception of the Eastern U.S. seaboard/northwest Atlantic region, where the temperature gradient is washed out in the absence of insolation changes. The SST changes induce SAT changes well inland, but their magnitude is overall quite small: 15% to 30% (depending on the estimate) of the CTL changes in northwest Africa, 50% in extratropical South America. SST also induces positive anomalies in northeast Brazil and in south-central Africa that are not present in the CTL annual cycle. The two experiments provide somewhat different estimates of the SST-induced June-March anomalies in the Guiana Highlands (northern South America), the Guinea region, and the eastern Sahara. In Guiana and Guinea the negative anomalies do not reach as far north in the PWSol run as in the PVE run; in Sahara the PWSol run is 3° C warmer than the PVE run.

The patterns of the September-March and December-March terrestrial surface air temperature anomalies due to SST are very similar to the June-March, and only the magnitude of the anomalies changes noticeably. The September-March SST produces SAT anomalies with a pattern very similar to the CTL case—especially in the PVE run, less so in the PWSol run, in which the negative anomalies over North Africa do not extend far enough

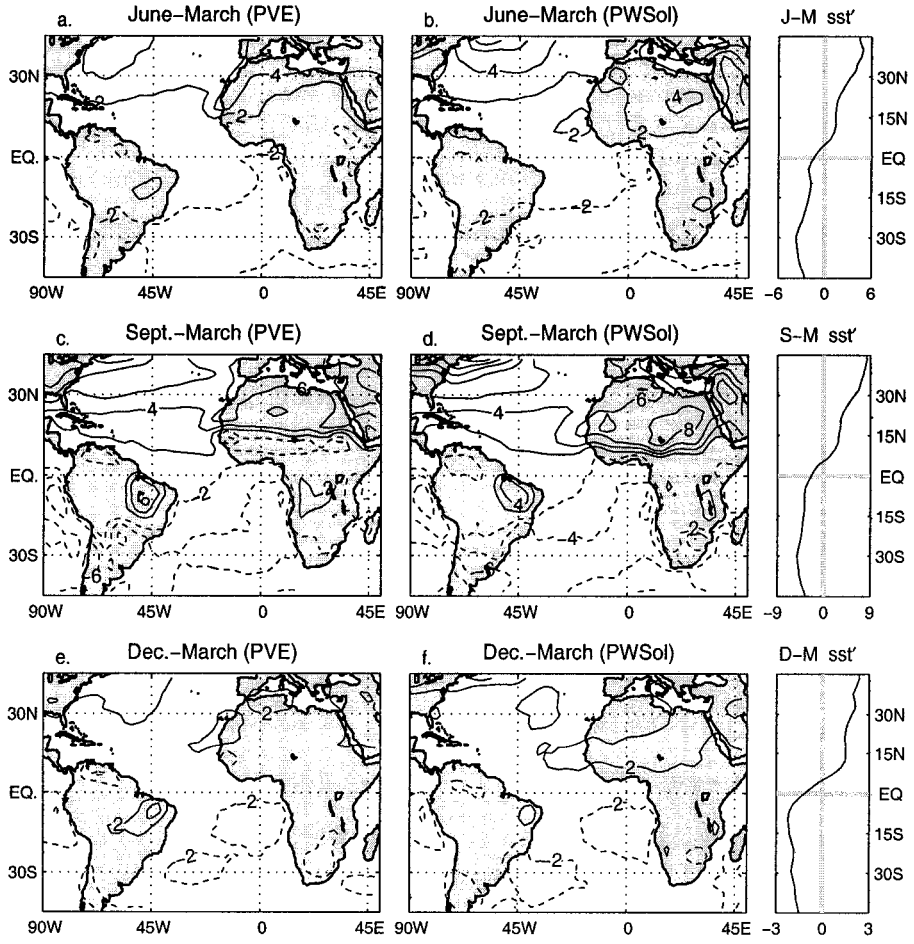

Figure 4.4: The portion of the annual cycle of surface air temperature (presented as anomalies from the month of March) that can be attributed solely to seasonal changes in SST. Left column: estimate obtained from PVE (March insolation boundary conditions). Center column: estimate obtained from PWSol (December insolation boundary conditions). Right column: zonally averaged Atlantic SST (°C). The contour interval is 2°C in all maps; the zero contour is omitted. Land surface temperature are affected by SST. The September-March anomalies due to SST are 60% to 100% of the total seasonal changes, shown in Fig. 4.3. SST plays a more modest role in the solstice months.

north—and 60% or more of the magnitude (compare Figs. 4.4c,d with Fig. 4.3c). The effect of SST on the December-March changes (Figs. 4.4e,f) is very small, and is more than counteracted by the effect of insolation nearly everywhere (cf. Fig. 4.3e with Figs. 4.4e,f). Only along the northeastern coasts of South America (in Guiana and northeast Brazil) is the December-March change in SAT determined by SST. (Note also that in this region SAT anomalies are larger in December than in June, and that, even if the basin-averaged forcing is smaller, the anomalous SST meridional gradient in the western equatorial Atlantic is actually larger in December.) Finally, we note that the terrestrial SAT response to SST is approximately linear, in the sense that the general features of the response of the system to a given SST change are similar in the two runs, regardless of the different insolation conditions.

Figure 4.5 presents the portion of the annual cycle of precipitation that is due to changing SST. It is structured as Fig. 4.4. Over the equatorial Atlantic Ocean, the anomalous precipitation field is a north-south dipole in all months, indicating that, as anticipated in Sec. 4.2.2, the oceanic ITCZ moves north with the warm SST in all months (inspection of the annual cycle in the PMAS confirms that only the Atlantic SST influences the position of the Atlantic ITCZ). The fact that the anomalous precipitation dipole is roughly symmetric about the zero line indicates that, in the PVE and PWSol runs, the intensity of precipitation in the ITCZ changes little from one season to the next. The influence of SST on the rainfall of coastal regions is apparent. The positive rainfall anomalies in the north equatorial Atlantic extend into the Guiana Highlands, the Caribbeans, and Central America. The negative anomalies to the south extend into north east Brazil (to 50°W in June and December, somewhat farther inland in September, when the SST anomalies are strongest). Note the correspondence between negative precipitation anomalies and positive temperature anomalies (and vice-versa) in this region, which indicates that SAT anomalies are due to changes in cloudiness and evaporation. In equatorial Africa, the influence of SST is substantial in June and September, but limited in December.

In the PVE run, the June-March SST anomalies induce positive rainfall anomalies in eastern Sudan and negative anomalies in Guinea, the Congo basin and the East Africa Highlands; in September, the rainfall anomalies intensify and extend over the entire Sahel/Sudan

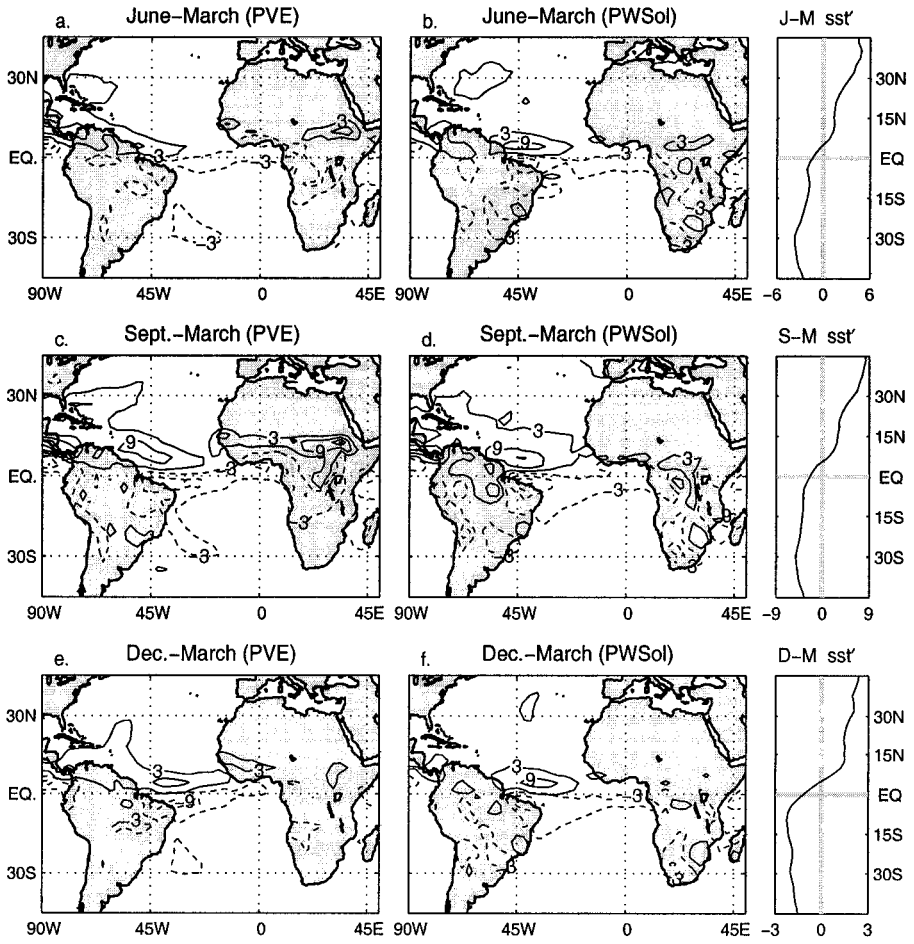

Figure 4.5: The portion of the annual cycle of precipitation (presented as anomalies from the month of March) that can be attributed solely to seasonal changes in SST. Left column: estimate obtained from PVE (March insolation boundary conditions). Center column: estimate obtained from PWSol (December insolation boundary conditions). Right column: zonally averaged Atlantic SST (°C). The contour interval is 6mm/day in all maps, starting at ±3mm/day. SST controls the position of the ITCZ. SST also affects the Guinea and Sudan regions in Africa and the Guiana Highlands and northeast Brazil in South America. SST is the dominant forcing over the tropical continents in September.

region and central equatorial Africa. The general pattern of rainfall anomalies simulated by the PWSol run over tropical Africa is similar to that of the PVE run: it indicates that a positive meridional SST gradient pushes rainfall farther north into the Guinea region, intensifies it in the central equatorial Africa, and reduces it in the Congo basin and in the East Africa Highlands. Nevertheless, the rainfall anomalies in the PWSol run are confined south of 10° N, and do not reproduce the strong effect of SST on the Sahel/Sudan rainfall captured by the PVE run. The PWSol run shows an influence of SST on African rainfall south of 15° S that is not reproduced in the PVE run.

4.4 The effect of Insolation

In this section we present results from the PMS and PSS runs, in which the SST boundary conditions are held fixed, while insolation varies seasonally. We will refer to our results as to the insolation-induced anomalies. In nature all seasonal changes are ultimately caused by the seasonal changes in insolation. In our simulations, instead, the state of the ocean is not modeled, but is prescribed as a boundary condition; thus insolation does not affect SSTs. Therefore when we say "insolation-induced anomalies" we mean it as a shorthand for "changes that are a direct response of the land-atmosphere system to changes in insolation, and that are not mediated by changes in the ocean surface temperature".

Figure 4.6 presents the portion of the surface air temperature (SAT) annual cycle due to insolation, along with the zonally averaged insolation forcing. Comparison with Fig. 4.3 confirms that insolation is the dominant forcing during the solstice months for SAT over both the land masses and the western North Atlantic, in the Gulf Stream region. Insolation-induced SAT anomalies in Fig 4.6 are typically 60-100% of the total change shown in Fig. 4.3.

Figs. 4.6a and 4.6b represent two estimates of the insolation-induced June-March anomalies associated with fixed March and September SST boundary conditions, respectively. The general pattern is quite similar in the two maps, but there are many small but interesting differences. For example, the SAT anomalies outside the deep tropics have smaller magnitude in PMS than in PSS and the negative anomalies in the Sahel region is weaker and displaced farther south. This suggests that, in this region, SAT anomalies are not generated

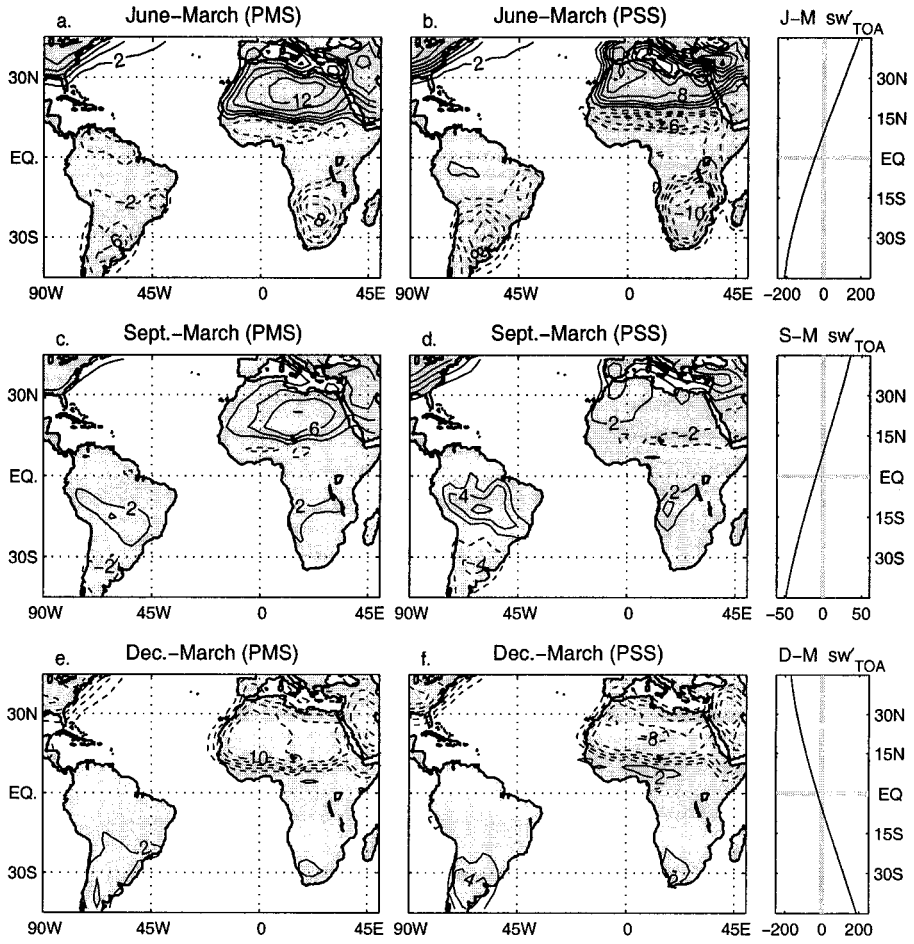

Figure 4.6: The portion of the annual cycle of surface air temperature (presented as anomalies from the month of March) that can be attributed solely to seasonal changes in insolation. Left column: estimate obtained from PMS (March SST boundary conditions). Center column: estimate obtained from PSS (September SST boundary conditions). Right column: zonally averaged insolation at the top of the atmosphere (Wm^{-2}). The contour interval is 2°C in all maps; the zero contour is omitted. Insolation alone suffices to determine the bulk of land surface temperature changes in June and December.

as a direct response to insolation, in fact differences between SAT anomalies in the Sahel in the PMS and PSS are reproduced in differences in the precipitation anomalies (see Fig. 4.7).

The two estimates of the SAT response to September-March insolation changes shown in Figs. 4.6c,d reproduce the coarser features of the control September-March changes (Fig. 4.3c), but are generally smaller. Moreover, the two estimates are quite different from each other, and where one experiment produces sizable anomalies (North Africa in the PMS, Brazil in the PSS), the other doesn't. This behavior is consistent with a minor role of insolation in determining land surface temperature in September (cf. Fig. 4.3c with Figs. 4.6c,d) and the predominance of SST established in Sec. 4.3 (cf. Fig. 4.3c with Figs. 4.4c,d).

As expected, the December-March SAT differences are produced by the changes in insolation almost everywhere over the continents. Notable exception are found only in the coastal regions of equatorial South America and South Africa, where SST produce sizable anomalies with the same sign of the CTL (cf. Fig. 4.3e with Figs. 4.4e,f and Figs. 4.6e,f). The two estimates of the insolation-induced anomalies shown in Figs. 4.6e,f are quite similar.

Figure 4.7 presents the portion of the rainfall seasonal changes due to insolation, along with the zonally averaged insolation forcing. By comparing Fig. 4.7 to Fig. 4.3 (right), we can conclude that (i) the bulk of the June-March and December-March anomalies over the continents is captured by imposing changes in insolation; (ii) for the September-March anomalies, insolation has a robust and dominant effect only in South Africa; and (iii) there is a sizable influence of insolation on the intensity of the oceanic precipitation. It is important to note that precipitation anomalies over the tropical Atlantic Ocean are produced only where there is significant precipitation in the basic state. When the basic state has March SST boundary conditions (PMS run, Fig. 4.7 left column), the precipitation anomalies over the ocean are confined to the equator. When the basic state has September SST boundary conditions, (PSS run, Fig. 4.7 right column) the largest precipitation anomalies over the ocean are in the Caribbeans and the Gulf of Mexico. During June and December there is an additional precipitation anomaly in the central Atlantic, at about 10°N. Precipitation anomalies, whether they are positive or negative, are colocated with the ITCZ of the basic state. Therefore this coincidence cannot be solely attributed to the fact that precipitation is a positive definite variable. While the position of the ITCZ is largely established by coupled

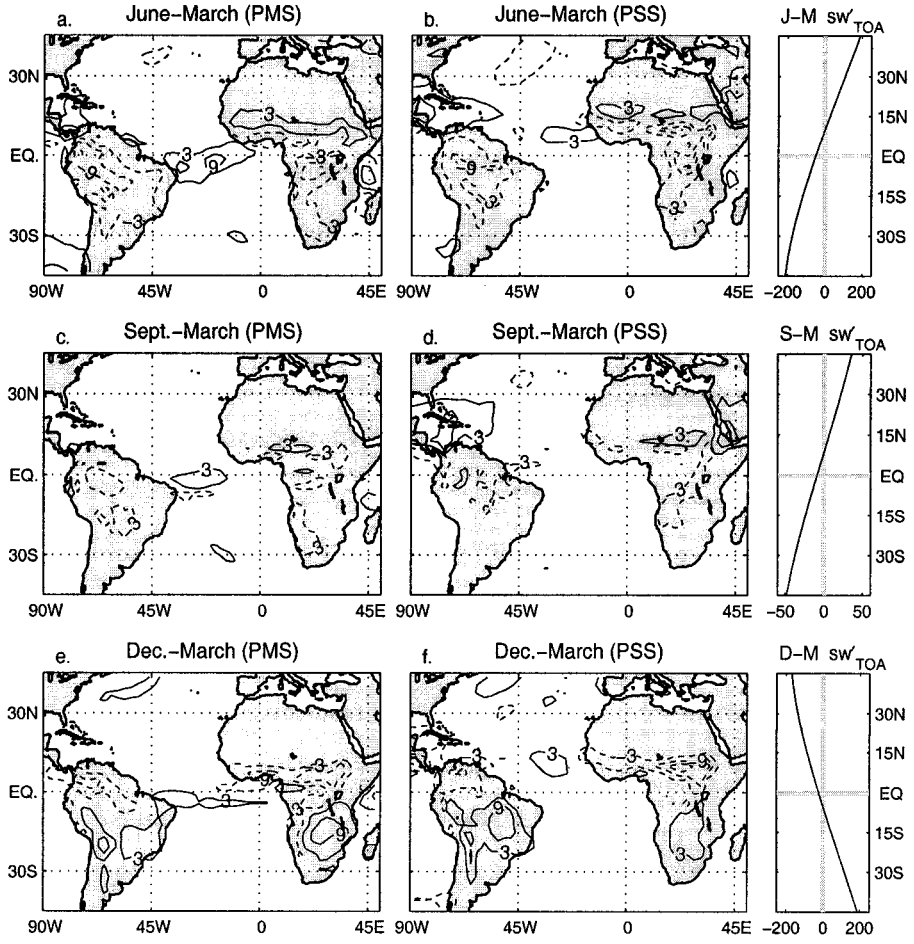

Figure 4.7: The portion of the annual cycle of precipitation (presented as anomalies from the month of March) that can be attributed to seasonal changes in insolation. Left column: estimate obtained from PMS (March SST boundary conditions). Center column: estimate obtained from PSS (September SST boundary conditions). Right column: zonally averaged insolation at the top of the atmosphere (Wm^{-2}). The contour interval is 6mm/day in all maps, starting at $\pm$3mm/day. Insolation controls the position of continental convection in June and December, and modulates the intensity of oceanic convection during all months.

atmosphere ocean interactions (ultimately also paced by insolation), the circulation induced over the continental land masses by changing insolation extends over the oceanic regions and greatly affects the intensity of oceanic convection.

4.5 Statistical Significance and Non-Additive Effects

The results presented in the previous two sections showed the SAT and precipitation responses to seasonal variation in SST and solar forcing. The responses were inferred by looking at the annual variations in experiments where the annual cycle of one of the two forcings had been suppressed. This method has the advantage of presenting the actual pattern of the response: for example, it indicates that the SST-induced northward shift of the ITCZ between March and September is associated with a 4°C warming of the northeast Brazil and a 2°C cooling in the Guiana Highlands. The disadvantage of the method is that it does not gauge the statistical significance of the response, and can only provide a qualitative indication of non-linear interactions existing between insolation and SST when they act together in generating the control annual cycle. The analysis of variance (ANOVA, Storch and Zwiers, 1999) is the appropriate statistical tool to investigate questions of significance and non-additivity of the responses.

The CTL, PMS, PVE, and PM runs form a complete set of experiments in which the two factors whose effect we are set out to prove—that is, the presence or absence of an annual cycle of insolation and the presence or absence of an annual cycle of SST—are combined in all possible ways (or "treatments"). In CTL, SST and insolation are annually varying; in PMS, SST is constant at the March value and insolation is annually varying; in PVE, SST is annually varying and insolation is constant at the March value; in PM, both SST and insolation are constant at the March value. Every year of a model integration can be considered as a member of an ensemble of experiments subject to the same treatment. Thus we have four eight-member ensembles.

Let's assume, for example, that we want to measure the effects of the SST treatment and insolation treatment on the June precipitation. For every June of any of the four

experiments, we can write:

$$P = \bar{P} + P_I + P_S + P_{IS} + \varepsilon$$

where $\bar{P}$ is the baseline, i.e. the grand mean of all June months in the four experiments; P_I represents the departure from the baseline due to the effect of insolation; P_S represents the departure due to the effect of SST; P_{IS} represents the departure due to the effect of interactions between insolation and SST treatments; and, finally, ε represents random interannual variability.

If annual variations of neither SST nor insolation had any effect, June would look the same, aside from random variability, in all experiments (it would look a lot like March, in our set-up), and P_I, P_S, and P_{IS} would all be statistically indistinguishable from zero. This is the null hypothesis that can be tested with the ANOVA technique.

Figures 4.8 and 4.9 show where the effects of SST, of insolation, and of their non-additive interaction are significant at the 95% level in producing the annual cycle of SAT and precipitation. In this set-up, "producing the annual cycle" is tantamount to say "making June, September, and December different from March". Therefore Figs. 4.8 and 4.9 indicate that the anomalies discussed in sections 4.3 and 4.4 are significant. Moreover, they confirm what was inferred by comparing PMS to PSS and PVE to PWSol, i.e. the existence of interactions between SST and insolation treatments in the ITCZ region, the Sahel, and northern South America.

4.6 Summary

In this chapter, we have described a set of GCM experiments performed with an uncoupled AGCM and intended to elucidate the relative role of changes in SST and insolation over land in producing the annual cycle of surface air temperature and precipitation over the tropical Atlantic, Africa, and South America. The simulated annual cycle replicates the general characteristics of the observed annual cycle, but there are substantial biases; in particular, the amount of continental precipitation is grossly overestimated by CCM3.

We have presented results from four modeling studies (PVE, PWSol, PMS, and PSS; see Table 3.1) designed to distinguish what portion of the annual cycle of temperature and

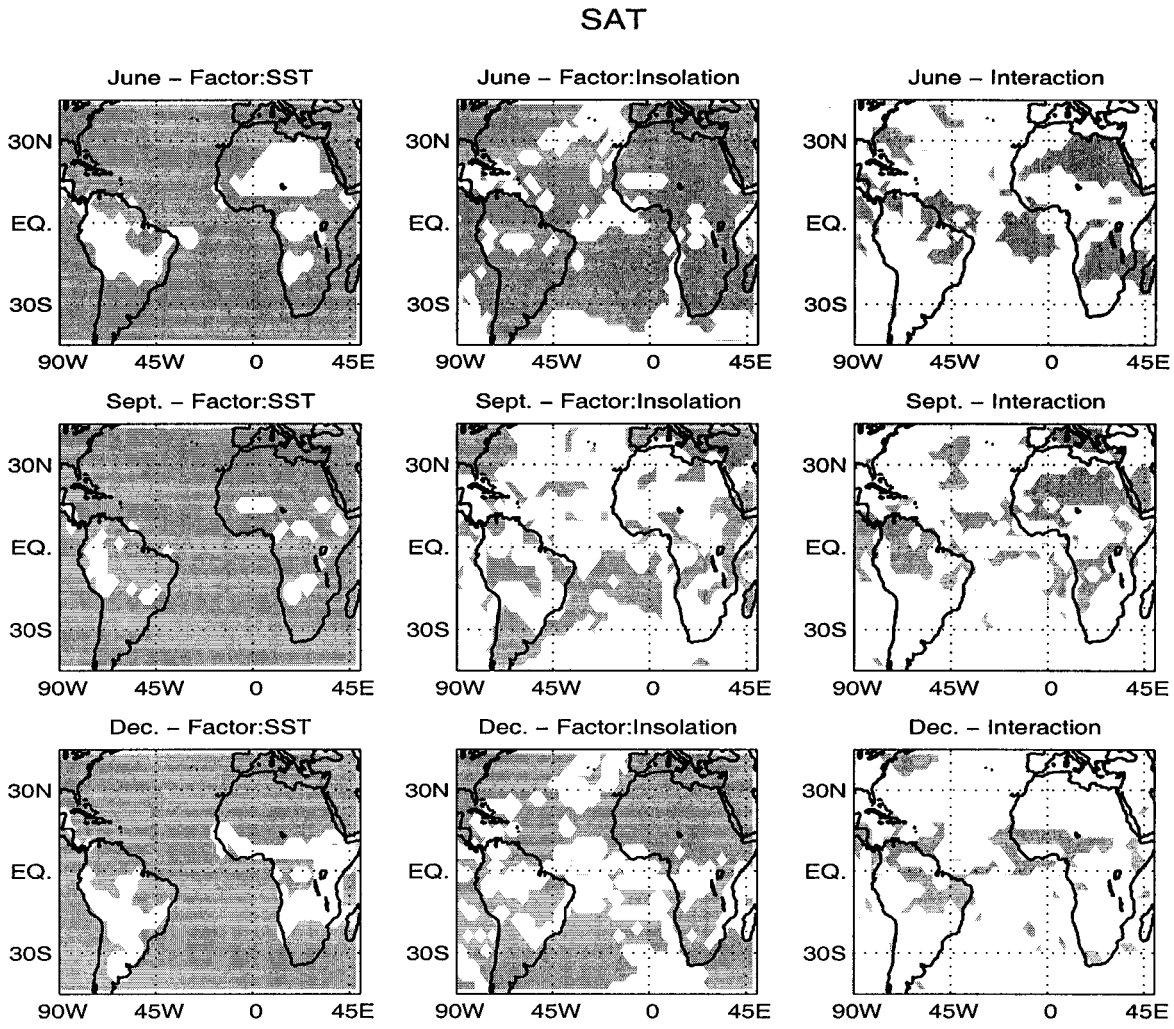

Figure 4.8: Regions where SST (left column), insolation (center column), and their interaction (left column) contribute significantly (at the 95% level) in making SAT values during June, September, and December different from SAT values in perpetual March conditions. The method used to establish significance is introduced in the text.

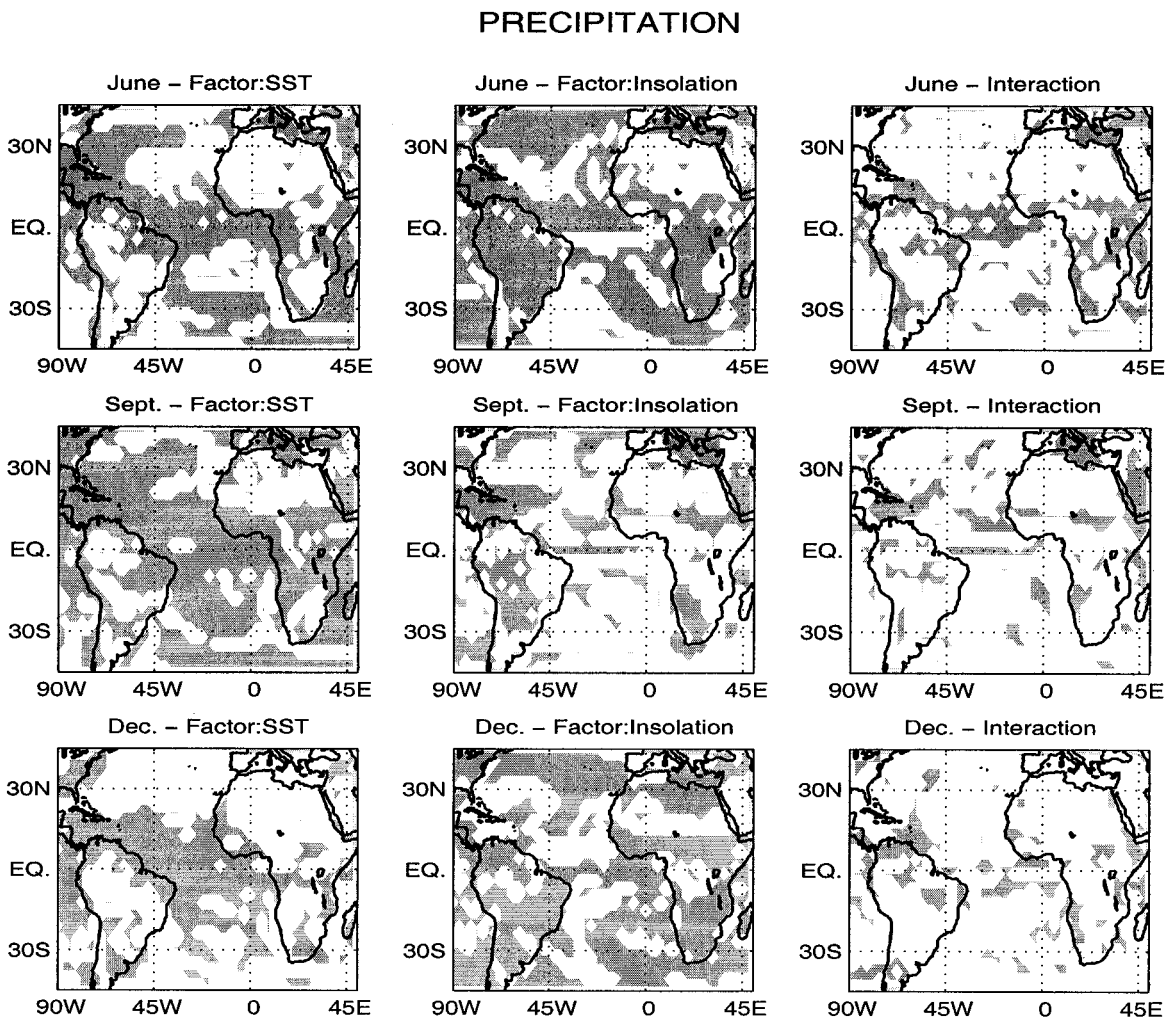

Figure 4.9: Regions where SST (left column), insolation (center column), and their interaction (left column) contribute significantly (at the 95% level) in making precipitation values during June, September, and December different from precipitation values in perpetual March conditions. The method used to establish significance is introduced in the text.

precipitation is due to a direct response of the land-atmosphere system to seasonal changes in insolation, and what portion is a response to changes in SST. In the PVE and PWSol runs the insolation at the top of the atmosphere is held fixed at the boreal vernal equinox and winter solstice values, respectively, while the SST is allowed to vary according to the observed climatology. Therefore comparison of two months extracted from the climatology of either the PVE or the PWSol run provides an estimate of the effect of SST changes. In the PMS and PSS runs the SST boundary conditions are held fixed at March and September values, respectively, while insolation changes. Therefore, the climatologies of the PMS and PSS runs reveal the direct response of the land-atmosphere system to insolation. The degree to which estimates obtained by the PVE and PWSol (PMS and PSS) runs differ gives a qualitative measure of the linearity of the response to SST (insolation) changes.

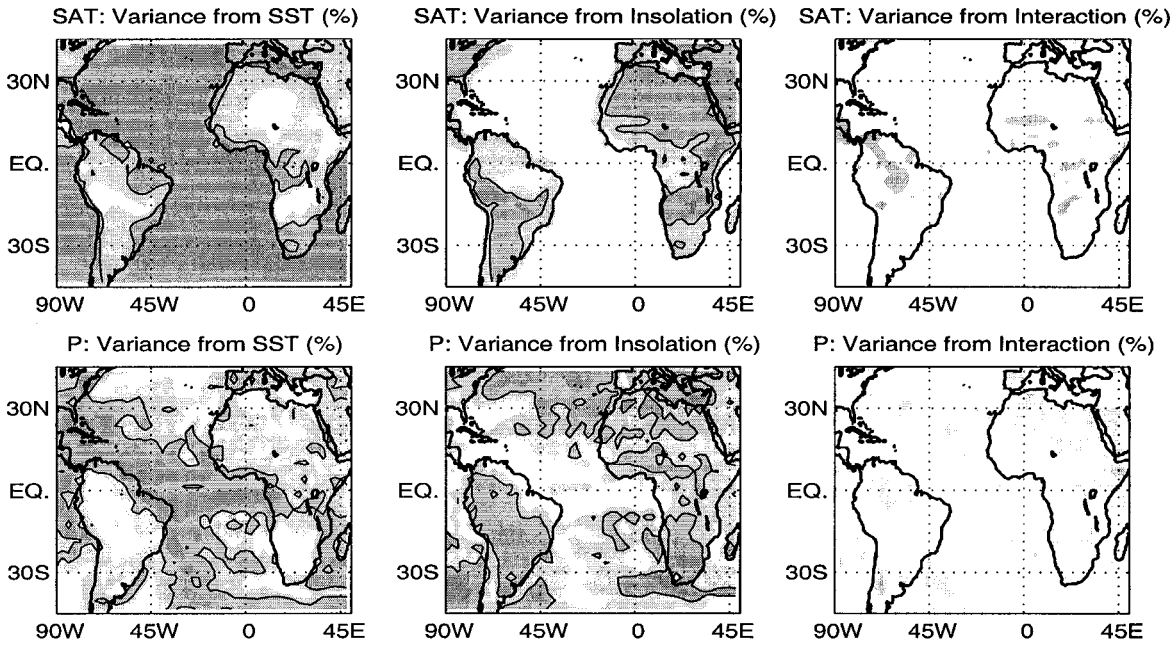

Figure 4.10: Percentage of the annual variations in SAT (top row) and precipitation (bottom row) that can be ascribed to SST (left column), insolation (center column), and their interaction (left column). Darker grey shading indicate a larger percentage of explained annual variations (the increment equals 25%); the solid line is the 50% contour. The method used to establish the relative importance of each factor is introduced in the text.

Figure 4.10 gives an estimate of the relative role of SST annual variations, insolation

annual variations, and their interactions. The annual signal of a variable (surface air temperature, SAT, or precipitation) is represented by its total variance minus the variance due to random fluctuation, and it can be expressed as the sum of the variance due to the SST treatments, the insolation treatments, and their interactions. The ratios of the factor- and interaction-induced variances to the annual signal are plotted in Fig. 4.10 by increments of 25% (the contour line indicates the 50% value). Although the significance of these ratios is not established, we find them to be a useful guidance in summarizing our results.

SST is the dominant forcing for the terrestrial SAT in northeast South America (the Guiana Highlands and northeast Brazil), the Gulf of Guinea, the Congo basin, and South Africa. The direct response to insolation anomalies explains the greatest part of the annual cycle of SAT over land outside the deep tropics (and except the southern tip of Africa).

Maritime precipitation in the tropics responds most strongly to SST changes (the location of the ITCZ shifts to follow closely the warmest waters). SST changes also account for the bulk of the annual cycle in precipitation over the Guiana Highlands, the northeast Brazil and the Gulf of Guinea region. The SST impact on precipitation over the Sahel is on average between 25 and 50%. The direct response of land to changes in insolation is responsible for the bulk of seasonal changes in precipitation over Africa and South America. The effect of insolation variations on the equatorial Atlantic precipitation is between 25% and 50%: the insolation-induced anomalies over land drive circulation anomalies that extend over the ocean and significantly affect the intensity, but not in the location, of maritime precipitation.

The interaction between SST and insolation, although significant in a larger portions of the domain, accounts for more than 25% of the total annual signal only in a small portion of the domain, which includes the Sahel.

Chapter 5

UNCOUPLED EXPERIMENTS: MECHANISMS OF LOCAL AND REMOTE RESPONSE TO SST AND INSOLATION

5.1 Outlook

In this chapter, we expand our analysis by focusing on the *mechanisms* that determine the annual cycle of precipitation in an atmospheric general circulation model (AGCM) with prescribed SST. In particular, our aim is to identify how changes in local insolation affect precipitation over the tropical continents, how changes in SST (which in our model experiments can be prescribed independently from insolation) affect precipitation in the ITCZ, and how temperature and rainfall over the ocean affect precipitation over the continents, and vice-versa.

The decomposition of the annual cycle of precipitation into locally and remotely forced components that was detailed in Chapter 4 is encapsulated in Figure 5.1. Shown is the first empirical orthogonal function (EOF) and first principal component (PC) of the annual cycle of precipitation in the tropical Atlantic sector in the CTL, the PMS, and the PVE simulations (see Table 3.2 for a complete list of the experiments presented in this chapter). The comparison of Figure 5.1c and Figure 5.1a indicates that the local insolation forces the bulk of the annual cycle of precipitation over the continents, with maximum precipitation occurring during the early summer months. Note that insolation causes African precipitation to reach the farthest north in June, and not in August as seen in observations and in the control experiment (this is apparent in the raw annual cycle as well, and is not an artifact of EOF analysis). Continental climate also influences the intensity of the maritime ITCZ rainfall, producing a stronger ITCZ when rainfall is weaker in South America and South Africa. Figure 5.1e shows that SST determines the position of the ITCZ: the ITCZ reaches its northernmost position in September and its southernmost position in March,

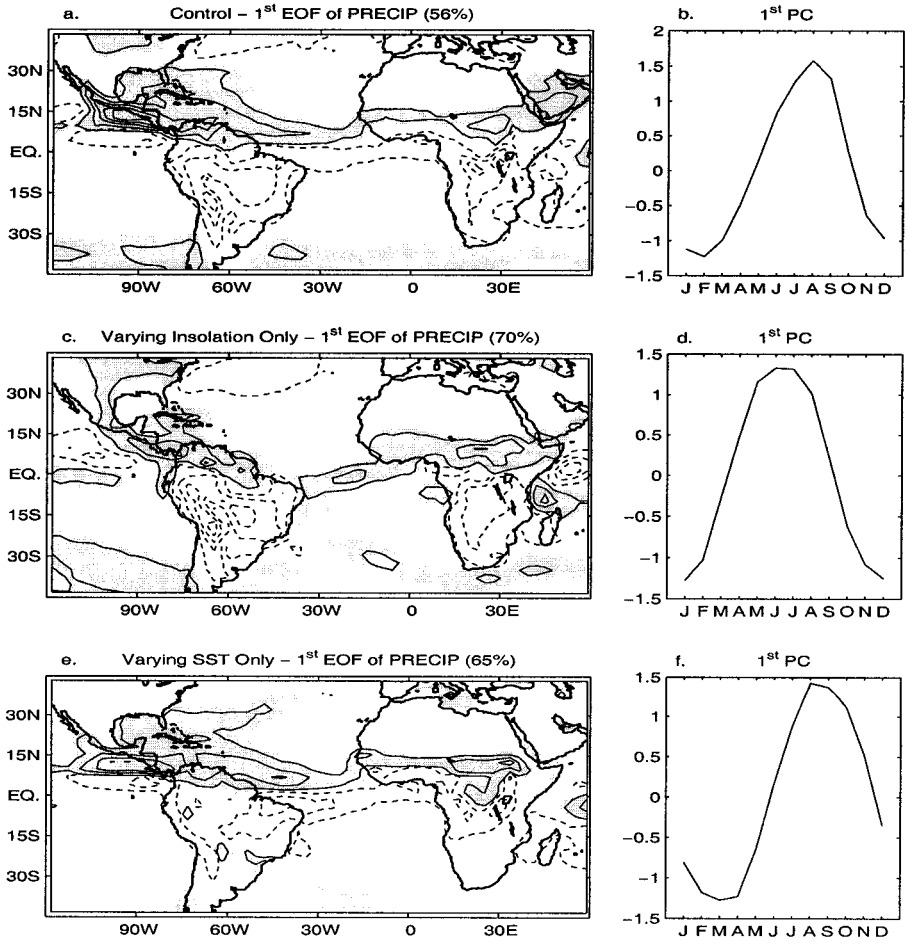

Figure 5.1: First EOF and PC of the annual cycle of precipitation in (a,b) the control run, (c,d) PMS, the experiment with varying insolation and SST fixed at March value, and (e,f) PVE, the experiment with varying SST and insolation fixed at March 21st value. The contour interval in a,c, and e is 2 mm day^{-1} per standard deviation, starting with ± 1. Dashed contours indicate negative values. The shading indicates positive values.

following the warmest SST. The same SST-induced north-south displacement is apparent in the precipitation field over the coastal regions in northeast South America and in central Africa, Sahel, and Sudan.

The rest of this chapter will detail the mechanisms by which changes in local insolation affect precipitation over the tropical continents (Section 5.2), changes in SST affect precipitation in the ITCZ (Section 5.3), and changes in temperature and rainfall over the ocean affect precipitation over the continents (Section 5.4), and vice-versa (Section 5.5).

5.2 Local control of continental precipitation

The theoretical work of Neelin and Held (1987) suggests that, in the Tropics, a net influx of energy in the atmospheric column (F_{net}, the downward radiative fluxes at the top of the column plus the upward radiative and turbulent fluxes at the surface) is balanced by rising motion and divergent circulation. Neelin and Held derive this conclusion from an analysis of the dominant balance in the equations of energy and moisture in the precipitating regions of the Tropics. They develop their argument in terms of the moist static energy; for consistency with the rest of the chapter, we will recast it in terms of equivalent potential temperature.

We describe the energy of a moist air parcel as $c_p\theta_e$, where c_p is the atmospheric heat capacity at constant pressure and θ_e is the equivalent potential temperature. The total rate of change in $c_p\theta_e$ equals the total energy input,

$$D_t c_p\theta_e = \partial_t c_p\theta_e + \nabla \cdot c_p\theta_e\mathbf{V} + \partial_p c_p\theta_e\omega = g\partial_p F,$$

where F is the total vertical energy flux, i.e. the sum of the radiative, sensible, and latent vertical heat fluxes. If we take the vertical integral over the atmospheric column (indicated with $\langle\cdot\rangle$), and the time mean, the first and third term in the l.h.s. vanish and we obtain: $\langle\nabla \cdot c_p\theta_e\mathbf{V}\rangle = F_{bottom} - F_{top}$.

Neelin and Held now make two major assumptions: the first is that the vertical structure in convective regions can be described by the first baroclinic mode (and thus the lower level convergence is equal and opposite to the upper level convergence), the second is that horizontal gradients of both temperature and moisture are negligible in the Tropics and so

is the transport by transients. Under these approximation, the equation for the vertically integrated mean equivalent potential temperature simplifies to:

$$(\theta_e^{lowerlevel} - \theta_e^{upperlevel})\nabla \cdot \mathbf{V}^{lowerlevel} \propto F^{bottom} - F^{top}.$$

In regions of deep convection, the adiabatic cooling and the diabatic heating nearly balance, so $\Delta\theta_e = \theta_e^{upper} - \theta_e^{lower} \approx 0$. Yet, Neelin and Held hold that requiring that the time-mean circulation be thermally direct is tantamount to require that $\Delta\theta_e$ be positive. Under this assumption, low level convergence and precipitation can only be possible when $F_{net} = F_{bottom} - F_{top}$ is positive. The intuitive interpretation is that a positive influx of energy is balanced by rising motion and a divergent circulation. $\Delta\theta_e$ behaves as a gross moist stability and determines the efficiency with which the incoming energy is converted into convective motion. Neelin and Held (1987) show that, over the ocean, $\Delta\theta_e$ is linked to SST via the proportionality of boundary layer moisture to temperature and it is the dominant factor in determining the spatial structure of oceanic precipitation.

Note that the model constructed by Neelin and Held (1987) assumes that the atmospheric column can be described by the first baroclinic mode, and thus should only be applied to describe an atmospheric column that is convecting. Nevertheless, recent studies indicate that it is warranted to use F_{net} as a zeroth order indication of where convection is possible. Sobel and Bretherton (2000) show that a model based on the balance of F_{net} and the divergent circulation captures the distribution of convective regions in the Tropics equatorward of 15°, although they also show that the addition of moisture advection improves the simulation. Chou and Neelin (2003) show an overall good correspondence between regions of positive F_{net} and precipitation during July both in observations and in an intermediate complexity model, but such correspondence breaks down in the observed Atlantic ITCZ. Our GCM simulations also reproduce the expected coincidence of positive rainfall and F_{net} over most of the tropical land, but not in the Atlantic ITCZ or in regions affected by the ITCZ (e.g. the Guinea coast). Because in these regions moisture gradients and the transport by the transients are not negligible, deviations from the simple theory outlined above is to be expected.

Over land, where the negligible heat capacity of the soil makes the energy flux into the surface vanish on timescales longer than a day, the requirement of a positive F_{net} for the development of convection translates into the requirement of a positive energy flux at the top of the atmosphere. Therefore, it is very tempting to explain the influence of insolation on the annual cycle of precipitation in the tropical continents in terms of F_{net}. Figure 5.2 shows the seasonal change in precipitation brought about by insolation only

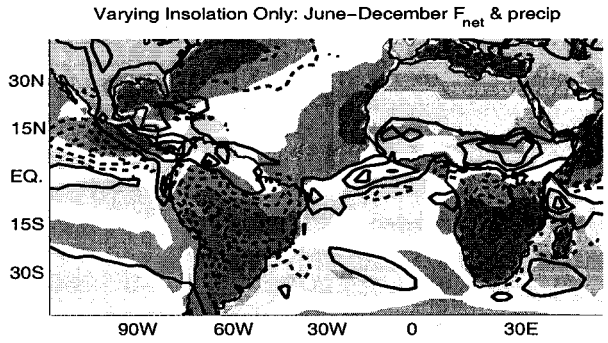

Figure 5.2: Varying Insolation Only run. June-December precipitation (contoured, c.i.=4mm/day, starting with ±2, negative values dashed) and total energy flux into the atmosphere F_{net} (shaded, interval of 50Wm^{-2} starting at $\pm 25 Wm^{-2}$, dark grey shading indicates negative values less then $-25 Wm^{-2}$, white indicates value between $\pm 25 Wm^{-2}$, light grey shading indicates positive values larger that $25 Wm^{-2}$).

(June-December in the PMS simulation), superimposed on the changes in total column energy flux (F_{net}). It is apparent that changes in F_{net} are responsible for the changes in precipitation *over land*: where the June-December F_{net} is negative, so is the precipitation change, and vice-versa, with the noticeable exception of the Sahara, where dryness and high albedo make F_{net} negative all year around in our simulations (not shown) as well as—to a lesser extent—in observations (Chou and Neelin, 2003).

Nevertheless, it is clear from Figure 5.2 that the spatial *details* of the seasonal changes in rainfall over Africa and South America cannot be explained by the changes in F_{net}. First, orography plays an obvious role in shaping the precipitation field in South America. Second, advection terms become more important the further we move from the equator, and the simple tropical model of correspondence between F_{net} and precipitation cannot be applied

into the subtropics. Third, the moist stability field determines the efficiency with which an F_{net} change is translated into a precipitation change: for example, if $\Delta\theta_e$ is negative, a positive F_{net} does not imply convection.

We conclude this section showing how the vertical structure of the atmosphere is influenced by insolation over two convective regions in Africa. Figure 5.3 shows the vertical

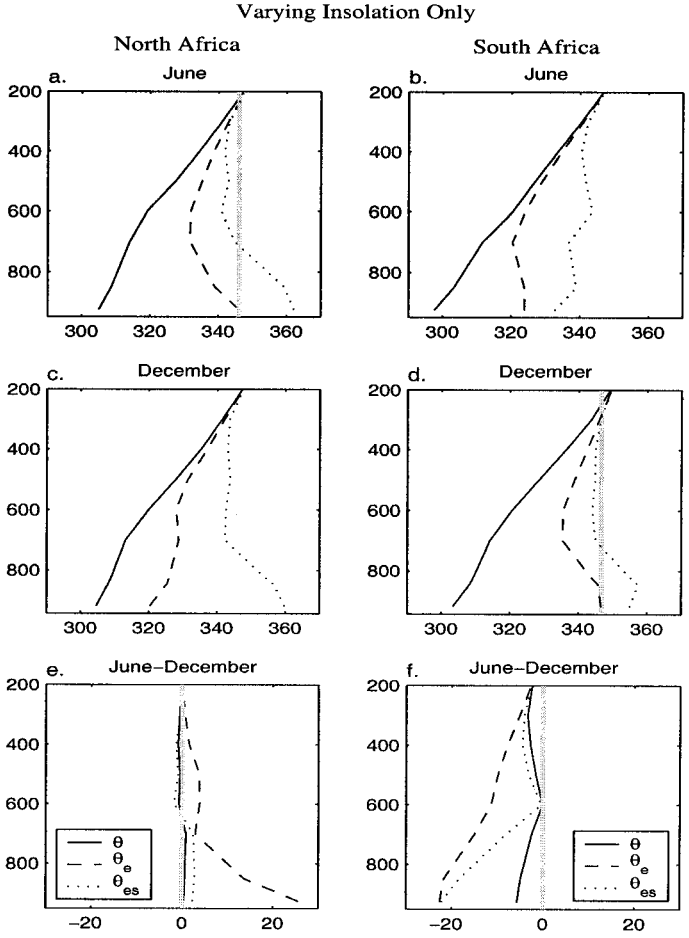

Figure 5.3: Vertical profiles of potential temperature (θ, solid), equivalent potential temperature (θ_e, dashed), and saturated equivalent potential temperature (θ_{es}, dotted) over northern Africa (6°N - 12°N, left column) and southern Africa (5°S - 20°S, right column) during (upper panels) June and (middle panels) December, and (lower panels) the June-December difference.

profiles of potential temperature (θ), equivalent potential temperature (θ_e), and saturated

equivalent potential temperature (θ_{es}) in northern Africa (20°E-40°E, 6°N-12°N) and southern Africa (15°E-35°E, 5°S-20°S). It is apparent that insolation influences the stability of different land regions in different ways. In South Africa, insolation induces a substantial change in the stability of the atmosphere. The low-level summer warming is responsible for the erosion of the wintertime inversion at 700mb. This change in stability is responsible, together with the increase in low level humidity, for making the December "sounding" conditionally unstable (the interception between the θ_{es} line and the gray line indicating the surface value of θ_e indicates that the level of free convection for surface plumes is at about 750mb) and therefore for making December precipitation increase in southern Africa.

Conversely, the "sounding" in northern Africa indicates that the surface temperature and atmospheric stability barely change between December and June. What makes the North Africa sounding conditionally unstable is the increased low level moisture (see θ_e in Figure 5.3c). Obviously, the additional low-level convergence of moisture is due to the monsoon flow. The role of large scale circulation is paramount for northern sub-Saharan Africa, while it is somewhat secondary in the Congo Basin, in southern Africa. As an aside, we note that, although the raison d'être for the monsoon is the warm continent / cold ocean summer contrast, the monsoon rain falls on land that is no warmer during the summer than it is in winter. It is a truism, but worth repeating: insolation drives the African monsoon by warming up the Sahara, not the regions where rainfall ends up falling. We will return to the role of the Sahara in the dynamics of monsoon circulation in section 5.4.

5.3 Local control of oceanic precipitation

Figure 5.4a shows the difference between September and March precipitation in the PVE simulation (in which only the SST boundary condition has an annual cycle, and insolation is fixed) and elucidates the response of precipitation to September-March changes in SST. In this section, we will focus on the oceanic portion of the response. SST determines the position of the ITCZ: when the highest SST migrates to the north, so does the ITCZ. This result is not at all surprising, and the mechanisms for the SST-ITCZ coupling are well understood. Lindzen and Nigam (1987) first suggested that departures from the zonal mean

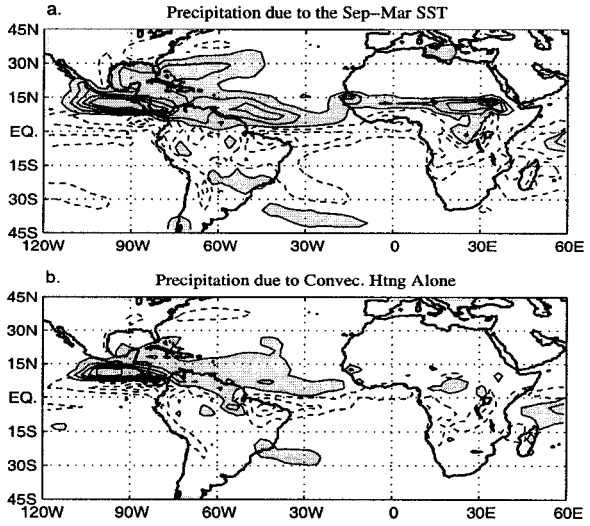

Figure 5.4: Top panel: September-March precipitation in the Varying SST Only run. Bottom panel: precipitation anomalies due to September-March elevated latent heating anomalies in the oceanic ITCZ (Perpetual March with September ITCZ Heating - Perpetual March) The contour interval is 4mm/day, starting with ± 2, negative values are dashed, positive values larger than 2mm/day are shaded.

in tropical convection can be explained through boundary layer dynamics. A positive surface temperature perturbation is communicated by turbulent mixing throughout the boundary layer, creating a negative low-level pressure anomaly which influences the boundary layer convergence that sustains convection. Hastenrath and Greischar (1993) have used the same argument to explain the coherent decadal variability in SST and rainfall in the tropical Atlantic. This interpretation also agrees with Neelin and Held's (1987) recognition that the spatial distribution of rainfall over the tropical oceans is determined by SST, via its influence on moisture convergence and thus gross moist stability.

While it is true that boundary layer processes drive the seasonal shift of the ITCZ, convective heating in the ITCZ has itself the potential to thermally drive changes in surface pressure and thus surface wind and low-level convergence. This suggests the possibility of a feedback in which SST anomalies drive anomalous low-level convergence and thus anomalous precipitation, which in turns drives more convergence. The role of elevated condensational heating in driving surface wind in the tropical Atlantic was quantified by Chiang et al.

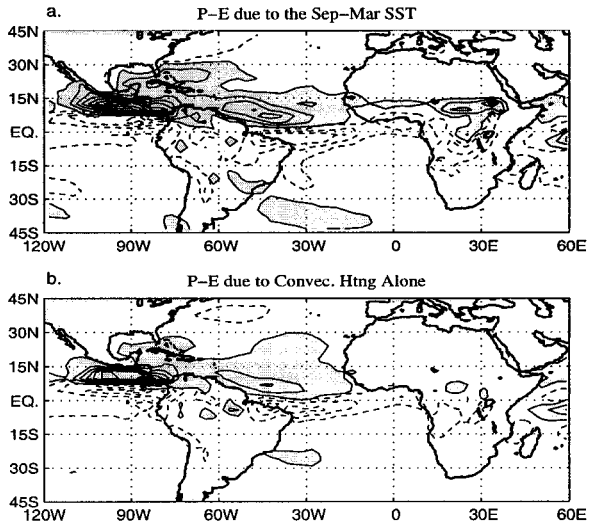

Figure 5.5: Top panel: September-March column-integrated moisture convergence in the Varying SST Only run, calculated as precipitation minus evaporation (P-E). Bottom panel: column-integrated moisture convergence (P-E) anomalies due to September-March elevated latent heating anomalies in the oceanic ITCZ (Perpetual March with September TCZ Heating - Perpetual March) The contour interval is 4 mm day^{-1}, starting with ± 2, negative values are dashed, positive values larger than 2mm day^{-1} are shaded.

(2001).

To identify the role of latent heating in amplifying the rainfall anomalies directly forced by SST, we performed a perpetual-March experiment in which we discarded the simulated latent heating due to convection in the maritime ITCZs and replaced it with a prescribed value, namely that associated with the September ITCZ (taken from the PVE experiment). Over land and outside the band between 20°S and 30°N the model remains free to determine the latent heating released in convection. The transition between the regions forced by prescribed and calculated latent heating is smoothed over two grid points in every direction. Note that the model is free to calculate its own precipitation everywhere, so the simulated precipitation and the imposed latent heating are not necessarily consistent in this experiment. We will refer to this run as the Perpetual March with September ITCZ Heating experiment (PMw/SIQ, see Table 3.2).

Figure 5.5b shows the difference in the column-integrated moisture convergence between this experiment and a control Perpetual March (PM) experiment, calculated as precipitation minus evaporation (P-E). Figure 5.5a shows the September-March difference in the same quantity in the PVE simulation. Because the anomalies in Figure 5.5b develop in the absence of SST forcing, comparing Figure 5.5a and Figure 5.5b gives a rough estimate of the importance of feedbacks triggered by the elevated condensational heating on convergence. In regions where Figure 5.5a and 5.5b are substantially different, boundary layer forcing primarily determines the low-level convergence and precipitation, and elevated heating (i.e., precipitation) can be thought of as a passive response. In regions where Figure 5.5a and 5.5b are similar, the circulation forced by the elevated condensational heating contributes substantially to the maintenance of the low-level convergence initiated by SST. The comparison of Figure 5.5a and 5.5b suggests that the elevated heating plays a substantial role, especially south of the equator.

We conclude noting that the precipitation and surface convergence response calculated by the model in response to the September-March difference in elevated heating in the tropical Atlantic (Figure 5.4b and 5.5b) are quite weaker than the anomalies generated by the SST (Figure 5.4a and 5.5a). This result can be easily explained in terms of the effect of an imposed heating on the stability of the atmospheric column and reminds us of the

caution one needs to use in treating convective heating as an external forcing. The imposed heating peaks at 600mb and drops off faster in the lower troposphere than in the upper troposphere; thus the upper troposphere becomes relatively warmer, and the stability of the column increases or, equivalently, the convective available potential energy decreases (not shown). In the region of imposed heating, deep convection is less efficient than in the original simulation (the simulation from which the heating field itself was taken) and precipitation is weaker.

5.4 Oceanic Control of Continental Precipitation

Figure 5.1e shows that SST influences the annual cycle of continental precipitation in those coastal regions of South America and Africa that border the ITCZ, and in a zonal band that spans the whole of Africa, at the latitude of the Sahel. Figure 5.1f shows that the SST seasonal cycle is responsible for the fact that the African monsoon reaches its northernmost position in late summer.

There are two possible ways for SST to influence continental climate: by directly changing the boundary layer wind and moisture that is advected onshore, or by causing anomalies in oceanic precipitation which, in turn, drive far-reaching circulation anomalies.

To sort out the relative importance of the boundary layer forcing and of the elevated convective heating forcing in inducing precipitation changes over land, we refer again to the Perpetual March with September ITCZ Heating (PMw/SIQ) experiment introduced in the previous section and presented in Figure 5.4b and 5.5b. We recall that, in this experiment, the heating field in the ITCZ is taken from the PVE experiment and corresponds to September SST conditions, making the precipitation difference between this run and a control Perpetual March run (Figure 5.4b) directly comparable to the September-March precipitation difference in the PVE simulation (Figure 5.4a). In the Guiana Highlands and Northeast Brazil, the response forced by the ITCZ heating 5.4b and that forced by SST Figure 5.4a are very similar, indicating that the influence of the ocean in these region can be explained in terms of the circulation changes that accompany the movement of the ITCZ,

in particular the changes in low-level convergence. [1]

Conversely, over Africa the precipitation response to SST is not reproduced by the PMw/SIQ simulation. The ITCZ heating forces anomalies of the right sign in equatorial central Africa, but their magnitude is too weak. More importantly, the ITCZ heating does not force any coherent anomaly over the Sahel. We conclude that SST has a direct influence on Sahel rainfall, by which we mean an influence not mediated through the circulation forced by changes in the ITCZ. The oceanic influence over the Sahel is exerted through the advection of SST anomalies over Northern Africa, which causes the development of anomalies in sea level pressure (SLP) and in surface wind convergence.

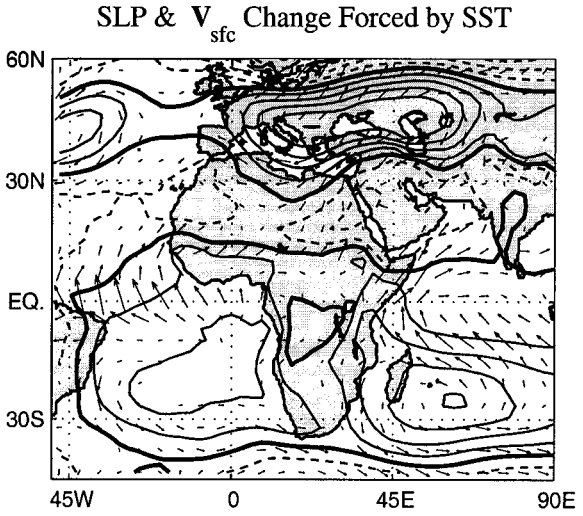

Figure 5.6: September-March sea level pressure and surface wind anomalies in the PVE simulation (s.l.p. c.i.=2mb, negative values are dashed, the zero line is thick; only wind anomalies greater than 1m/s are plotted).

Figure 5.6 shows the SLP and surface wind changes generated by the September-March SST. A cross-isobaric southerly wind converges in the Sahel region, where it generates the

[1]Note that the PMw/SIQ experiment underestimates the anomalies in Colombia and Venezuela, but we attribute this to the fact that the forcing in the eastern Pacific and the Gulf of Mexico is not applied at full strength, because in those regions the forcing is a linear interpolation between the full forcing (over the open ocean) and zero forcing (over the Central American continent and the Caribbean Islands).

observed enhancement in precipitation. the similarity between the changes in SLP and the corresponding changes in surface air temperature (SAT) in north Africa (cf. Figure 5.6 and Figure 5.7c) supports the interpretation that the SLP changes in response to warmer anomalies in boundary layer air temperature.

How is the seasonal change of SST communicated inland, across the entire African continent? The differences in the temperature advection and subsidence between March and September in the PVE run (not shown) indicate that the anomalies are maintained in equilibrium by horizontal advection [2], but do not tell us much about how those anomalies are established.

To understand how the temperature gradient across the Sahel is established we need to turn to a thought experiment. Let's imagine an experiment in which the September-March SST differences are imposed as an instantaneous forcing upon the atmosphere. Immediately after the forcing is switched on, the situation is that depicted in Figure 5.7a. In response to the SST forcing, the ITCZ shifts to the north. The precipitation shift induces a a remote response over land: changes in subsidence induce precipitation and temperature anomalies over Africa, the Arabian peninsula and the Indian region. The shift of the ITCZ also generates anomalous surface wind in the western Sahara, which carry inland the warm temperature anomalies imposed in the Mediterranean. At the same time, the mean westerly winds north of 30°N (Figure 5.7b) advect the SST anomalies into Mediterranean Africa and the Near East, thus intensifying the warm anomalies there (Figure 5.7c). The mean northeasterly trade winds (Figure 5.7b) and the anomalous wind in northeast Africa (Figure 5.7a) combine to advect those temperature anomalies into the central Sahara (Figure 5.7c).

At this point the anomalous North-South gradients in SAT and SLP are established across the Sahel; the resulting monsoon-like circulation (Figure 5.7c) brings in moisture from the ocean and the equatorial rain forest generating a band of enhanced precipitation at about 15°N. Finally, the precipitation anomalies over land change the soil moisture and soil evaporation, producing drier and warmer surface conditions in southern central Africa

---

[2]the advection of mean temperature by the anomalous wind, the advection of anomalous temperature by the mean wind, and the advection of anomalous temperature by the anomalous wind all play a comparable role

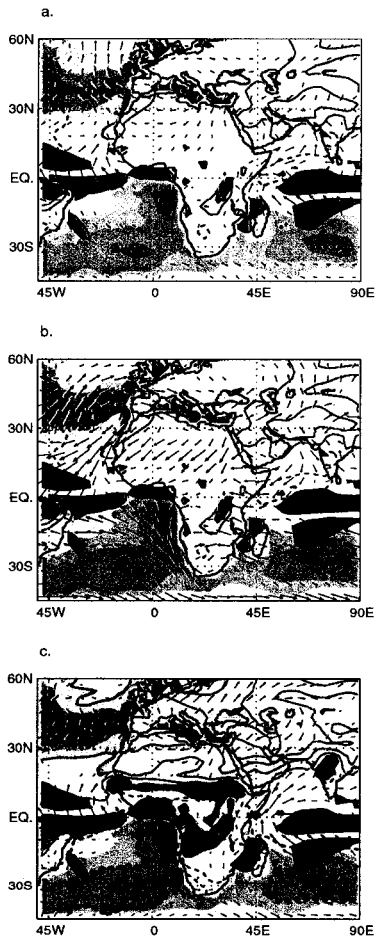

Figure 5.7: The development of SAT, wind, and precipitation anomalies over Africa in response to the September-March SST change. The (a) circulation forced by the displacement of oceanic precipitation and (b) the advection of SST anomalies by the mean wind cause (c) warm anomalies in the Sahara, and a monsoon-like circulation converging into the Sahel, where they induce precipitation and surface cooling by evaporation. (a.): September-March SST difference (red-blue shading, c.i.=2°C) and oceanic precipitation difference (positive anomalies larger than 4mm/day are shaded in green, negative anomalies less than -4mm/day are shaded in brown) from the Varying SST Only run. Surface air temperature difference (red and blue contours, c.i.=2°C), surface wind difference (only wind differences greater than 1m/s are plotted), and land precipitation difference (positive anomalies larger than 4mm/day are shaded in green, negative anomalies less than -4mm/day are shaded in brown) between the Perpetual March with September Heating run and the Perpetual March run. (b.): As in (a.), but the wind vectors represent the March mean surface wind in the Varying SST Only run (only wind vectors greater than 1m/s are plotted). (c.): September-March SST difference, precipitation difference, surface air temperature difference, and surface wind difference from the Varying SST Only run. Plotting conventions are as in (a.).

and wetter and colder surface conditions in the Sahel (Figure 5.7c).

The insight gained from this thought experiment leads us to infer that as the SST smoothly changes from its March value to its September value, the same advective processes outlined above smoothly produce the September-March anomalies in SAT over the Sahara, and the precipitation anomalies across the Sahel.

In the above discussion we have argued that anomalies in SLP are responsible for the anomalous southwesterly wind converging into the Sahel. Yet, SLP is not the best predictor for the location of precipitation: the maximum precipitation is not collocated with the minimum in SLP. A better predictor is the mean boundary layer equivalent potential temperature (θ_e). This makes intuitive sense, because $\theta_e$contains information about both temperature and humidity of the surface atmosphere. This correspondence can also be expected in light of the study by Emanuel et al. (1994), who showed that when atmospheric moist convection is in statistical equilibrium, the thickness of the convective layer is in one-to-one correspondence with the boundary layer θ_e.

Figure 5.8 portrays the effect of SST changes on African climate in terms of its effect on boundary layer θ_e, SLP, and precipitation. The solid (dashed) lines in Figure 5.8a,b portray θ_e (SLP), averaged over 15°W-15°E (Figure 5.8a, West Africa and Eastern Atlantic), and 15°E-45°E (Figure 5.8b, Central Africa), as a function of latitude, for September and March SST conditions (in the PVE run). The hatched vertical bands indicate regions of precipitation greater than 5mm/day. The correspondence between the precipitation and θ_e maxima is apparent.

During September SST conditions, the maxima of both θ_e and precipitation are shifted to the north, in both West and Central Africa. To the south of West Africa, the September-March difference in θ_e is a direct expression of the changes in SST; in the Sahara, the September increase in θ_e is due to changes of land surface temperature, and in the Sahel region it is due to changes in humidity. Similarly, θ_e anomalies in Central Africa are due to temperature outside the Sahel and to humidity in the Sahel region. The profiles of θ_e show the important role of changes *in the Sahara* in shifting the maximum θ_e and precipitation, in both western and central Africa.

We conclude this section with a comment on the differences between the structure of

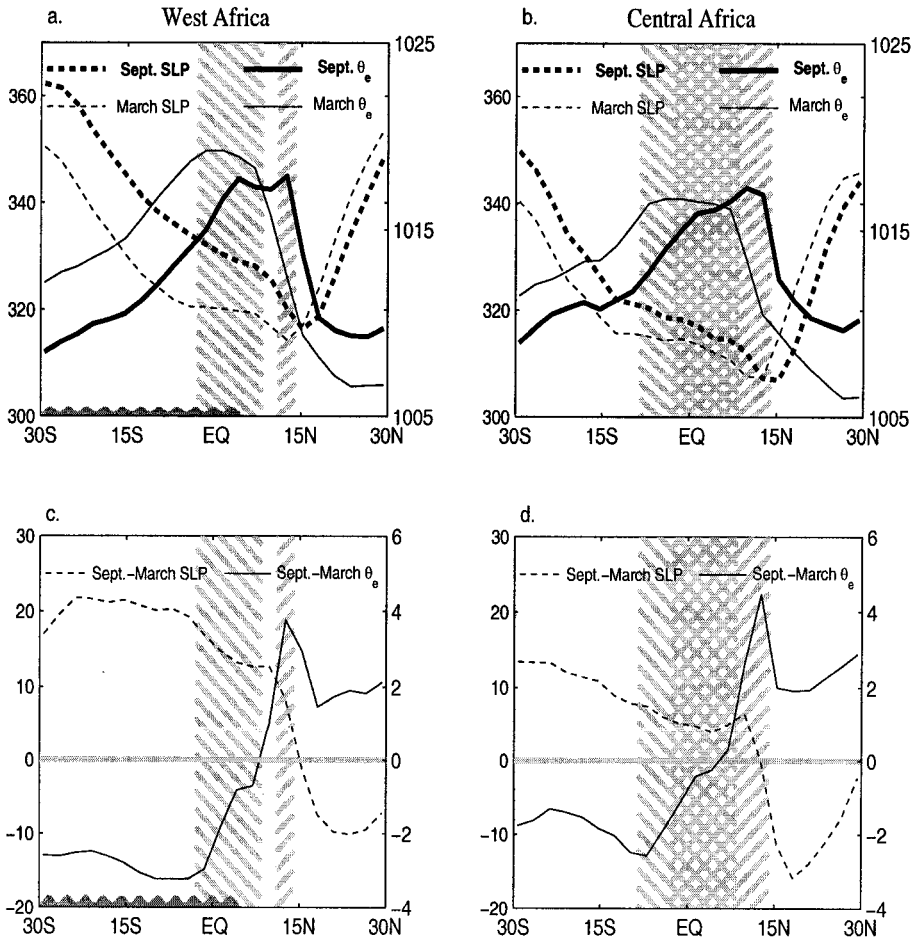

Figure 5.8: September (thick lines, a. and b.), March (thin lines, a. and b.), and September minus March (c. and d.) latitudinal profiles of boundary layer equivalent potential temperature (θ_e, solid) and sea level pressure (SLP, dashed) over West Africa (15°W - 15°E, a, c), and East Africa (15°E - 45°E, b, d) in the PVE simulation. The hatched gray vertical bands indicate latitudinal bands of precipitation larger than 5mm/day in September (positive slope) and in March (negative slope). The wavy line at the bottom of panels a. and c. indicates the extent of the oceanic region.

the precipitation field in western and central Africa. Over the Sahel, the pattern of the precipitation anomalies induced by the September-March SST changes (Figure 5.4a and Figure 5.7c) is remarkably uniform in the zonal direction. Yet, there are some interesting differences in how SST affects west and central Africa. In central Africa, the SST forcing leaves the latitudinal extent of the precipitation maximum unchanged and the area of maximum precipitation straddles the equator whether SST assumes March or September values (Figure 5.8b). The anomalous circulation is mostly limited to the latitude of the Sahel (Figure 5.7c). In western Africa, September SST conditions both shift the location of the precipitation maximum and reduce its extent to a narrow band at about 15°N (Figure 5.4a). In this region, the anomalous circulation is a cross-equatorial, monsoon-like circulation.

5.5 Continental Control of Oceanic Precipitation

Figure 5.9a shows the June minus March difference in the PMS simulation, i.e. the precipitation changes forced by the June-March changes in insolation over land. Recall that, in this experiment, SST conditions are fixed at March value and the position of the ITCZ is anchored by the SST gradient to be near the equator throughout the year. The remote effect of changes over land is to increase the precipitation intensity of about 6mm/day, with peak anomalies of 10mm/day. The location of the ITCZ—*when SSTs are prescribed*—is not affected by changes over land.

How is the variation of oceanic precipitation intensity achieved? There are two main possibilities. The first is that the insolation-induced changes in land surface temperature directly affect the sea level pressure field in such a way as to change the intensity of the low-level convergence into the ITCZ. The second possibility is that changes in land temperature force changes in land convection, which in turn induce anomalies in the stability in the atmosphere over the ocean.

The total remote effect of land on the vertical structure of the atmosphere in the ITCZ region is presented in Figure 5.10 (left column), which shows the vertical profiles of θ, θ_e, and θ_{es} averaged over the equatorial Atlantic for the month of June and March. Under June and March insolation conditions alike (Figure 5.10a and c), the atmosphere is conditionally

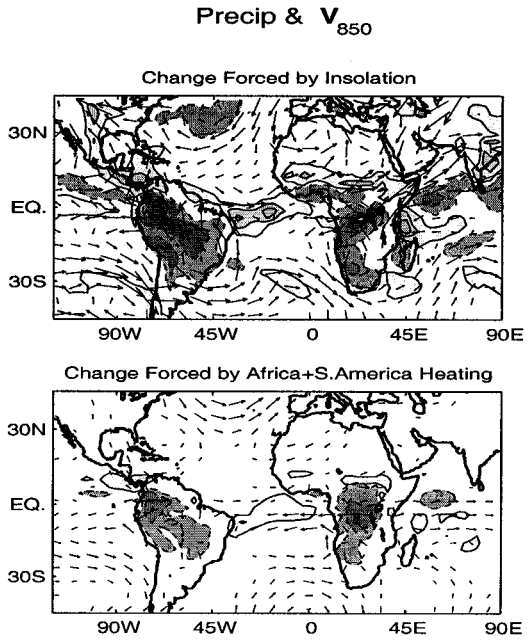

Figure 5.9: (a.): June-March precipitation and 850mb wind anomalies in the Varying Insolation Only run (precipitation c.i.=4mm/day, starting at ± 2 negative values are dashed and shaded in dark grey, positive values are solid and shaded in lighter grey; only wind anomalies greater than .75m/s are plotted). (b.): Precipitation and 850mb wind difference between the Perpetual March with June Africa and South America Heating run and the Perpetual March run (plotting convention as in a.)

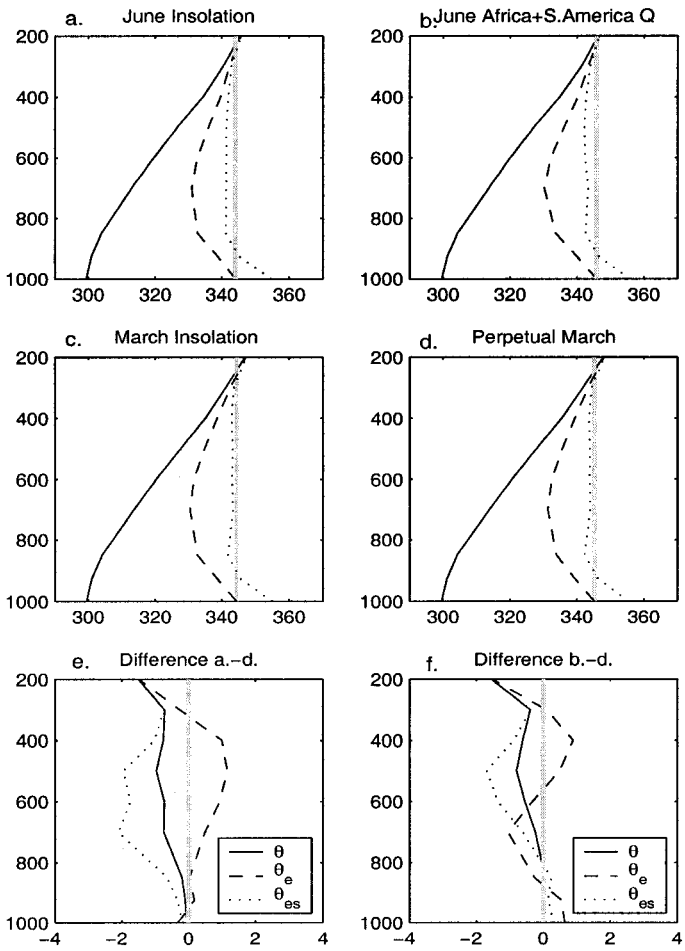

Figure 5.10: Vertical profiles of potential temperature (θ, solid), equivalent potential temperature (θ_e, dashed), and saturated equivalent potential temperature (θ_{es}, dotted) over the location of the March maritime ITCZ (40°W-5°W, 7°N - Equator) in the (left column) Varying Insolation Only run and (right column) the Perpetual March with June Africa and South America Heating run and the Perpetual March run.

unstable and the level of free convection (indicated in Figure 5.10 by the intersection of θ_{es} with the light gray line) is reached just below 900mb. Figure 5.10e suggests that the precipitation increase under June insolation condition over land follows a cooling of the upper troposphere over the Atlantic, which is, most likely, due to the reduced convection over the tropical continents. [3]

We hypothesize that June-March land surface temperature changes do not have a direct on oceanic precipitation, instead they cause a reduction in deep convection over Africa and South America, which cools the tropical free troposphere and makes the equatorial Atlantic more convective. To test this hypothesis, we have run some additional experiments (see Table3.2) with a Perpetual March configuration of insolation and SST, but imposed June elevated condensational heating (taken from the PMS simulation) over selected areas (Africa only, South America only, both Africa and South America, and the whole tropical belt *except* the Atlantic Ocean). Any change in the intensity of precipitation in the Atlantic ITCZ between one of these simulations and a control Perpetual March run should be interpreted as forced by June-March changes in convection in the selected area.

Figure 5.9b shows precipitation and 850-mb wind changes forced by the June-March elevated condensational heating difference in both South America and Africa (Perpetual March w/ June Africa and S. America Heating minus Perpetual March, PMw/JAf+SAQ - PM). We first note that, as was seen in section 5.3 in reference to the ITCZ, forcing the atmosphere with a given elevated heating does not induce a consistent precipitation intensity at the location of the forcing (cf. Figure 5.9a and b over South America and Africa). More importantly, we note that the elevated condensational heating in the African and South American convection centers does force more intense rainfall in the Atlantic ITCZ, but the response in the central and western Atlantic is only a third of that caused by the full continental forcing (cf. Figure 5.9a and b over the Atlantic). The experiments

[3]Note that Figure 5.10e does not indicate an increase in low-level moisture, but that would not necessarily be expected: because the basic state is convective to begin with, any increase in moisture through low-level convergence would likely show up in stronger updrafts and precipitation, and a moistening of the free troposphere, rather than a moister surface. Surface convergence is indeed larger when precipitation is more intense (not shown), but this correspondence shows only consistency, not causality.

in which the elevated condensational heating is imposed over Africa only and over South America only indicate that the two continental convection centers play comparable roles in producing the rainfall anomalies in the ITCZ (not shown). The experiment in which the elevated condensational heating is imposed over the entire tropical belt *but* the Atlantic, presents a response in the Atlantic ITCZ that is closer to what seen in Figure 5.9a in spatial extent (it reaches the northeast coast of South America) and intensity (it reaches a peak value of 6mm/day), but is still too weak.

Figure 5.10 (right column) shows the profiles of θ, θ_e, and θ_{es} in the equatorial Atlantic for March and June elevated condensational heating conditions in South America and Africa. It is apparent that the reduction in continental convection is responsible for cooling the upper troposphere, but cannot cool the lower half of the column. This induces a small increase of stability at about 700mb, and limits the increase in precipitation.

A better match between the response to continental convection and the response to changes in insolation over land (or, equivalently, to changes in both convection and surface temperature) can be achieved by adjusting the imposed heating over Africa and South America to mimic changes in radiative heating and thus better match the vertical profile of heating associated with convection simulated in the PMS run. We conclude that the ITCZ responds to remote convection, as hypothesized, but that the response is quite sensitive to the details of the heating profile.

Another interesting feature of the response to continental heating is its spatial scale. Dry models would suggest a tropics-wide response to a deep convective heating (small, widespread subsidence would compensate for a positive isolated heating, and vice-versa). Instead, experiments in which elevated condensational heating is imposed over one continent at a time (not shown) indicate that the response is inhomogeneous in precipitation, vertical motion, and low-level wind. The reason for the inhomogeneity in the precipitation response can be explained in terms of stability threshold: if, for example, the profile is very stable, a small upper level cooling will not create a precipitation anomaly. Thus, we expect a larger response where the basic state already has precipitation. To understand why the circulation is also inhomogeneous, one has to invoke the most basic balance in the tropics: diabatic heating and adiabatic heating balance each other. The diabatic heating response

depends on the basic state, therefore the same must hold true for the vertical motion field and the associated divergent circulation. How the atmosphere achieves this adjustment in our experiments has not been established.

5.6 Summary and Discussion

In this chapter we have identified the mechanisms that determine the local and remote response of precipitation to the annual cycle of SST and insolation over land. We have discussed how changes in local insolation affect precipitation over the tropical continents, how changes in SST (which in our model experiments can be prescribed independently from insolation) affect precipitation in the ITCZ, and how temperature and rainfall over the ocean affect precipitation over the continents, and vice-versa.

5.6.1

The response of continental precipitation in the Tropics to insolation can be explained in the context of the simple theoretical model put forth by Neelin and Held (1987) for the case of the ocean and revisited by Zeng and Neelin (1999) for the case of land. According to their theory, in the Tropics one can reasonably neglect mean horizontal advection and transient transport of moisture and temperature, and can moreover assume that the first baroclinic mode describes the vertical structure of the atmosphere. Under these assumptions, a simple balance is obtained: the atmosphere balances a positive net energy input in the atmospheric column (the net energy flux, $F_{net} = F_{top} - F_{bottom}$) by convection, convergent circulation at the lower levels, and divergent circulation at the upper levels. To zeroth order, the PMS experiment supports the conclusions of this simple model: the seasonal changes in precipitation mimic the seasonal changes in F_{net} in most of the tropical land masses, with the noticeable exception of the Sahara, where F_{net} never becomes positive and convection cannot be sustained—even if the seasonal changes in F_{net} are substantial.

5.6.2

The ITCZ response to seasonal changes in SST is direct, the ITCZ lies over the warmest waters, and can be interpreted in terms of boundary layer processes, as first described by Lindzen and Nigam (1987). The boundary layer hydrostatically adjusts to an increase in SST and produces a low-level thermal low. The resulting wind converges moisture into the low, sustaining convection. Although boundary layer processes are the fundamental reason why the ITCZ follows the warmest SST, the ITCZ might be more than a passive tracer, and might aid the SST in generating the low-level convergence. By comparing the PVE simulation to experiments in which the elevated condensational heating in the ITCZ is prescribed to vary independently of the SST, we find that the circulation driven by the ITCZ itself indeed generates a substantial fraction of the moisture convergence and the of meridional flow seen in the PVE simulation.

This result is somewhat at odds with the work of Chiang et al. (2001), which found that at interannual-to-decadal timescales the SST gradient, and not the heating anomalies associated with the displacement of the ITCZ, forces surface convergence and meridional wind. This apparent discrepancy between our study and theirs might be explained by the difference in the forcings used. In the study of Chiang et al. (2001), the convective heating anomalies used to force the model are mostly confined to the equator. In our study they extend to 15°N. Another possible explanation is that the simulated atmospheric response to elevated heating is dependent on the characteristics of the model, such as the treatment of the boundary layer processes, or the radiative parameterizations.

The strong surface response to elevated heating suggests the possibility of feedbacks between the ITCZ and the SST in experiments in which the SST is interactive. One implication is that we can expect the Atlantic ITCZ to have larger variability in POGA+MXL simulations (Pacific Ocean Global Atmosphere and Mixed Layer: experiments in which the observed time series of SST is prescribed in the tropical Pacific, and SST is calculated by a mixed layer model elsewhere) than in GOGA simulations (Global Ocean Global Atmosphere: experiments in which the observed time series of SST is prescribed everywhere). A preliminary analysis of runs provided by P. Chang and R. Saravanan supports this conclu-

sion.

We note that prescribing the convective condensational heating associated with a given precipitation anomaly does not ensure that the model will produce the same precipitation anomaly back. On the contrary, the upper level warming due to the prescribed heating stabilizes the column, making convection less efficient in producing rain.

5.6.3

The response of continental precipitation to SST is concentrated in the coastal regions adjacent to the ITCZ and in the African Sahel. The seasonal changes in precipitation in coastal regions appear to be an indirect response to SST changes, and can be forced by applying the changes in elevated condensational heating associated with the latitudinal movement of the ITCZ. Instead, precipitation in the Sahel responds directly to the basin-wide changes of SST. Seasonal changes of SST are advected into the interior of the Sahara and generate surface pressure anomalies, which in turn force low-level wind changes and convergence at the latitude of the Sahel. This chain of events can also be described in terms of the latitudinal shift of the maximum of zonal mean boundary layer θ_e, which determines a shift in the location of the precipitation maximum.

Eltahir and Gong (1996) have explained the effect of SST anomalies on West Africa precipitation variability at the interannual timescale in terms of the SST influence on the meridional gradient of θ_e at the equator. Following Emanuel (1995), they maintain that a flat meridional profile of θ_e at the equator is associated with a weak monsoon flow and with atmospheric conditions closer to a motionless radiative-convective equilibrium, while a positive gradient of θ_e at the equator is associated with the development of a strong, thermally direct, monsoon circulation. This condition on the profile of θ_e is derived under the assumption of a moist convective atmosphere in quasi-equilibrium, and is evolved from the condition for the onset of meridional circulations in a zonally-symmetric dry atmosphere forced by off-equatorial heating identified by Plumb and Hou (1992). In the framework developed by Eltahir and Gong (1996), Sahel precipitation is affected by SST variability because SST anomalies in the Gulf of Guinea are responsible for determining the equatorial

gradient of θ_e.

In our experiments, we find that the influence of SST on Sahel precipitation at the annual timescale is better explained in terms of the influence of SST on the location of the θ_e maximum, and is determined by the SST field in the *whole* Atlantic basin. Specifically, the θ_e profile seems to evolve into its September value by means of an interactive adjustment involving first the response of the boundary layer atmosphere in the Atlantic basin to SST changes directly underneath, then the advection of temperature anomalies from the northern Atlantic over the Sahara, and finally the advection of moisture from the Gulf of Guinea and the equatorial rain forest into the Sahel. To the extent that similar mechanisms are relevant for both the annual cycle and interannual variability, we suggest that interannual variability in Sahelian rainfall might be forced by SST variability in the subtropical Atlantic, as well as by SST variability in the Gulf of Guinea.

Explaining the effect of SST on Sahel rainfall in terms of its effect on the meridional profile of boundary layer entropy also helps us explain why the latitudinal shift of Sahel rainfall in response to seasonal SST changes depends on the basic state of the land. In particular, we have shown in Chapter 4 that the September-March SST difference pattern induces a larger shift in the Sahel precipitation in an experiment with perpetual March insolation than it does in an experiment with perpetual December insolation. Moderate temperature anomalies in the northern subtropics are sufficient to substantially displace the maximum of θ_e to the north when the meridional profile of θ_e is somewhat flat (as it is for equinoctial insolation), but are too weak to do so when the θ_e meridional profiles drops sharply from its maximum value (as it is for solstitial insolation). Thus the precipitation response is muted in the latter case.

5.6.4

The intensity of oceanic precipitation in the ITCZ responds to the intensity of precipitation over the tropical continents: less precipitation over the continents induces a cooling of the upper troposphere and a more unstable environment (or equivalently, more convective available potential energy, CAPE) in the Atlantic. It stands to reason, then, that a larger upper

level cooling will force a larger response in the Atlantic ITCZ. Indeed, the ITCZ response is quite linear in the sense that, for example, the responses to the convective heating forcing imposed over only Africa and over only South America add up to the response obtained by applying the forcing over Africa and South America at the same time. Sensitivity experiments in which the heating was adjusted to reproduce the vertical profile of the full convective forcing (i.e. the sum of the condensational and radiative heating associated with convection) suggest that the ITCZ response to remote elevated heating is quite sensitive to the details of the heating profile.

The fact that the oceanic convection responds to the intensity of precipitation in the tropical continents via its response to changes in upper-troposphere temperature explains why land-induced precipitation anomalies over the ocean are co-located with the basic state ITCZ (cf. Chapter 4). An upper-level change of temperature is felt as an increase of CAPE in regions where the atmosphere is conditionally unstable to begin with, but is not enough to make a stable column unstable. Conversely, if the SLP changes induced by land surface temperature were the main drive for ocean precipitation changes, we would expect that the basic state of SST would not matter as much, because surface wind responds linearly to SLP changes (Lindzen and Nigam, 1987).

Chapter 6

COUPLED EXPERIMENTS: TERRESTRIAL INFLUENCE ON THE ATLANTIC ITCZ

6.1 Outlook

When SSTs are prescribed underneath an AGCM, the response of the simulated oceanic ITCZ to annual changes in insolation over the adjacent continents is a change in intensity, but not in position (cf. Chapter 4). In uncoupled experiments the ITCZ responds to temperature changes in the free troposphere, which are in turn caused by changes in continental convection; the changes in land surface temperature do not directly affect the oceanic precipitation (cf. Chapter 5). What is the response of the ITCZ to continental forcing when we expand our model to include thermodynamic atmosphere-ocean interactions? What other mechanisms come into play? We approach this question by steps: we first investigate what is the response of the Atlantic SST and ITCZ to a steady elevated condensational heating imposed over South America and Africa (Section 6.2). We then show the ITCZ response to insolation-induced annual variations in land surface temperature and precipitation over the continents (Section 6.3). The question of how the ocean responds to local insolation and ocean heat transport convergence is addressed in Section 6.4.

6.2 The ITCZ response to a steady continental forcing

This section describes the ITCZ response to a steady elevated heating over South America and Africa. The imposed forcing (Figure 6.1) is the difference in condensational heating over South America and Africa between the months of June and March (as simulated by CCM3 in an experiment with prescribed March SST and climatologically varying insolation, the Perpetual March SST simulation, PMS). Figure 6.1a shows the horizontal pattern at 500mb. Figure 6.1b shows the average vertical profile.

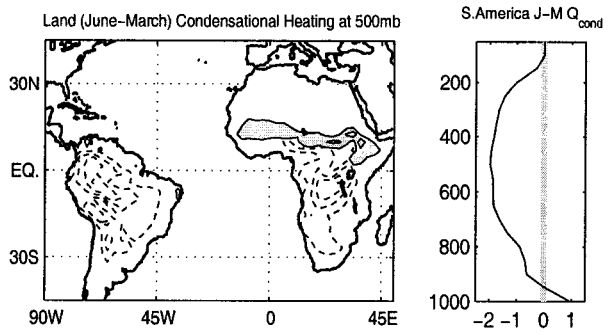

Figure 6.1: The June-March difference in condensational heating over South America and Africa, taken from a simulation with perpetual March SST and climatologically varying insolation over land. (a.) Heating difference at 500mb. The contour interval is $2 * 10^{-5}$ Ks^{-1}, starting with $\pm 10^{-5}$. Negative contours are dashed, the zero line is omitted, shading indicates values larger than $10^{-5} Ks^{-1}$. (b.) Vertical profile as a function of pressure (in millibars) of the heating difference averaged over South America (in units of 10^{-5} Ks^{-1}).

Figures 6.2a,b show the oceanic response in precipitation and surface winds to the forcing shown in Figure 6.1 in *uncoupled* simulations with different basic states (see Table 3.3 for a list of the uncoupled experiments presented in this chapter). Figure 6.2a refers to simulations with March SST and insolation conditions; Figure 6.2b to simulations with September conditions. Specifically, Figure 6.2a shows the PMw/JQ-PM differences, where PM simulates a perpetual March, and PMw/JQ simulates a perpetual March with imposed June condensational heating over the continents. Figure 6.2b shows the PSw/JQ-PSw/MQ differences, i.e. the difference between two perpetual September simulations, but with different imposed condensational heating over the continents (the climatological June condensational heating is imposed in PSw/JQ, and the climatological March condensational heating is imposed in PSw/MQ).

The mechanisms responsible for the uncoupled response have been described in Chapter 5 and can be summarized as follows. A prescribed negative heating over the continents causes a cooling of the free troposphere, which is homogenized by the atmospheric circulation, thus changing the stability profile of the tropical atmosphere. In the Atlantic ITCZ, this enhances CAPE and makes precipitation more vigorous. In regions that are non-convective in the basic state, the change in stability is not sufficient to induce deep convection, and thus the

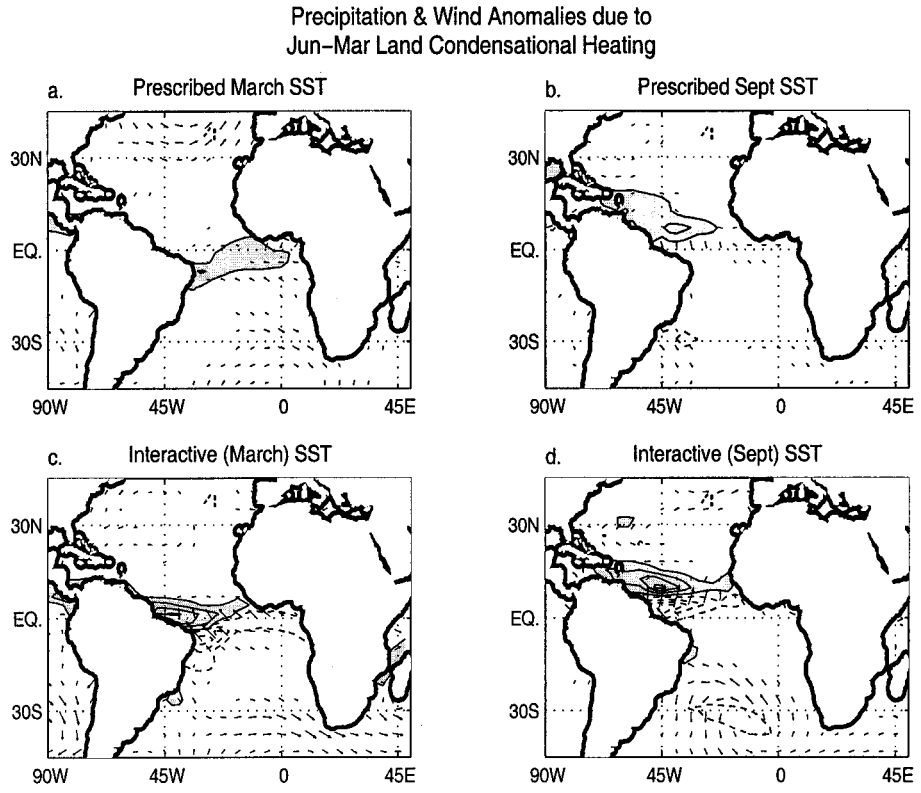

Figure 6.2: The surface wind and ITCZ response forced over the ocean by the constant condensational heating anomalies shown in Fig 6.1. In experiments with prescribed SST, the response of the Atlantic ITCZ is more intense precipitation, the wind response is concentrated to the south of the ITCZ. In experiments with interactive SST, the ITCZ is both more intense (by about 20%) and shifted to the north. Associated with the northward shift of the ITCZ is a strong southerly wind anomaly. (a.) Perpetual March with June continental elevated heating minus Perpetual March (PMw/JQ - PM). (b.) Perpetual September with June continental elevated heating minus Perpetual September with March continental elevated heating (PSw/JQ - PSw/MQ). (c.) Perpetual June continental elevated heating minus perpetual march continental elevated heating (CpldPJQ - CpldPMQ) during March. (d.) As in (c.) but for September insolation and SST conditions. The contour interval is 4 mm day^{-1}, starting with the ± 2 contour, negative contours are dashed, the zero line is omitted, and shading denotes anomalies larger than 2mm day^{-1}; only wind anomalies larger than 1 m s^{-1} are plotted. Anomalies over land have been masked out.

precipitation response is muted outside of the ITCZ region.

Figures 6.2a,b show that the surface wind response is more intense at the equator and to the south edge of the precipitation anomalies. The analysis of sensitivity experiments in which the elevated heating is applied only in South Africa or only in South America suggests that the wind anomalies shown in Figures 6.2a,b should be interpreted as the combination of the Rossby wave response to African heating with the response to the anomalous elevated heating in the ITCZ.

How is the ITCZ response affected by the coupling? Figures 6.2c,d show the difference in precipitation and surface winds between the CpldPJQ and CpldPMQ runs, i.e. between runs where condensational heating over Africa and South America is prescribed to be fixed at the June and March values, respectively, but otherwise the climate is forced by the annual cycle of insolation and Q-flux (see Table 3.4 for a list of the coupled experiments presented in this chapter). Therefore, the difference between the simulations is forced by a steady forcing equal to the June-March continental condensational heating (shown in Figure6.1) but the coupled runs have an annual cycle in their basic state. Figure 6.2c shows the CpldPJQ-CpldPMQ anomalies during March (to be compared with Figure 6.2a), and Figure 6.2d during September (to be compared with Figure 6.2b).

As in the uncoupled case, the intensity of precipitation in the ITCZ is enhanced (by roughly 20%, when averaged over the whole ITCZ) when continental precipitation is depressed. But the coupled response is drastically different from the uncoupled response in that, in the coupled case, the ITCZ has shifted 7 degrees northward in response to the continental condensational heating anomalies. This suggests that precipitation over the African and South American land masses has the ability to affect the annual meridional march of the ITCZ.

The northward shift of the ITCZ could have been anticipated in light of the surface wind response in the uncoupled case (Figures 6.2a,b): the southeasterly trades to the south of the ITCZ are anomalously strengthened in response to the continental forcing. Stronger winds mean stronger evaporation and latent heat loss from the ocean. When a slab ocean model is coupled to the AGCM, this anomalous latent heat flux cools the SST to the south of the mean ITCZ, establishing a cross-equatorial gradient that pushes the ITCZ northward.

Associated with the SST gradient and the ITCZ shift is an enhanced meridional wind response.

Note that over the ocean the wind response to the continental elevated heating forcing of Figure 6.1 is comprised of two components: the direct Rossby response to African heating (Gill, 1980) and the response to the changes in oceanic precipitation. Because the precipitation intensity response is locked to the annual cycle of the mean ITCZ, the surface wind response is locked to the annual cycle of the mean ITCZ as well. This behavior is maintained in the coupled case and the northward displacement of the ITCZ is tightly locked to the annual cycle of the basic state.

The comparison of the uncoupled and coupled response in Figure 6.2 sheds light on how the coupled anomalies are established. We next focus on how the equilibrated response is maintained by the coupled system. Figure 6.3 shows the annual cycle of the CpldPJQ-CpldPMQ anomalies in precipitation, SST, surface winds and heat flux into the surface ocean at 30°W, in the central Atlantic, as a function of month and latitude. Also shown is the annual cycle of the mean position of the ITCZ (in this case identified by the confluence line) in both runs. The ITCZ in the CpldPJQ run is always about 7 degrees to the north of that in the CpldPMQ run, with the largest displacement of the ITCZ rainfall occurring in boreal spring, the smallest in boreal winter (Fig. 6.3a). The ITCZ displacement is associated with a positive anomalous meridional SST gradient and southerly wind (Fig. 6.3b). There is a band of strong heat flux anomalies (Fig. 6.3c) in proximity of the mean ITCZ. These anomalies are strongly negative from March to August, and strongly positive for the rest of the year. Away from the ITCZ region, the heat flux anomalies are much weaker, but maintain the same sign nearly throughout the whole year: they are mostly positive in the northern tropical Atlantic and mostly negative in the southern tropical Atlantic. The weak but constant heat flux anomalies poleward of ±5°are as important as the strong but oscillating anomalies in the equatorial region for maintaining a year-round positive anomaly in the meridional gradient of SST across the mean position of the ITCZ.

Figure 6.3d shows the CpldPJQ-CpldPMQ anomalies in wind speed squared; because evaporation depends on the square of the wind, the similarity in the patterns in Figure 6.3d and Figure 6.3c indicates to what extent heat flux anomalies can be explained by wind-

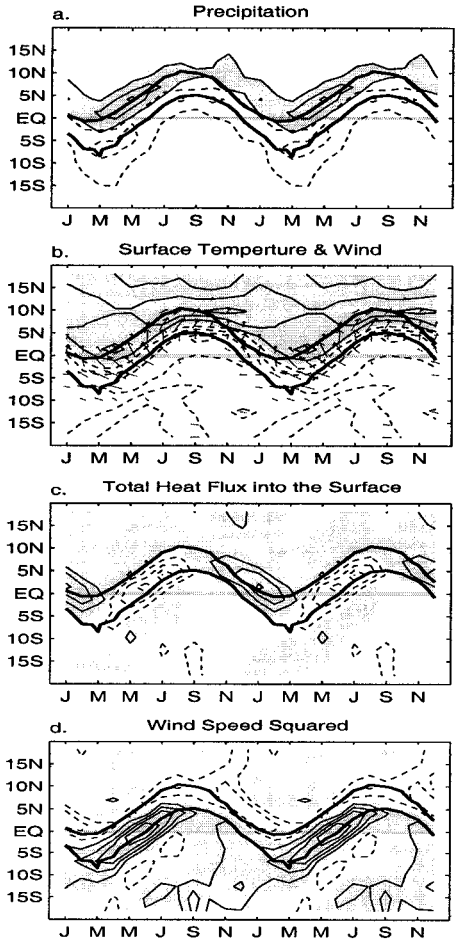

Figure 6.3: The annual cycle of the response of the Central Atlantic (30°W) to the forcing in land condensational heating shown in Fig 1, as a function of month and latitude [Perpetual June continental elevated heating minus perpetual March continental elevated heating (CpldPJQ - CpldPMQ)]. (a.) CpldPJQ - CpldPMQ precipitation anomalies (contour interval of 4 mm day^{-1}, starting with ± 2). (b.) CpldPJQ - CpldPMQ SST anomalies (contour interval of 0.5°C, the zero line is omitted) and surface wind anomalies (only wind anomalies larger than 2 m s^{-1} are plotted). (c.) CpldPJQ - CpldPMQ total heat flux anomalies into the ocean (contour interval of 30 W m^{-2}, the zero line is omitted). (d.) CpldPJQ - CpldPMQ wind speed squared anomalies (contour interval of 16 m^2 s^{-2}, the zero line is omitted). In every panel the thick lines indicate the climatological position of the confluence line in CpldPJQ (further to the north) and CpldPMQ (further to the south), the dashed lines indicate negative values, and the shading indicates positive values (b,c,d) or values larger than the value of the first positive contour line (a).

induced anomalies in evaporation (a faster wind means more evaporation and a cooling of the ocean). Radiative fluxes anomalies have a smaller, but still non-negligible, magnitude in the ITCZ region, and are comparable to the changes in latent heat flux poleward of $\pm 5°$(not shown).

We can describe the anomalies in wind speed in terms of the meridional and zonal wind components (Figure 6.3b). The meridional wind anomalies are mostly southerly and maximize to the north of the CpldPMQ confluence line. They induce a reduction of the wind speed everywhere north of the CpldPMQ confluence line, therefore contribute to the warming there all year-round. Everywhere else they have a much smaller impact. The zonal wind anomalies are mostly easterly to the south of the equator and are the major cause for the boreal spring-time cooling there; during boreal summer and fall the anomalies are westerly north of 5°N, where they induce warming.

To summarize, a reduction in continental precipitation induces a remote cooling of the free troposphere and a reduction in stability. In the ITCZ, this translates in more active deep convection and larger low-level convergence. The surface wind anomalies (generated in response to both the prescribed elevated heating over land and the precipitation changes in the ITCZ) induce a cooling to the south of the mean ITCZ (Figure 6.2a,b). Finally, SST, surface wind, and oceanic precipitation adjust to each-other in an interactive way, establishing the anomalies portrayed in Figure 6.2c,d and Figure 6.3.

6.3 The ITCZ response to an annually varying continental forcing

In this section we present the response of the Atlantic ITCZ to annually varying forcing over the continents. Specifically, we compare two simulations: one is a control run, with climatologically varying forcings, the other is an experiment with insolation over land fixed at the boreal vernal equinox (see Tables 3.3 and 3.4 for lists of the uncoupled and coupled experiemnts presented in this chapter). The difference between the two simulations is the response to the insolation differences shown in Figure 6.4. It can be thought of as the response to the annual cycle of insolation over land.

Before presenting the results of the coupled experiments, we will review the experiments

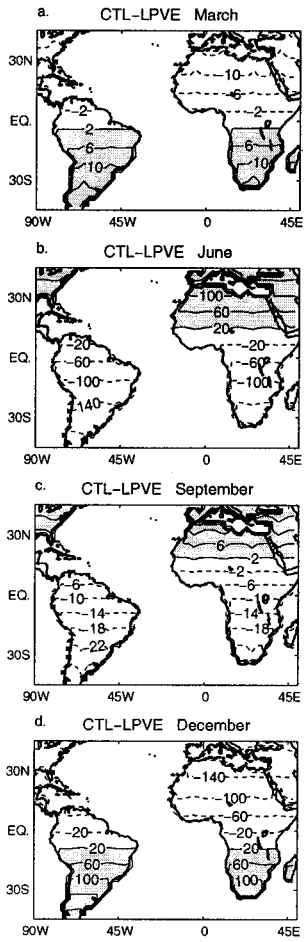

Figure 6.4: The annual cycle of insolation over land, shown as differences from the (boreal) vernal equinox value. (a.) March CTL - March LPVE (i.e., March mean - March 21st). (b.) June CTL - June LPVE. (c.) September CTL - September LPVE. (d.) December CTL - December LPVE. The contour interval is 4 W m^{-2} (40 W m^{-2}), starting with $\pm 2(20)$, in panels a. and c. (b. and d.); the dashed contours indicate negative values and the shading indicates positive values larger than 2 W m^{-2} (20 W m^{-2}).

with prescribed SST. Figures 6.5a,c,e,g show the difference between the uncoupled CTL simulation and the uncoupled LPVE simulation (forced with perpetual vernal equinox insolation over land) during March, June, September, and December. The precipitation anomalies are forced by the corresponding difference in insolation over land from the equinox value (Figure 6.4) and are somewhat modified by soil processes, which hold memory of the forcing from one month to the next (Chapter 4). Figures 6.5a,c,e,g present an alternate view of the insolation-induced anomalies presented in Chapter 4 (cf. Figure 4.7). The left column of Figure 6.5 shows that, over land, precipitation to zeroth order increases with increasing insolation and that, over the ocean, the intensity of the ITCZ is sensitive to continental forcing, but—*when SST are prescribed*—the location of the ITCZ is not. We have shown in Chapter 5, and reviewed in Section 6.2, that the changes in ITCZ intensity are a response to the temperature changes in the free troposphere that accompany changes in continental precipitation. The concomitant changes in land surface temperature do not have a direct effect on oceanic precipitation in the uncoupled experiment.

Figures 6.5b,d,f,h show the CpldCTL-CpldLPVE difference in precipitation during March, June, September, and December. The forcing is the same of that for the uncoupled case (Figure 6.4), but now SST is allowed to change in response to changes in turbulent and radiative surface heat fluxes. Over land, the precipitation anomalies present, as expected, the same picture of the uncoupled case. Over the ocean, the precipitation anomalies are similar to those in the uncoupled case during June, September, and December, but show a markedly different pattern during March. In the uncoupled case (Figure 6.5a), the March anomalies show a slightly weakened ITCZ. In the coupled case (Figure 6.5b), the ITCZ is both weakened and shifted farther south in the CpldCTL simulation, compared to the CpldLPVE simulation.

Figure 6.6 provides a better description of how significant the precipitation differences of Figure 6.5 are. It shows the annual cycle of precipitation and SST in the central Atlantic (at 30°W) in the CpldCTL and the CpldLPVE simulation. In the control simulation (Figure 6.6a) the main ITCZ stays north of 5°S, and a secondary precipitation center develops during boreal spring at about 10°S. In the CpldLPVE experiment, in which the annual cycle of both temperature and precipitation over the continents is suppressed (Figure 6.6b),

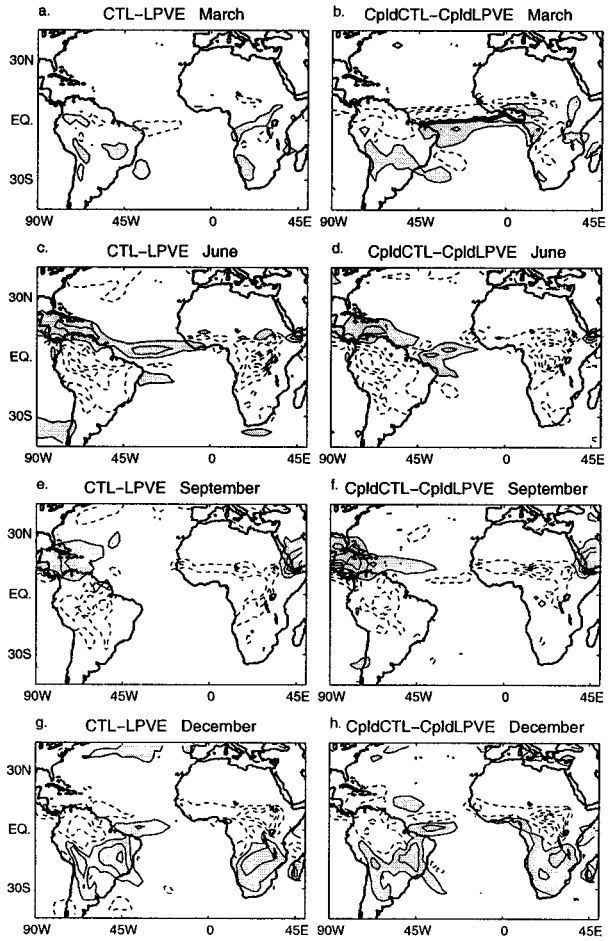

Figure 6.5: The precipitation response to the annual cycle of insolation over land in the case of (left column) prescribed SST and (right column) interactive SST. The effect of having an interactive SST is to allow the ITCZ to move, as can be easily inferred by comparing the coupled and uncoupled March anomalies. (a.) March CTL - March LPVE. (b.) March CpldCTL - March CpldLPVE. (c.) June CTL - June LPVE. (d.) June CpldCTL - June CpldLPVE. (e.) September CTL - September LPVE. (f.) September CpldCTL - September CpldLPVE. (g.) December CTL - December LPVE. (h.) December CpldCTL - December CpldLPVE. The contour interval is 4 mm day^{-1}, starting with ± 2, the dashed contours indicate negative values and the shading indicates positive values larger than 2mm day^{-1}.

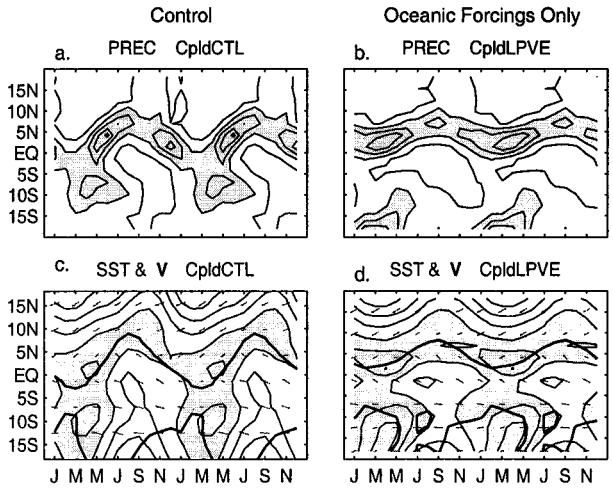

Figure 6.6: The annual cycle of precipitation, SST, and surface wind in the Central Atlantic (30°W) in simulations with different annual forcings. (a.), (c.) CpldCTL: annual cycle due to both local (insolation and Q-flux) forcings and remote (land insolation) forcing. (b.), (d.) CpldLPVE: annual cycle due only to local forcings (insolation and Q-flux); the remote forcing coming from the annual cycle over land has been suppressed. The contour interval for precipitation is 3 mm day^{-1}, starting with ± 1.5, values larger than 4.5mm day^{-1} are shaded. The contour interval for SST is 1°C, values larger than 27°C are saded . Only surface wind vectors larger than 1.5 m s^{-1} are plotted.

the northern ITCZ does not reach as far south, while the southern precipitation develops earlier in the year and is limited to farther south. We see by comparing Figures 6.6a,b that suppressing the annual cycle over the continents suppresses the annual cycle in the position of the ITCZ.

We can further decompose the effect of land on oceanic precipitation into the effect of land precipitation and the effect of land surface temperature. To do so, we will com-

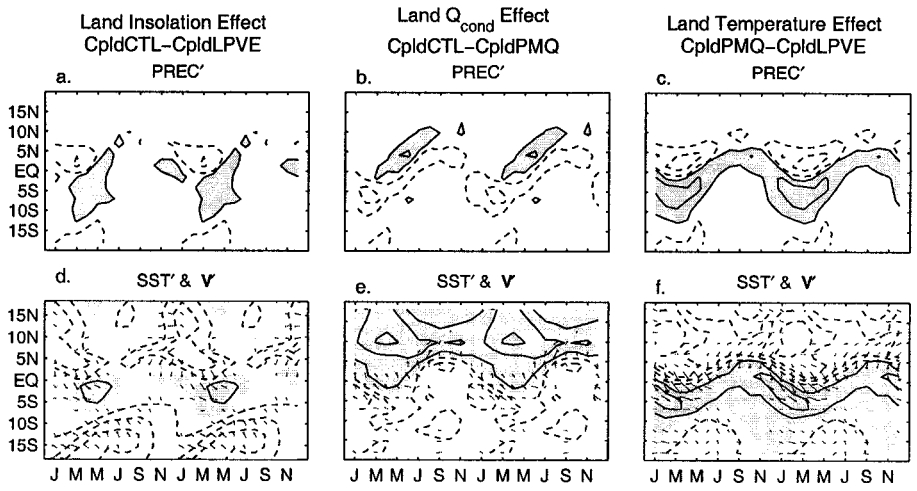

Figure 6.7: The annual cycle of the response of precipitation, SST, and surface wind in the Central Atlantic (30°W) to annually varying continental forcing as a function of month and latitude. (a.), (d.) CpldCTL - CpldLPVE: anomalies due to insolation over land. (b.), (e.) CpldCTL - CpldPMQ: anomalies due to precipitation over land. (c.), (f.) CpldPMQ - CpldLPVE: anomalies due to surface temperature over land. The contour interval for precipitation anomalies is 6 mm day^{-1}, starting with ± 3, dashed contours indicate negative values, shading indicates positive values larger than 3 mm day^{-1}. The contour interval for SST anomalies is 0.5°C, the zero line is omitted, dashed contours indicate negative values, shading indicates positive values. Only surface wind anomalies larger than 1.5 m s^{-1} are plotted.

pare the CpldLPVE and CpldPMQ experiment with the coupled control CpldCTL. In the CpldLPVE run the insolation over land is fixed to March value, so that the difference CpldCTL-CpldLPVE (Figure 6.7a,d) shows the impact of insolation over land, and includes both land surface temperature and land precipitation changes due to the seasonal cycle in land insolation. In the CpldPMQ run land insolation and ocean forcings cycle

through their climatology, but the elevated condensational heating associated with precipitation over Africa and South America is kept fixed at March value. Therefore the difference plots CpldCTL-CpldPMQ (Figure 6.7b,e) show how elevated heating changes over Africa and South America (due to the annual cycle of insolation over land) impact the seasonal march of the ITCZ. To the extent that changes in the mid-latitudes climate can be neglected and that the effect of land surface temperature and land convective heating add up linearly, the difference CpldPMQ-CpldLPVE (Figure 6.7c,f) can be thought of as showing the ITCZ response to land surface temperature in Africa and South America. Figure 6.7 shows that the CpldCTL-CpldPVE precipitation and SST differences are the result of large but opposite responses to changes in the continental precipitation and in the continental surface temperature, with surface temperature being the dominant forcing.

Note that the annual cycle of both land surface temperature and land precipitation force an *annual mean* anomaly in the position of the ITCZ. There are two reasons for this. The principal reason is that the forcings itself have a non-zero annual mean. For example, the CpldLPVE is warmer in the mean than the CpldCTL, and the June CpldCTL-CpldLPVE land temperature difference is smaller in amplitude than the December difference (see Figure 6.11), so the oceanic response is biased toward the response to boreal winter anomalies. A secondary reason is that the feedbacks between the SST, the ITCZ, and the surface winds tend to maintain an original displacement of the ITCZ.

Figure 6.7d shows that associated with the boreal spring displacement of the ITCZ are large anomalies in equatorial SST meridional gradient and surface wind. The spatial pattern of March CpldCTL-CpldLPVE surface air temperature (SAT) difference (over the ocean SAT closely mimics SST) is shown in Figure 6.8 . As a reference for the position of the precipitation difference dipole during the same month plotted in Figure 6.5, we have also plotted the zero line in precipitation anomalies. Again, it is clear that the southward displacement of the ITCZ is associated with an anomalous negative meridional gradient of SST at the equator. How is this anomalous gradient established?

Figure 6.9 shows the anomalies in total heat flux and latent heat flux integrated over December, January, and February. The latent heat flux makes up the bulk of the total heat flux in the equatorial area, but radiative fluxes are also important, especially in the

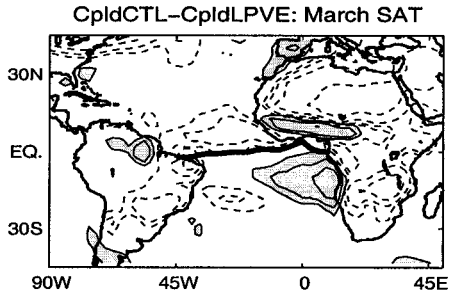

Figure 6.8: The surface air temperature response to the annual cycle of insolation over land in the case of interactive SST (March CpldCTL - March CpldLPVE). The contours are spaced logarithmically: $\pm.5, \pm1, \pm2, \pm4, \pm8°C$, negative values are dashed and positive values larger than 2°C are shaded.

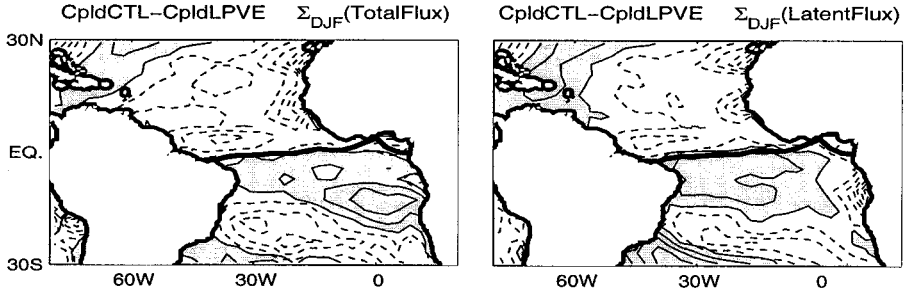

Figure 6.9: The winter-time (the sum of December, January, and February) latent heat flux response to the annual cycle of insolation over land in the case of interactive SST (CpldCTL - CpldLPVE). The contours interval is 40 W m^{-2}, starting with ±20. The thick line is the zero line of the March CpldCTL - March CpldLPVE precipitation anomalies.

stratus region off the South African coast. It is apparent that wintertime latent heat flux anomalies are responsible for the generation of the anomalous equatorial SST gradient during March—and thus for the shift of the ITCZ. (When comparing Figures 6.8 and 6.9, recall that poleward of 20°the calculated SST are linearly merged with the prescribed SST.) Therefore we next focus on how the latent heat flux anomalies are generated.

Figure 6.10 shows the surface wind and latent heat flux anomalies for each winter month in both the uncoupled and the coupled experiments. Let's first focus on the coupled results. During December (Figure 6.10b) the largest surface latent heating anomalies occur offshore of the Sahara, in the northern tropical Atlantic; at and south of the equator the latent heating anomalies are positive and weaker. A linear analysis [following Saravanan and Chang (2000)] indicates that the latent heat flux anomalies are mostly a consequence of wind speed anomalies (latent heat fluxes anomalies due to changes in air-sea temperature difference are also large off the Saharan coast, but warm the SST, the opposite of the wind speed effect). The enhanced trades in the northern tropical Atlantic are a consequence of the insolation-induced cold anomalies and high surface pressure over the Sahara (not shown). This conclusion is consistent with our analysis of Figure 6.7, and with a larger effect of continental temperature than of continental convection.

The December latent heat flux anomalies extend to the equatorial region, where they force a negative meridional gradient in SST. In January (Figure 6.10d), northerly cross-equatorial wind anomalies are in place and cause a strengthening of the latent heat flux anomalies dipole in the equatorial region. By February (Figure 6.10f) the latent heat anomalies off of northern Africa have changed sign, while the negative cross-equatorial gradient of SST is maintained, and intensified, by a narrow patch of cross-equatorial wind. A comparison with the uncoupled case shows that the coupling amplifies the cross-equatorial wind and latent heat flux anomalies in the equatorial region (cf. Figures 6.10c and 6.10d and especially 6.10e and 6.10f). There is a positive feedback between the wind and the SST: the wind-induced latent heat anomalies strengthen the SST gradient, which in turn drives a stronger cross-equatorial wind. This wind-evaporation-SST feedback was first introduced in an idealized study of the annual cycle of the ITCZ by Xie and Philander (1994), and later invoked to explain the tropical Atlantic decadal variability (Chang et al., 1997). Neverthe-

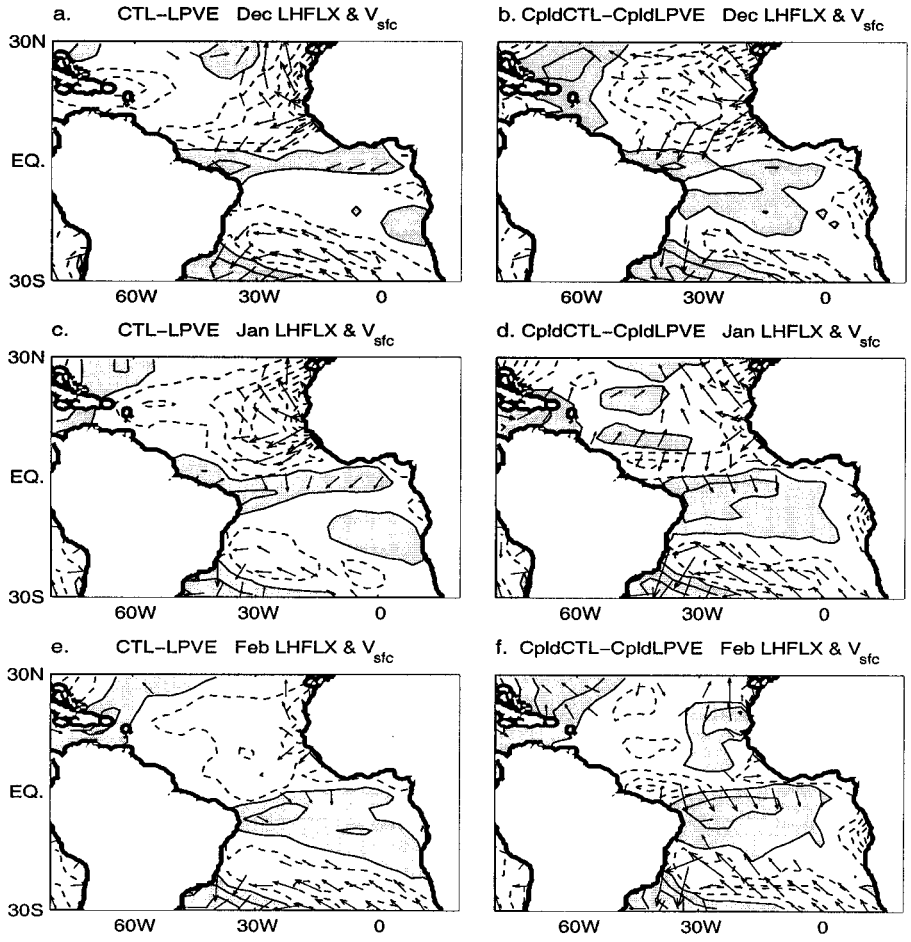

Figure 6.10: The latent heat flux and surface wind response to the annual cycle of insolation over land in the case of interactive SST. The contour interval is 20 W m^{-2}, starting with ± 10, dashed contours indicate negative values and the shading indicates positive values larger than 10W m^{-2}; only wind anomalies larger than 1.5 m s^{-1} are plotted. (a.) December CTL - December LPVE (b.) December CpldCTL - December CpldLPVE (c.) January CTL - January LPVE (d.) January CpldCTL - January CpldLPVE (e.) February CTL - February LPVE (f.) February CpldCTL - February CpldLPVE

less, we note that the latent heat flux anomalies in the uncoupled case (Figures 6.10a,c,e) are by themselves sufficient to induce a negative SST gradient at the equator; in this sense, the wind-evaporation-SST feedback, while undoubtedly an integral part of the development and the maintenance in time of the SST gradient and the displacement of the ITCZ in our coupled experiment, is not crucial for either.

An alternate view of the development of the March displacement of the ITCZ is portrayed in Figure 6.11. The top panel shows the annual cycle of the (insolation-induced) SAT over the Sahara. The vertical gray line in Figure 6.11a highlights the coldest SAT anomaly, during December. (In the other panels of Figure 6.11 the gray lines extend from December to the time when the plotted anomalies reach their maximum amplitude, and give a visual estimate of the response time of each variable.) The cold anomaly in the Sahara produces a high sea level pressure anomaly and easterly wind in the northern tropical Atlantic, strengthening the Trades (Figure 6.11b) and cooling the SST by evaporation. The maximum cooling in the northern tropical Atlantic is achieved in February (Figure 6.11d), at what time virtually all of the cross-equatorial SST gradient is also established (Figure 6.11d). The ITCZ responds to the SST gradient by shifting south, achieving the largest southward displacement in March (according to the confluence line, Figure 6.11e) or April (according to precipitation maximum, Figure 6.11f).

It is obvious from the above discussion, that the timing of the maximum displacement of the ITCZ is controlled by the response time of the mixed layer, which in this simple model is just proportional to the mixed layer depth. A similar set of experiments, in which we had reduced the depth of the mixed layer to 1 meter to make the ocean respond instantaneously to the atmospheric forcing, shows that in that case the maximum ITCZ displacement occurs in December (not shown).

We conclude this section with a caveat. In the above discussion we have disregarded the state of the midlatitudes. Obviously the insolation forcing has a large impact on the temperature of the northern midlatitude continents, and therefore on the midlatitude jets (but not on the midlatitude ocean temperature, because those are prescribed in our model configuration). The fact that the changes in tropical SST and precipitation can plausibly be explained in terms of the insolation-induced temperature changes in the Sahara makes us

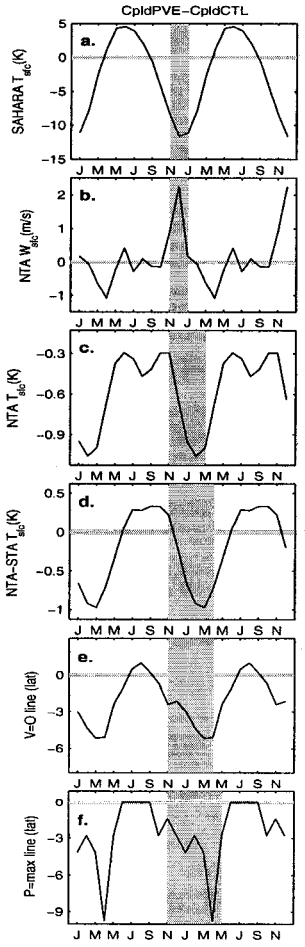

Figure 6.11: The response to the annual cycle of insolation over land in the case of interactive SST (CpldCTL - CpldLPVE). (a.) Surface air temperature in the Sahara. (b.) Wind speed in the north tropical Atlantic. (c.) SST in the north tropical Atlantic. (d.) SST in the north tropical Atlantic - SST in the south tropical Atlantic. (e.) Position of the Atlantic ITCZ as measured by the confluence line (f.) Position of the Atlantic ITCZ as measured by the maximum precipitation. The grey vertical line indicates the elapsed time between the time of the minimum surface temperature in the Sahara, December, and the time when the other indeces reach an extrema. The wind response in the northern tropical Atlantic is instantaneous. The minimum SST in the tropical Atlantic is reached within two months, in February. The maxima in cross-equatorial SST gradient and in the dispalcement of the ITCZ is reached in March/April.

confident that the mid-latitude jets have—in these experiments—a secondary role at best. Sensitivity experiments are underway in order to verify that this is indeed the case.

6.4 The ITCZ response to annually varying local forcings

Figure 6.6 highlights a surprising result of this study: the annual march of the Atlantic ITCZ is greatly reduced when the annual cycle over land is suppressed. This might indicate that the annual variations of the local forcings in the Atlantic ocean (insolation and ocean heat transport) are secondary in generating the annual cycle of the Atlantic ITCZ, but given the large amplitude of the annual cycle in both insolation and ocean heat transport, one is inclined to conclude that the two forcings counteract each other. In this section we investigate what is the role of the insolation over the ocean and the Q-flux, singularly taken, in generating the annual cycle of the tropical Atlantic ITCZ.

We show results from two additional experiments (see Table 3.4). In CpldLPVE$\overline{\text{Qflux}}$ the only annually varying forcing is insolation over the ocean, while insolation over land is fixed at the vernal equinox value and the Q-flux is annually averaged. In CpldLOPVE the only annually varying forcing is the Q-flux, while insolation is fixed at the vernal equinox value everywhere. Figure 6.12 shows the annual cycle of precipitation, SST, and surface winds in the CpldLPVE$\overline{\text{Qflux}}$ and CpldLOPVE simulations. The annual cycle in the *position* of the ITCZ is small in both simulations (especially in the CpldLOPVE, in which the annual variations derive entirely from the Q-flux), at the same time that the annual cycle in the intensity of the ITCZ is maintained or augmented. In both simulations, the equilibrium state has a year-round ITCZ in the north, and a second maximum of precipitation in the southern tropics that lasts only few months. A caveat in the interpretation of these results derives from the fact that the annually averaged insolation is different in the two simulations. In particular the northern Tropics receive in the annual mean more insolation in perpetual vernal equinox conditions then they do for climatological insolation. This additional insolation contributes to the pronounced warming at about 7°N seen in Figure 6.12d.

We conclude this section noting that the above results are only valid in the context of

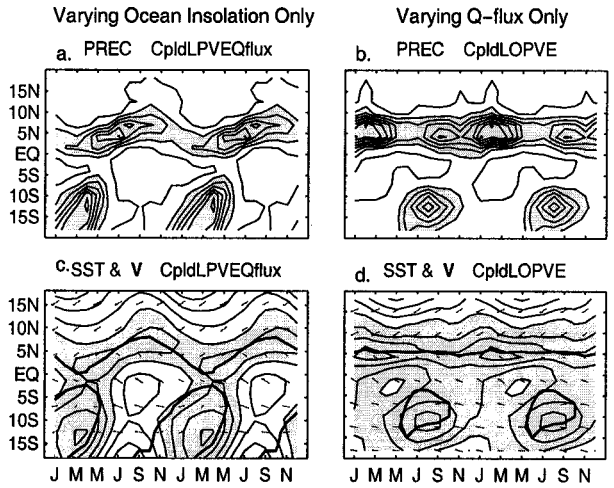

Figure 6.12: The annual cycle of precipitation, SST, and surface wind in the Central Atlantic (30°W) in simulations with different annual forcings. (a.), (c.) CpldLPVE$\overline{\text{Qflux}}$: annual cycle due to local insolation. (b.), (d.) CpldLOPVE: annual cycle due only to the Q-flux. The contour interval for precipitation is 3 mm day^{-1}, starting with ± 1.5, values larger than 4.5mm day^{-1} are shaded. The contour interval for SST is 1°C, values larger than 27°C are saded . Only surface wind vectors larger than 1.5 m s^{-1} are plotted.

AGCM+SOM experiments. While it is appropriate to refer to the Q-flux forcing as a local forcing in the context of AGCM+SOM experiments, in reality the ocean heat transport that we parameterize with the Q-flux is the result of ocean dynamics that is, in principle, the result of both local and remote forcings. Sorting out the cause of annual variations in ocean heat transport requires a dynamical ocean, and cannot be done in our simpler model configuration. Furthermore, the SOM uses a constant, uniform mixed layer depth of 50 m. In the real world, the depth of the mixed layer varies in space and time, introducing another modulation in the response of the ocean to surface fluxes. The depth of the mixed layer is determined by the the strength of the wind and by advective processes in the ocean, and thus depends in a non-trivial way on both local and remote forcings. Finally, although we have interpreted the Q-flux as a parameterization of the ocean heat transport convergence, in reality it also correct for model biases, which might present a non-trivial annual cycle.

6.5 Summary and Discussion

In Sections 6.3 and 6.4 we have shown that the simulated control climatology of the Atlantic ITCZ is the result of a balance between the annual variations of local insolation, ocean heat transport, continental surface temperature and continental precipitation, and that no single forcing is dominant. The annual variations in oceanic local forcings (insolation over the ocean and heat transport) modulate the intensity of precipitation in the tropical Atlantic, both north and south of the equator, but do not force the migration of the ITCZ seen in the control simulation. On the contrary, the annual variations in terrestrial forcings (continental surface temperature and precipitation) affect the position of the ITCZ more than its intensity, with the effect of the continental precipitation forcing partially counteracting the effect of the continental surface temperature forcing.

The main conclusion of this chapter is that variations in precipitation and temperature over the continents are as important as variations in insolation over the ocean and in ocean heat transport convergence in forcing the annual march of the Atlantic ITCZ observed in the control simulation.

Figure 6.13 offers an alternate summary of our results. It shows the annual harmonic of precipitation and surface temperature in response to annually varying insolation and ocean heat transport (CpldCTL, Figures 6.13a,b), land insolation only (CpldCTL-CpldLPVE, Figures 6.13c,d), ocean forcings only (CpldLPVE, Figures 6.13e,f) ocean insolation only (CpldLPVE$\overline{\text{Qflux}}$, Figures 6.13g,h), and Q-flux only (CpldLOPVE, Figures 6.13i,l). The length of each vector gives a measure of the amplitude of the annual cycle (more precisely, it represents the amplitude of the annual harmonic of the climatology) at that location, and the direction represents its phase, with an arrow pointing upward indicating a maximum in January, and time progressing clockwise.

A comparison of the annual harmonic of temperature and precipitation in the control run is interesting in its own right: it shows that the largest amplitude in the annual variations of oceanic precipitation in this model is achieved in the western equatorial basin, where the annual harmonic of SST is negligible. SST has a much larger annual harmonic in the eastern equatorial region, in the Gulf of Guinea. This local "decoupling" of the SST and the ITCZ

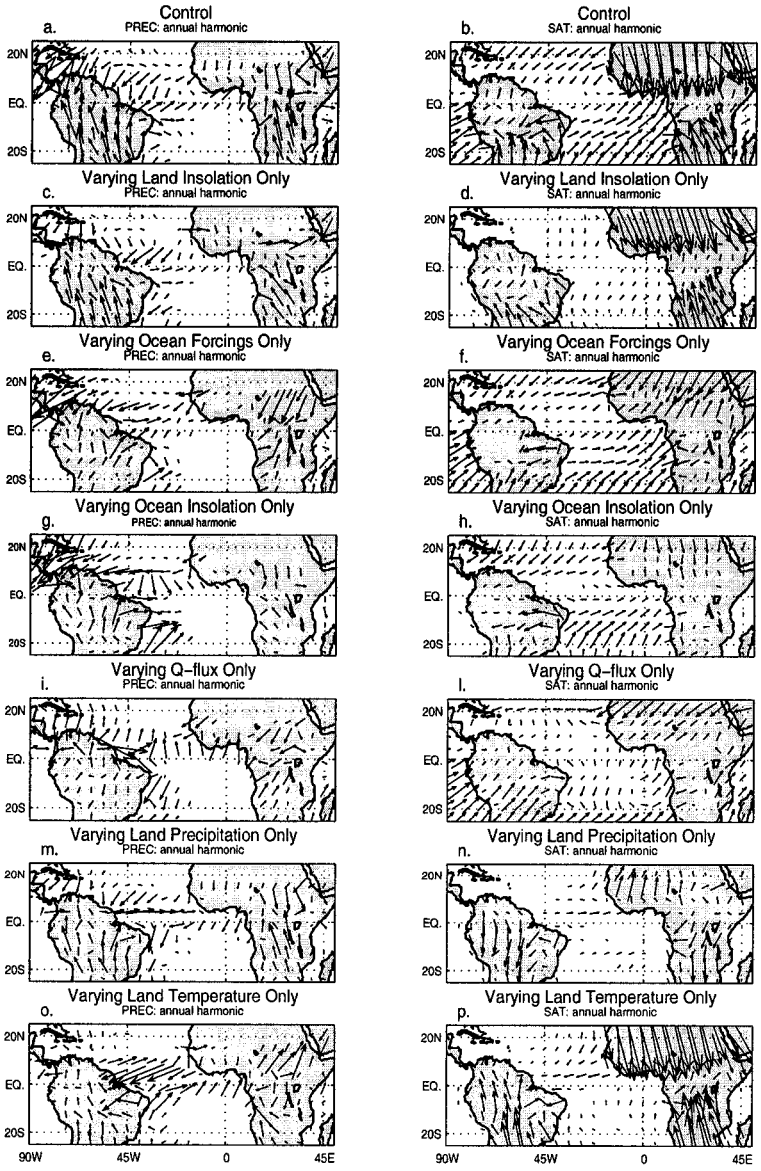

Figure 6.13: Harmonic dial of the annual cycle of (left column) precipitation and (right column) surface air temperature in (a.) and (b.) CpldCTL, (c.) and (d.) CpldCTL-CpldLPVE, (e.) and (f.) CpldLPVE, (g.) and (h.) CpldLPVE$\overline{\text{Qflux}}$, (i.) and (l.) CpldLOPVE, (m.) and (n.) CpldCTL-CpldPMQ, (o.) and (p.) CpldPMQ-CpldLPVE. The direction of the arrows indicates the maximum in the annual harmonic, with January pointing upward and time increasing clockwise. The length of the arrows indicates the amplitude of the annual harmonic. The smallest arrow in the precipitation plots indicates an amplitude of 0.5 mm day^{-1}. The smallest arrow in the surface air temperature plots indicates an amplitude of 0.25°C.

is even more apparent in the annual harmonic simulated in response to the annual cycle of insolation over land: the ITCZ response is very strong (and strikingly similar to the control annual harmonic in the equatorial region), while the remotely forced annual harmonic of SST is weak. The remotely forced annual harmonic of the ITCZ is the result of a cancellation between the response to continental precipitation (Figures 6.13m) and continental surface temperature (Figures 6.13o). The locally forced annual harmonic in oceanic precipitation (i.e. that forced by insolation over the ocean and by the Q-flux) is of the same amplitude of that forced remotely (cf. Figures 6.13c and e) , and is the result of partial cancellation between the effect of the insolation and the Q-flux (cf. Figures 6.13g and i).

The annual harmonic of SST appears to be mainly a response to local insolation, although variations in Q-flux are also important, especially in the Gulf of Guinea. This result seems at odds with those of Carton and Zhou (1997). Their study concluded that insolation had little effect between 5°S and 10°N (and that ocean dynamics was dominant between 10°S and the latitude of the mean ITCZ, and the latent heat flux was dominant from the latitude of the mean ITCZ to to 10°N). The contradiction is not irreconcilable, and stems at least in part from the difference in the experimental design and the model used. In Carton and Zhou (1997) the insolation can only directly heat the ocean, but does not drive surface winds (the annual cycle of surface wind is taken from observations). In the northern equatorial Atlantic, our study will agree with Carton and Zhou (1997) if insolation drives the annual cycle of SST by driving the annual cycle of surface winds. Our conclusions about the role of ocean heat transport in determining the annual cycle of SST agree with that of Carton and Zhou (1997) qualitatively, but not quantitatively. This might be a consequence of the fact that in our Q-flux Only experiment there are significant changes to the surface wind—and thus surface heat flux—due to atmosphere-ocean coupling. Moreover, extrapolating our conclusion on the relative role of annual variations in the Qflux in generating the annual cycle of SST to the role of ocean dynamics is probably not warranted: the Q-flux also corrects for the choice of a uniform constant mixed layer depth, and is contaminated by biases in the atmospheric fluxes.

In regard to the Q-flux we also note that, in this model configuration, the Q-flux can be interpreted as a local forcing, but in reality the ocean heat transport convergence contains

the effect of horizontal advection by ocean currents, upwelling, and the deepening and shoaling of the mixed layer depth. Thus, it is the product of local and remote forcings alike. In particular, Mitchell and Wallace (1992) in an observational study and Li and Philander (1997) in a modeling study have suggested that the southerly wind in the (land-driven) African monsoon is the main driver for the dynamics of the Atlantic cold tongue. A recognition of the total effect of the continents on the oceanic climate requires the use of a dynamical ocean model and is beyond the scope of this study.

Chapter 7

CONCLUSIONS

This thesis describes a set of GCM experiments intended to elucidate the relative role of local and remote forcings in producing the annual cycle of surface temperature and precipitation over the tropical Atlantic ocean, Africa, and South America. We have used the NCAR CCM3 atmospheric GCM in an uncoupled configuration, in which case SST is prescribed and can be treated as an external forcing, and coupled to a motionless slab ocean model, in which case SST is interactive and can respond to surface heat fluxes, albeit not to wind stress. This experimental design allows us to sequentially isolate the processes that determine the annual cycle in simpler models, and is a starting point for understanding the annual cycle in the more complex, fully-coupled GCMs and in nature.

We will focus our discussion on the annual cycle of precipitation, and especially on the role of mutual influences between the Atlantic ocean and the African and South American continental masses.

7.1 Results

Our uncoupled experiments show that the ITCZ response to seasonal changes in SST is direct: the ITCZ lies over the warmest waters. Such response can be interpreted in terms of boundary layer processes, as first described by Lindzen and Nigam (1987). The boundary layer hydrostatically adjusts to an increase in SST and produces a low-level thermal low. The resulting wind converges moisture into the low, sustaining convection. Experiments in which we have imposed the elevated condensational heating associated with precipitation in the ITCZ indicate that the ITCZ is more than a passive tracer of SST gradients, and aids the SST in generating the low-level convergence: the circulation driven by the ITCZ itself generates a substantial fraction of the moisture convergence and of the meridional flow seen in response to SST changes.

The seasonal changes in precipitation in the equatorial coastal regions (Northeast Brazil, Guiana, Gulf of Guinea) are primarily determined by SST. They appear to be an indirect response to SST changes, in that they can be forced by applying the changes in elevated condensational heating associated with the latitudinal movement of the ITCZ.

The seasonal changes of SST are responsible for a substantial portion of the seasonal changes of precipitation over the Sahel. The Sahel responds directly to the basin-wide changes of SST: seasonal changes of SST are advected into the interior of the Sahara and generate surface pressure anomalies, which in turn force low-level wind changes and convergence of moisture from the Gulf of Guinea and the equatorial rain forest into the Sahel. We stress that the SST of the *whole* Atlantic basin influence the annual cycle of Sahelian rainfall. Note also that the remote influence of SST and the local influence of insolation interact in a non-linear fashion in producing the observed annual cycle of precipitation in the Sahel.

Insolation determines the bulk of the seasonal changes in precipitation over Africa and South America through its influence on the net energy influx in the atmospheric column (F_{net}).

In the experiments with prescribed SST, changes in insolation over land also have the effect of modulating the intensity of the ITCZ. If, for example, insolation forces a reduction in precipitation over the continents, the corresponding reduction in elevated condensational heating induces a cooling of the upper troposphere and a more unstable environment (or equivalently, more convective available potential energy, CAPE) in the Atlantic. The intensity of precipitation in the oceanic ITCZ will thus increase.

When we expand our model to include thermodynamic atmosphere-ocean interactions, we find that variations in precipitation and temperature over the continents are as important as variations in insolation over the ocean and in ocean heat transport convergence in forcing the annual march of the Atlantic ITCZ observed in the control simulation. The simulated control climatology of the Atlantic ITCZ is the result of a balance between the annual variations of local insolation, ocean heat transport, continental surface temperature and continental precipitation, and that no single forcing is dominant. The annual variations in oceanic local forcings (insolation over the ocean and heat transport) modulate the intensity

of precipitation in the tropical Atlantic, both north and south of the equator, but do not force the migration of the ITCZ seen in the control simulation. On the contrary, the annual variations in terrestrial forcings (continental surface temperature and precipitation) affect the position of the ITCZ more than its intensity, with the effect of the continental precipitation forcing partially counteracting the effect of the continental surface temperature forcing.

7.2 Implications

7.2.1 Implications for modeling the annual cycle

Our results from the uncoupled experiments allow us to draw some implications for modeling the annual cycle of precipitation over the tropical continents in a coupled GCM. Outside of the equatorial belt and the Sahel, where the influence of remote SST is important, gross shortcomings in the simulation of precipitation are most likely attributable to the atmosphere-land component of the model, and not to the effect of coupling. In particular, the land albedo, determined by soil type, soil moisture, and vegetative cover, can strongly affect F_{net} and thus can have a large impact on precipitation.

Furthermore, the uncoupled response of the Atlantic ITCZ to continental precipitation suggests the idea that the CCM3 biases in tropical precipitation—wherein precipitation over land is overestimated and precipitation over the ocean is underestimated—are two sides of the same coin. This indicates that changing the land surface properties in a way that reduces land precipitation could be a viable way to address both problems.

Our results from the AGCM+SOM experiments suggests that a correct simulation of the annual cycle of the Atlantic ITCZ in fully coupled GCMs will only be possible when the models will get everything right: no single process is the dominant influence on the ITCZ. This means, in particular, that the AGCMs must correctly simulate the annual cycle over land before we can hope to correctly simulate the maritime climate in coupled GCMs.

7.2.2 Implications for interannual-to-decadal variability

Although the subject of this paper is the annual cycle, we believe that the following additional conclusions regarding the interannual climate variability in the tropical Atlantic region are warranted.

We have shown that SST is an important forcing of the annual cycle of precipitation in the same regions where it is an important forcing of interannual precipitation variability, namely, northeast Brazil, Gulf of Guinea, Sudan, and Sahel (e.g. Nobre and Shukla, 1996; Rowell et al., 1995). This finding supports the suggestion (by, for example, Hastenrath, 1984; Mitchell and Wallace, 1992) that the same mechanisms might be at play in shaping both the annual cycle and the interannual variability, and that we can indeed gain some understanding of the variability by examining the much larger signal in the annual cycle.

Our results for the annual cycle suggest that interannual variability in Sahelian rainfall might be forced by SST variability in the subtropical Atlantic, as well as by SST variability in the Gulf of Guinea. Moreover, the co-variability between Sahel rainfall and the Atlantic ITCZ appears to be due to the presence of a common forcing (the SST), and not to the fact that the circulation associated with the ITCZ forces anomalies in the Sahel. Conversely, precipitation in the Nordeste, the Guiana Highlands, and the Guinea region is affected by the elevated heating in the ITCZ, and thus only indirectly by the Atlantic SST.

Our coupled experiments have shown that annual variations in the continental (and especially African) climate easily trigger a coupled response in the tropical Atlantic surface wind, the ITCZ, and the cross-equatorial SST, alike to the meridional-mode seen in the interannual-to-decadal variability, whose net effect is the meridional displacement of the ITCZ. Therefore, we would expect that variability in continental climate—either internal to the land-atmosphere coupled system, or forced by our land use practices—would have a signature in the oceanic variability.

Moreover, we can expect a linkage between the African and the South American climate, mediated by the ITCZ. For example, precipitation changes over Africa might induce a displacement of the ITCZ and affect rainfall in northeast Brazil.

Finally, we suggest that the fact that the response of oceanic precipitation to terrestrial

forcing is tightly locked to the annual cycle implies that a linear analysis of tropical Atlantic variability, or an analysis not stratified by season, might fail to fully capture a substantial effect of land processes.

7.2.3 Implications for paleo-climate

We maintain that our decomposition of the annual cycle in the Atlantic sector is also a valuable help in understanding past climates. For example, let's consider the greening of the Sahara of the mid-Holocene. Our results regarding the land response to seasonal changes in insolation suggest that surface albedo would be a limiting factor for the northward march of the African monsoon, and that a model must be able to accurately reproduce the changes in albedo following a change in soil moisture and vegetation cover in order to accurately simulate the greening of the Sahara. At the same time, we have shown that the precipitation at the edge of the Sahara depends on the basin-wide SST, and thus knowledge of the state of the Atlantic is also a prerequisite for simulating the greening of the Sahara.

Similarly, our coupled experiments have evidenced how a change in the climate of Africa sets off a coupled interaction between the Trades, the SST, and the ITCZ which results in a meridional displacement of the ITCZ. Thus, we can expect that the mid-Holocene greening of the Shara, which involves substantial changes in both surface temperature and precipitation, will be traceable in paleo records from the equatorial Atlantic.

BIBLIOGRAPHY

Biasutti, M., D. S. Battisti and E. S. Sarachik, 2003a: Mechanisms controlling the annual cycle of precipitation over the tropical Atlantic sector. *J. Climate*, In preparation.

Biasutti, M., D. S. Battisti and E. S. Sarachik, 2003b: Terrestrial influence on the annual cycle of the Atlantic ITCZ. *J. Climate*, In preparation.

Biasutti, M., D. S. Battisti and E. S. Sarachik, 2003c: The annual cycle over the tropical Atlantic, South America, and Africa. *J. Climate*, In press.

Bonan, G. B., 1996: A land surface model (LSM version 1.0) for ecological, hydrological, and atmospheric studies: Technical description and user's guide. Tech. Rep. NCAR/TN-417+STR, NCAR, pp. 150.

Bonan, G. B., 1998: The land surface climatology of the NCAR Land Surface Model coupled to the NCAR Community Climate Model. *J. Climate*, **11**, 1307–1326.

Carton, J. A. and Z. Zhou, 1997: Annual cycle of sea surface temperature in the tropical Atlantic Ocean. *J. Geophys. Res.*, **102 C13**, 27,813–27,824.

Chang, P., J. Li and H. Li, 1997: A decadal climate variations in the tropical Atlantic Ocean from thermodynamic air-sea interactions. *Nature*, **385**, 516–518.

Chiang, J., M. Biasutti and D. S. Battisti, 2003: Sensitivity of the atlantic itcz to last glacial maximum boundary conditions. *Paleoceanography*, Submitted.

Chiang, J., S. Zebiak and M. Cane, 2001: Relative roles of elevated heating and surface temperature gradients in driving anomalous surface winds over tropical oceans. *J. Atmos. Sci.*, **58**, 1371–1394.

Chou, C. and J. D. Neelin, 2003: Mechanisms limiting the northward extent of the northern summer convection zones . *J. Climate*, **16**, 406–425.

Davey, M. K. and co authors, 2002: STOIC: a study of coupled model climatology and variability in tropical ocean regions. . *Clim. Dyn.*, **18**, 403–420.

Dickinson, R. E., A. Henderson-Sellers and P. J. Kennedy, 1993: Biosphere-Atmosphere Transfer Scheme (BATS) Version 1e as coupled to the NCAR Community Climate Model. Tech. Rep. NCAR/TN-387+STR, NCAR, pp. 72.

Eltahir, E. A. B. and C. Gong, 1996: Dynamics of wet and dry years in West Africa. *J. Climate*, **9**, 1030–1042.

Emanuel, K. A., 1995: On thermally direct circulations in moist atmospheres. *J. Atmos. Sci.*, **52**, 1529–1534.

Emanuel, K. A., J. Neelin and C. Bretherton, 1994: On large-scale circulations in convecting atmospheres. *Q. J. R. Meteorol. Soc.*, **120**, 1111–1143.

Folland, C. K., A. W. Colman, D. P. Rowell and M. K. Davey, 2001: Predictability of Northeast Brazil rainfall and real-time forecast skill,1987-98. . *J. Climate*, **14**, 1937–1958.

Folland, C. K., T. N. Palmer and D. Parker, 1986: Sahel rainfall and worldwide sea temperature . *Nature*, **320**, 602–687.

Fu, R., R. E. Dickinson, M. Chen and H. Wang, 2001: How do tropical sea surface temperatures influence the seasonal distribution of precipitation in the equatorial Amazon? *J. Climate*, **14**, 4003–4026.

Gill, A. E., 1980: Some simple solutions for heat-induced tropical circulation. *Q. J. R. Meteorol. Soc.*, **106**, 447–462.

Hack, J., J. Kiehl and J. Hurrell, 1998: The hydrologic and thermodynamic characteristics of the NCAR CCM3 . *J. Climate*, **11**, 1207–1236.

Hastenrath, S., 1984: Interannual variability and the annual cycle: mechanisms of circulation and climate in the tropical Atlantic sector. *Mon. Wea. Rev.*, **112**, 1097–1107.

Hastenrath, S. and L. Greischar, 1993: Further work on the prediction of Northeast Brazil rainfall anomalies. *J. Climate*, **6**, 743–758.

Huffman, G. J., R. F. Adler, P. Arkin, A. Chang, R. Ferraro, A. Gruber, J. Janowiak, R. Joyce, A. McNab, B. Rudolf, U. Schneider and P. Xie, 1997: The Global Precipitation Climatology Project (GPCP) Combined Precipitation Data Set. *Bull. Amer. Meteor. Soc.*, **78**, 5–20.

Kalnay, E., M. Kanamitsu, R. Kistler, W. Collins, D. Deaven, L. Gandin, M. Iredell, S. Saha, G. White, J. Woollen, Y. Zhu, M. Chelliah, W. Ebisuzaki, W. Higgins, J. Janowiak, K. Mo, C. Ropelewski, J. Wang, A.Leetmaa, R. Reynolds, R. Jenne and D. Joseph, 1996: The NCEP/NCAR 40-year reanalysis project. *Bull. Amer. Meteor. Soc.*, **77**, 437–471.

Kiehl, J. T., J. J. Hack, G. B. Bonan, B. A. Boville, D. L. Williamson and P. J. Rasch, 1998: The National Center for Atmospheric Research Community Climate Model: CCM3. *J. Climate*, **11**, 1131–1150.

Li, T. and S. G. H. Philander, 1997: On the seasonal cycle of the equatorial Atlantic. *J. Climate*, **10**, 813–817.

Lindzen, R. S. and S. Nigam, 1987: On the role of sea-surface temperature-gradients in forcing low-level winds and convergence in the tropics. *J. Atmos. Sci.*, **44**, 2418–2436.

Mitchell, T. P. and J. M. Wallace, 1992: The annual cycle in equatorial convection and sea-surface temperature. *J. Climate*, **5**, 1140–1156.

Neelin, J. D. and I. M. Held, 1987: Modeling tropical convergence based on the moist static energy budget. *Mon. Wea. Rev.*, **115**, 3–12.

Nobre, P. and J. Shukla, 1996: Variations of sea surface temperature, wind stress, and rainfall over the tropical Atlantic and South America. *J. Climate*, **9**, 2464–2479.

Parker, D. E., C. K. Folland, A. Bevan, M. Ward, M. Jackson and K. Maskell, 1996: *Marine surface data for analysis of climatic fluctuations on interannual to century timescales.* pp. 241–250. National Academy Press, Washington, DC.

Philander, S. G. H., D. Gu, D. Halpern, G. Lambert, N.-C. Lau, T. Li, and R. Pacanowski, 1996: Why the ITCZ is mostly north of the equator. *J. Climate*, **9**, 2958–2971.

Plumb, R. and A. Hou, 1992: The response of a zonally symmetric atmosphere to subtropical thermal forcing: threshold behavior. *J. Atmos. Sci.*, **49**, 1790–1799.

Reynolds, R. W. and T. M. Smith, 1994: Improved global sea surface temperature analyses. *J. Climate*, **7**, 929–948.

Rowell, D. P., C. K. Folland, K. Maskell and M. N. Ward, 1995: Variability of summer rainfall over tropical north Africa (1906-92): Observations and modelling. *Q. J. R. Meteorol. Soc.*, **121**, 669–704.

Saravanan, R. and P. Chang, 1999: Oceanic mixed layer feedback and tropical Atlantic variability. *Geophys. Res. Lett.*, **26**, 3629–3632.

Saravanan, R. and P. Chang, 2000: Interaction between tropical Atlantic variability and El Niño-Southern Oscillation. *J. Climate*, **13**, 2177–2194.

Seager, R., Y. Kushnir, P. Chang, N. Naik, J. Miller and W. Hazeleger, 2001: Looking for the role of the ocean in the tropical Atlantic decadal climate variability. *J. Climate*, **14**, 638–655.

Shea, D. J., K. E. Trenberth and R. W. Reynolds, 1992: A global monthly sea surface temperature climatology. *J. Climate*, **5**, 987–1001.

Shukla, J. and M. Fennessy, 1994: Simulation and predictability of Monsoons. In Proceedings of the International Conference on Monsoon Variability and Prediction : International Centre for Theoretical Physics, Trieste, Italy, 9-13 May 1994. in *Proceedings of the International Conference on Monsoon Variability and Prediction : International Centre for Theoretical Physics, Trieste, Italy, 9-13 May 1994*, WMO/TD-No.619, pp. 567–575.

Sobel, A. H. and C. Bretherton, 2000: Modeling tropical precipitation in a single column. *J. Climate*, **13**, 4378–4392.

Storch, H. V. and F. W. Zwiers, 1999: *Statistical Analysis in Climate Research.* Cambridge University Press.

Uvo, C. B., C. A. Repelli, S. Zebiak and Y.Kushnir, 1998: The relationships between tropical Pacific and Atlantic SST and Northeast Brazil monthly precipitation. *J. Climate*, **11**, 551–562.

Ward, M. N., 1998: Diagnosis and short-lead time prediction of summer rainfall in Tropical North Africa at interannual and multidecadal timescales. . *J. Climate*, **11**, 3167–3191.

Xie, S. P. and S. G. H. Philander, 1994: A coupled ocean-atmosphere model of relevance to the ITCZ in the eastern Pacific. *Tellus*, **46A**, 340–350.

Zeng, N. and J. D. Neelin, 1999: A land-atmosphere interaction theory for the tropical deforestation problem. *J. Climate*, **12**, 857–872.

VITA

Michela Biasutti

EDUCATION

July 2003 (expected): Ph.D., Department of Atmospheric Sciences, University of Washington, Seattle, WA. Dissertation title: On the Annual Cycle over the Atlantic Sector. The Relative Role of Land and Ocean.

2000: M.S. Atmospheric Sciences, University of Washington, Seattle, WA. Thesis Title: Decadal Variability in the Tropical Atlantic as simulated by the Climate System Model and the CCM3 coupled to a Slab Ocean Model.

1995: "Laurea in Fisica" cum laude, Universita' degli Studi di Trieste, Italy. Thesis topic: A Comparison of Internal and Forced Atmospheric Variability in the COLA GCM.

EMPLOYMENT

1996–Present: Research Assistant, Department of Atmospheric Sciences, University of Washington, Seattle, WA. Work done in JISAO, under the supervision of D. S. Battisti and E. S. Sarachik.

Spring 1998: Teaching Assistant for undergraduate level "Introduction to Weather and Climate".

January-September 1996: Research Assistant, IMGA-CNR, Modena, Italy. Work under the supervision of Antonio Navarra.

Autumn 1995: Internship at COLA, Calverton, MD. Work under the supervision of J. Shukla.

JOURNAL PUBLICATIONS

2003 Biasutti, M., D. S. Battisti, and E. S. Sarachik: "Terrestrial influence on the annual cycle of the Atlantic ITCZ." In preparation for *J. Climate.*

2003 Biasutti, M., D. S. Battisti, and E. S. Sarachik: "Mechanisms controlling the annual cycle of precipitation in the tropical Atlantic sector." In preparation for *J. Climate.*

2003 Chiang, J.C.H., M. Biasutti, and D. S. Battisti: "Sensitivity of the Atlantic ITCZ to millennial-timescale forcing." *Paleoceanography*, conditionally accepted.

2003 Biasutti, M., D. S. Battisti, and E. S. Sarachik: "The Annual Cycle over the Tropical Atlantic, South America, and Africa." In print. *J. Climate.*

2000 Navarra, A., M. Biasutti, S. Gualdi, E. Roeckner, U. Schlese, and U. Shulzweida: "Sensitivity experiments to mountain representations in spectral models." *Annali di Geofisica*, **43**(3), 559–584.

DOCTORAL DISSERTATION

July 2003 (expected) Biasutti, M.: On the Annual Cycle over the Atlantic Sector. The Relative Role of Land and Ocean. Ph.D. Thesis, University of Washington.

MASTER'S THESIS

2000: Biasutti, M.: Decadal Variability in the Tropical Atlantic as simulated by the Climate System Model and the CCM3 coupled to a Slab Ocean Model. M.S. Thesis, University of Washington.

OTHER PUBLICATIONS

2000 David S. Battisti, John C.H. Chiang, and Michela Biasutti: " Developing a Theory for ENSO." Lecture notes for 2000 NCAR ASP on Decadal and Centennial Climate Variability.

2000 David S. Battisti, John C.H. Chiang, and Michela Biasutti: "Competing Theories for the Observed Decadal ENSO-like Variability." Lecture notes for 2000 NCAR ASP on Decadal and Centennial Climate Variability.

ADDITIONAL EDUCATION

NCAR Advanced Study Program on Decadal and Centennial Variability (July, 2000) (presented).

SEMINARS PRESENTED:

A recipe for Decadal Variability in the Climate of the Tropical Atlantic. Part I: Ingredients. Department of Atmospheric Sciences, University of Washington, Seattle, WA (2000), IAOS, Bologna, Italy (2000).

A Possible Mechanism for Low Frequency Variability in the Climate of the Tropical Atlantic. NCAR Advanced Study Program on Decadal and Centennial Variability. Boulder, CO (2000).

On the Annual Cycle over the Atlantic Sector. The Relative Role of Land and Ocean. CGD, Boulder, CO (2002). ICTP, Trieste, Italy (2002). INGV, Bologna, Italy (2002).

CONFERENCES ATTENDED:

NCAR CSM workshop, Breckenridge CO (1998); US CLIVAR ATLANTIC meeting, Boulder, CO (2001); US CLIVAR workshop on the dynamics and predictability of the Atlantic ITCZ and its regional climatic influences, Palisades, NY (2002)